Physics – Uspekhi **42** (8) 737 – 778 (1999)

REVIEWS OF TOPICAL PROBLEMS PACS numbers: **04.40.–b**, **26.60.+c**, **95.30.–k**, 97.60.Jd

Cooling of neutron stars and superfluidity in their cores

D G Yakovlev, K P Levenfish, Yu A Shibanov

Contents

Abstract. We study the heat capacity and neutrino emission reactions (direct and modified Urca processes, nucleon–nucleon bremsstrahlung, Cooper pairing of nucleons) in the supranuclear density matter of neutron star cores with superfluid neutrons and protons. Various superfluidity types are analysed (singlet-state pairing and two types of triplet-state pairing, without and with gap nodes at the nucleon Fermi surface). The results are used for cooling simulations of isolated neutron stars. Both the standard cooling and the cooling enhanced by the direct Urca process are strongly affected by nucleon superfluidity. Comparison of the cooling theory of isolated neutron stars with observations of their thermal radiation may give stringent constraints on the critical temperatures of the neutron and proton superfluidities in the neutron star cores.

1. Introduction

Neutron stars (NSs) are unique astrophysical objects. First, their observational manifestations are numerous (radio and X-ray pulsars, X-ray bursters, X-ray transients, etc. [1]). Second, their structure and evolution are determined by properties of matter under extreme conditions which cannot be reproduced in the laboratory (supranuclear densities, superstrong magnetic fields, superfluidity of the baryon component of superdense matter, etc.).

It is widely accepted (see, e.g., Refs [2, 1]) that NSs are born at the final stage of evolution of normal stars of mass $M \gtrsim 8M_\odot$ in gravitational collapse of their cores ($M_\odot$ is the solar mass). During collapse, the matter of central layers is compressed to nuclear densities and enriched by neutrons. As a result, a compact NS is created of mass $M \sim M_\odot$ and radius $\mathcal{R} \sim 10$ km. The core consists mainly of neutrons (with some admixture of protons, electrons, and — possibly — hyperons and other particles). A NS is born hot, with an internal temperature of about 10^{11} K, but cools down rapidly due to powerful neutrino emission from the internal layers.

NSs possess strong gravitational fields; gravitational acceleration on their surfaces is as large as $\sim (2-3) \times 10^{14}$ cm s^{-2}. The stellar radius $\mathcal{R}$ is only 2 – 3 times larger than the gravitational radius $\mathcal{R}_g = 2GM/c^2$, where G is the gravitational constant and c is the speed of light. Therefore, the effects of General Relativity are important in NS life.

In this review, we restrict ourselves to a consideration of the structure and thermal evolution of isolated NSs of age $t \lesssim 10^6$ yr. The evolution of NSs in close binaries is more complicated; it has been described, for instance, by Lewin et al. [3].

D G Yakovlev, K P Levenfish, Yu A Shibanov. Ioffe Physical-Technical Institute Politekhnicheskaya 26,
194021 St.-Petersburg, Russian Federation
Tel. (7-812) 247-91-80. Fax (7-812) 550-48-90
E-mails: yak@astro.ioffe.rssi.ru; ksen@astro.ioffe.rssi.ru;
shib@stella.ioffe.rssi.ru

Received 24 March 1999
Uspekhi Fizicheskikh Nauk **169** (8) 825 – 868 (1999)
Translated by D G Yakovlev; edited by S D Danilov

The superfluidity and superconductivity of nucleons in NS interiors play an important role in the evolution of isolated NSs. For instance, sudden changes of spin periods (glitches) demonstrated by some pulsars are commonly explained [4] by the interaction of the normal and superfluid components of matter in the stellar crusts. Superfluidity affects the heat capacity and neutrino luminosity of the star, and therefore its cooling. The effect of superfluidity on the cooling is the main subject of the present review.

At a certain cooling stage ($10^2 - 10^5$ yr) the NS internal temperature can strongly depend on critical temperatures of transitions of nucleons into the superfluid state. This feature was first mentioned by Page and Applegate [5] who called NSs 'thermometers' for measuring the nucleon critical temperatures in asymmetric nuclear matter. Microscopic calculations of such temperatures are complicated owing to the absence of an explicit many-body relativistic quantum theory which would describe adequately strong interactions of particles of various species. However, the critical temperatures can be studied by the astrophysical method, by confronting cooling simulations with observations of thermal radiation of isolated NSs. This work is not finished yet but certain results have already been obtained. The aim of this review is to describe the above method and main results obtained to-date (by January 1999).

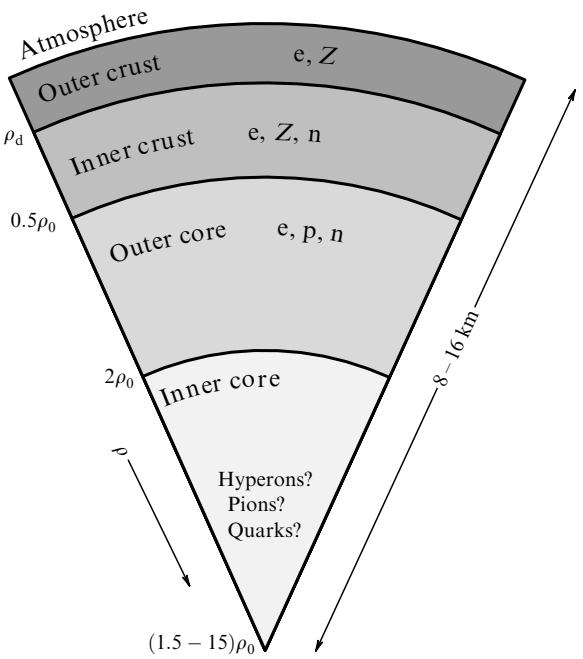

Figure 1. Schematic cross section of a $1.4\,M_\odot$ neutron star. The stellar parameters depend strongly on the equation of state of internal layers.

2. Overall properties of neutron stars

2.1 Structure

If standard measurements are used, neutron stars (NSs) are hot objects. Several hundred thousand years after their birth their internal temperature exceeds 10^7 K. However, the equation of state of internal NS layers is practically independent of temperature since the main contribution to the pressure comes from strongly degenerate fermions of high energy [1].

A NS can be subdivided into the *atmosphere* and four internal regions: *the outer crust, the inner crust, the outer core*, and *the inner core* as shown in Fig. 1.

The atmosphere is a thin plasma layer, where the spectrum of thermal electromagnetic NS radiation is formed. In principle, this radiation contains valuable information on the stellar parameters (on the temperature, gravitational acceleration and chemical composition of the surface, on the magnetic field, etc., see Section 8.1) and, as a result, on the internal structure. The geometrical depth of the atmosphere varies from some ten centimeters in a hot NS down to some millimeters in a cold one. Very cold NSs may have no atmosphere at all but a solid surface.

NS atmospheres have been studied theoretically by many authors (see, e.g., review articles by Pavlov et al. [6, 7] and references therein). The construction of atmosphere models, especially for cold NSs (with a surface temperature $T_s \lesssim 10^6$ K) with strong magnetic fields $10^{11} - 10^{14}$ G, is far from complete owing to the complexity of calculations of the equation of state and the spectral opacity of the atmospheric plasma (Section 8.1.2).

The outer core (outer envelope) extends from the atmosphere bottom to the layer of density $\rho = \rho_d \approx 4.3 \times 10^{11}$ g cm^{-3} and has a depth of some hundred meters [1]. Its matter consists of ions and electrons. A very thin (no more than several meters in a hot NS) surface layer contains a non-degenerate electron gas. In deeper layers, electrons constitute a strongly degenerate, almost ideal gas, which becomes relativistic at $\rho \gg 10^6$ g cm^{-3}. For $\rho \gtrsim 10^4$ g cm^{-3}, atoms are fully ionized by the electron pressure, being actually bare atomic nuclei. The electron Fermi energy grows with increasing ρ, and the nuclei suffer beta-decays and are enriched by neutrons (see, e.g., Ref. [8]). At the base of the outer core ($\rho = \rho_d$) neutrons start to drip from nuclei producing a free-neutron gas.

The depth of the inner crust (inner envelope) may be as large as several kilometers. The density ρ in the inner crust varies from ρ_d at the upper boundary to $\sim 0.5\rho_0$ at the base. Here, $\rho_0 = 2.8 \times 10^{14}$ g cm^{-3} is the saturation nuclear matter density. The matter of the inner crust consists of electrons, free neutrons and neutron-rich atomic nuclei [9, 10]. The fraction of free neutrons increases with growing ρ. At the crust bottom (in the density range from 10^{14} to about 1.5×10^{14} g cm^{-3}) the nuclei may form clusters and have non-spherical shapes [11, 10]. The nuclei disappear at the crust-core interface. Neutrons in the inner crust may be in a superfluid state (Section 3.1).

The outer core occupies the density range $0.5\rho_0 \lesssim \rho \lesssim 2\rho_0$ and can be several kilometers in depth. Its matter consists of neutrons n with some (several per cent by particle number) admixture of protons p and electrons e (the so called *standard* nuclear composition). The composition of matter is determined by the conditions of electric neutrality and beta-equilibrium with respect to the reactions $n \to p + e + \bar{\nu}_e$, $p + e \to n + \nu_e$, where ν_e and $\bar{\nu}_e$ stand for electron neutrino and antineutrino, respectively. The electric neutrality requires equality of the electron and proton number densities: $n_p = n_e$. The beta-equilibrium establishes a relationship between the chemical potentials of the particles: $\mu_n = \mu_p + \mu_e$. The neutrino chemical potential is omitted here since immediately after the birth a NS becomes fully transparent for neutrinos which freely escape the star [12, 1].

All npe-plasma components are strongly degenerate. The electrons form almost ideal relativistic Fermi gas. The neutrons and protons, which interact via nuclear forces, constitute a strongly non-ideal non-relativistic Fermi-liquid. It can be described using the formalism of quasi-particles [13, 14]. The Fermi momentum p_{F_j} of particle species j is related to their number density n_j as $p_{\mathrm{F}_j} = \hbar(3\pi^2 n_j)^{1/3}$. Therefore, the electric neutrality implies the equality of the Fermi momenta of protons and electrons: $p_{\mathrm{F_p}} = p_{\mathrm{F_e}}$.

Calculations show (e.g., Ref. [1]) that for $\rho \sim \rho_0$ the chemical potentials of neutrons and electrons are $\mu_{\mathrm{n}} \approx \mu_{\mathrm{e}} \approx 60-100$ MeV, while the chemical potential of protons is much lower, $\mu_{\mathrm{p}} \approx 3-6$ MeV. With increasing density, the Fermi energies of particles grow, so that new particles can be created. First of all, these are muons which, like electrons, constitute a strongly degenerate, almost ideal gas. The appearance of particles in the inner NS core will be discussed below.

Let us emphasize that properties of the NS crust ($\rho \lesssim 0.5\rho_0$) are described by sufficiently reliable microscopic theories. The situation with matter of supranuclear density, $\rho \gtrsim \rho_0$, is quite different. Laboratory data on the properties of this matter are incomplete, and the reliability of the theories decreases with growing ρ. An exact self-consistent quantum theory of matter of supranuclear density has not been constructed yet. Many theoretical equations of state have been proposed which can be subdivided conventionally into the *soft*, *moderate* and *stiff* ones with respect to compressibility of matter. These equations of state are considerably different for $\rho > \rho_0$. For instance, at $\rho \approx 4\rho_0$ a soft equation of state proposed by Pandharipande [15] (based on the Reid [16] nucleon–nucleon soft-core potential) gives a pressure which is about an order of magnitude lower than that given by a stiff equation of state constructed by Pandharipande and Smith [17] using the mean field approach.

Almost all microscopic theories predict the appearance of neutron and proton superfluidity in the outer NS core (Section 3.1). The proton superfluidity is accompanied by superconductivity (most likely, of the second type) and affects evolution of the internal magnetic fields (see, e.g., Ref. [18]).

The outer core of a low-massive NS extends to the stellar center. More massive NSs also possess an inner core. Its radius may reach several kilometers, and its central density may be as high as $(10-15)\rho_0$. The composition and equation of state of the inner core are poorly known. It should be emphasized that they are most crucial for determining the structure and evolution of massive NSs, and that they constitute the main NS 'mystery'. Several hypotheses have been put forward and are being discussed in the literature; it is impossible to reject any of them at present:

(1) Hyperonization of matter — the appearance of Σ- and Λ-hyperons (see, e.g., Ref. [1]). The fractions of p and e may be so high that the powerful direct Urca process of neutrino emission becomes allowed [19] as well as similar reactions involving hyperons [20]. In these cases, the neutrino luminosity of the star is enhanced by 5–6 orders of magnitude (see, e.g., Ref. [21]) as compared to the standard neutrino luminosity of the outer core produced mainly by the modified Urca process. This accelerates considerably NS cooling (Sections 2.2 and 7).

(2) The second hypothesis, proposed in different forms in Refs [22–26], assumes the appearance of pion condensation. The condensates soften the equation of state and enhance the neutrino luminosity by allowing direct Urca type reactions [22, 23, 27, 28]. However, many modern microscopic theories of dense matter predict weakly polarized pionic degrees of freedom which are not in favor of pion condensation [21].

(3) The third hypothesis predicts a phase transition to strange quark matter composed of almost free u, d and s quarks with a small admixture of electrons (see, e.g., Refs [29, 30]). In these cases the neutrino luminosity is thought to be considerably higher than the standard luminosity due to switching on the direct Urca processes involving quarks [31, 32, 21]. However, in some models (e.g., Ref. [33]) the presence of quarks does not enhance the neutrino luminosity.

(4) Following Kaplan and Nelson [34], Nelson and Kaplan [35] and Brown et al. [36], several authors considered the hypothesis on kaon condensation in dense matter. Kaon condensates may also enhance the neutrino luminosity by several orders of magnitude [21]. A critical analysis of contemporary theories of kaon condensation was given in Ref. [37].

For any equation of state, one can build a set of NS models with different central densities ρ_{c}. This can be done by solving numerically the equation of hydrostatic equilibrium with account for the effects of General Relativity (the Oppenheimer–Volkoff equation, see, e.g., Ref. [1]). With increasing ρ_{c}, the stellar mass M usually grows, and the radius $\mathcal{R}$ decreases (a star becomes more compact). As a rule, the mass ρ_{c} reaches maximum at some M, which corresponds to the most compact stable stellar configuration. The mass M_{c} of this configuration is the *maximum* NS mass, for a given equation of state. Stellar models with a higher central density are usually unstable (with respect to collapsing into a black hole) and cannot exist for a long time. Using a set of NS models, one can construct a 'mass–radius' diagram which depends strongly on the equation of state in the NS core. The softer the equation of state, the more compact NS, and the lower the maximum mass. For instance, this mass ranges from 1.4 to 1.6 $M_\odot$ for different soft equations of state; from 1.6 to 1.8$M_\odot$ for moderate equations of state, and from 1.8 to 3$M_\odot$ for stiff equations of state. The problem of maximum NS mass is crucial for the identification of black holes in binary systems [38].

The equation of state in the NS cores can be studied by confronting theory with observations in different ways. The majority of methods are based on the determination (constraint) of NS mass and/or radius and comparison of these observational results with the mass-radius diagrams for different equations of state (see, e.g., Ref. [1]). Unfortunately, no absolutely decisive arguments have been given so far in favor of the stiff, moderate or soft equations of state. One can definitely rule out only the ultra-soft equations of state which give a maximum NS mass lower than 1.44 $M_\odot$, the mass of the Hulse–Taylor pulsar (PSR 1913+16), which is the most massive known star in close double neutron-star binaries (where the NS masses are determined very accurately). In this review, we will discuss another method to explore properties of superdense matter — by NS cooling.

2.2 Neutrino emission

About 20 s after its birth, a NS becomes transparent for neutrinos [1] generated in its interior. Leaving the star, neutrinos carry away energy and cool the star. Therefore, a study of neutrino reactions is important for NS cooling theories. The most powerful neutrino emission is produced in the NS core. Thus we will not discuss the neutrino reactions in the NS crust. A detailed description of these can be found,

for instance, in the review article by Imshennik and Nadyozhin [39] as well as in Refs [40 – 45]. Typical neutrino energies are much higher than their assumed rest mass energies; therefore, neutrinos can usually be considered as massless particles.

There are many neutrino reactions in the NS core (see, e.g., Refs [1, 21]). Their efficiency is determined by the equation of state of matter which is poorly known (see above). For certainty, we will not consider exotic models of strange matter, pion or kaon condensates, but outline the main neutrino reactions in npe matter. A more detailed analysis of these reactions, particularly in the presence of nucleon superfluidity, is given in Sections 4 – 6.

2.2.1 Modified Urca processes. Starting from the classical article by Chiu and Salpeter [46] these processes have been treated as the main neutrino generation mechanism for *standard* NS cooling. Cooling is called *standard* provided very powerful neutrino reactions are absent, like the direct Urca process or analogous processes in exotic models of dense matter.

The modified Urca reaction is similar to the familiar reactions of beta decay and beta capture, but involves an additional spectacular nucleon. In the npe-matter, the reaction can go through two channels

$$\mathrm{n}+\mathrm{n}\to\mathrm{n}+\mathrm{p}+\mathrm{e}+\bar{\nu}_\mathrm{e},\ \mathrm{n}+\mathrm{p}+\mathrm{e}\to\mathrm{n}+\mathrm{n}+\nu_\mathrm{e}\,; \qquad (1)$$

$$\mathrm{n}+\mathrm{p}\to\mathrm{p}+\mathrm{p}+\mathrm{e}+\bar{\nu}_\mathrm{e},\ \mathrm{p}+\mathrm{p}+\mathrm{e}\to\mathrm{n}+\mathrm{p}+\nu_\mathrm{e}\,, \qquad (2)$$

which we define as the *neutron* and *proton* branches of the modified Urca process, respectively.

The spectacular nucleon is needed to conserve the momentum of reacting particles. The familiar beta-decay and beta-capture reactions (called the direct Urca process discussed below) are forbidden (strongly suppressed) in the outer NS core. The suppression is due to the relatively low fractions of electrons and protons, owing to which the Fermi momenta of n, p, and e do not obey the 'triangle rule', $p_{\mathrm{F_n}}\leqslant p_{\mathrm{F_e}}+p_{\mathrm{F_p}}$, required for momentum conservation (the momenta of emitting neutrinos $p_\nu\sim k_\mathrm{B}T/c$ can be neglected: they are determined by the temperature of matter, T, and are much smaller than the momenta of other particles; here k_B is the Boltzmann constant). The neutrino energy emission rate (emissivity) $Q^{(\mathrm{Mn})}$ in the neutron branch (1) of the modified Urca process for $\rho\sim\rho_0$ can be estimated as [12] $Q^{(\mathrm{Mn})}\sim$ $\sim 10^{22}T_9^8$ erg cm^{-3} s^{-1}, where $T_9=T/10^9$ K. The proton branch is nearly as efficient: $Q^{(\mathrm{Mp})}\sim Q^{(\mathrm{Mn})}$ (Section 5.1).

2.2.2 Neutrino bremsstrahlung due to nucleon–nucleon scattering. The standard neutrino luminosity is also determined by the processes of neutrino bremsstrahlung radiation in nucleon–nucleon collisions

$$\mathrm{n}+\mathrm{n}\to\mathrm{n}+\mathrm{n}+\nu+\bar{\nu},\quad \mathrm{n}+\mathrm{p}\to\mathrm{n}+\mathrm{p}+\nu+\bar{\nu}\,,$$
$$\mathrm{p}+\mathrm{p}\to\mathrm{p}+\mathrm{p}+\nu+\bar{\nu}\,, \qquad (3)$$

allowed throughout the NS core. Here ν means a neutrino of any flavor (ν_e, ν_μ, ν_τ). In normal (non-superfluid) matter the bremsstrahlung processes [12] are weaker than the modified Urca process: $Q^{(\mathrm{NN})}\sim(10^{19}-10^{20})T_9^8$ erg cm^{-3} s^{-1}. However, they can be important in superfluid matter (Section 5).

2.2.3 Direct Urca process. As mentioned above, the sequence of beta-decay and beta-capture reactions,

$$\mathrm{n}\to\mathrm{p}+\mathrm{e}+\bar{\nu}_\mathrm{e},\quad \mathrm{p}+\mathrm{e}\to\mathrm{n}+\bar{\nu}_\mathrm{e}\,, \qquad (4)$$

called the *direct Urca process*, is forbidden in the outer NS core due to insufficiently high fractions of e and p. It had been thought for a long time that the process is also forbidden in the inner NS core.

However, process (4) becomes allowed [19], if the fraction of protons (among all baryons) $x_\mathrm{p}=n_\mathrm{p}/n_\mathrm{b}$ exceeds some critical value $x_\mathrm{p}=x_\mathrm{c}$. In npe-matter, this happens for $p_{\mathrm{F_n}}\leqslant 2p_{\mathrm{F_p}}$, which gives $x_\mathrm{c}=1/9=0.111$. If muons are present for the same number density of baryons n_b, the proton fraction appears to be slightly higher than in the npe matter, and the electron fraction slightly lower. In this case, x_c is higher and reaches 0.148 for relativistic muons [19].

In the simplest model of superdense matter as a gas of non-interacting Fermi particles [1] the proton fraction is not high: $x_\mathrm{p}<x_\mathrm{c}$ for any density. However, this may not be so for realistic equations of state. This circumstance was first outlined by Boguta [47] in 1981 but his article was unnoticed for a long time.

It was the paper by Lattimer et al. [19] which initiated wide discussion of the direct Urca process. The authors showed that, for many realistic models of matter, x_p slightly exceeded x_c at densities several times higher than the standard nuclear matter density. Therefore, the nucleon direct Urca process can be allowed in the inner cores of rather massive NSs. Moreover, practically all equations of state in the inner stellar core, which predict the appearance of hyperons, open direct Urca reactions involving hyperons [20].

According to Ref. [19] the neutrino emissivity in the reaction (4) is $Q^{(\mathrm{D})}\sim 10^{27}T_9^6$ erg cm^{-3} s^{-1}. For $T\sim 10^9$ K, the direct Urca process is about 5 – 6 orders of magnitude more efficient than the modified Urca. Therefore, sufficiently massive NSs suffer *enhanced cooling* (Section 7).

In a series of papers initiated by Voskresensky and Senatorov [48, 49] direct Urca type neutrino reactions have been studied for models of dense matter with highly polarized pion degrees of freedom. Pion condensation in this matter takes place at $\rho\sim\rho_0$ and is very efficient. Even for lower ρ, before the condensation occurs, the neutrino emissivity appears to be much higher than the standard one due to the polarizability of pion vacuum. Cooling of NSs with this equation of state has been simulated recently by Schaab et al. [50]. We will not consider these models.

2.2.4 Neutrino emission due to Cooper pairing of nucleons. The onset of nucleon superfluidity switches on a new neutrino generation mechanism concerned with the creation of Cooper pairs. The process had been proposed and calculated in the pioneering article by Flowers et al. [51] and rediscovered independently by Voskresensky and Senatorov [49, 52] ten years later. Until recently, the process had been forgotten for unknown reasons and was not included in NS cooling simulations. It was Page [53] who 'recalled' the process and introduced it into the cooling theory. Cooling simulations including this process have been performed recently in several papers, in particular, in Refs. [50, 54 – 57]. The process in question actually represents [56] neutrino pair emission (any neutrino flavor) by a nucleon N (neutron or proton) whose dispersion relation contains an energy gap:

$$\mathrm{N}\to\mathrm{N}+\nu+\bar{\nu}\,. \qquad (5)$$

The reaction cannot occur without superfluidity: the emission of a neutrino pair by a free nucleon is forbidden by energy–momentum conservation. According to Yakovlev et al. [56]

the neutrino emissivity due to pairing of neutrons is $Q^{(\mathrm{CP})} \sim 10^{21} T_9^7 F(\tau)$ erg cm^{-3} s^{-1}, where $\tau = T/T_\mathrm{c}$, T_c is the critical temperature of superfluidity onset, and $F(\tau)$ is a function, which has maximum $F \sim 1$. The main neutrino energy release takes place in the temperature range $0.2\,T_\mathrm{c} \lesssim T \lesssim T_\mathrm{c}$. The efficiency of the process in this range can be comparable to or even larger than (Sect. 6.2) the efficiency of the modified or even the direct Urca processes suppressed partly by the superfluidity. This determines the importance of 'Cooper' neutrinos for NS cooling. Neutrino emission due to pairing of protons appears to be much weaker owing to the smallness of the vector constant of the weak neutral current involving protons.

2.3 Cooling

Initially a NS cools mainly via neutrino emission from its core. However, direct detection of the neutrino flux is possible only during NS birth in supernova explosion. So far this has been done only once, from the Supernova 1987A in the Large Magellanic Cloud (see, e.g., Ref. [39]). A powerful neutrino outburst in a supernova explosion lasts for about 20 s. Afterwards the neutrino flux decreases rapidly in time.

The cooling of a NS is accompanied by the loss of its thermal energy which is mainly stored in the stellar core. The energy is carried away through two channels: first, by neutrino emission from the entire stellar body (mostly from the core), where the most powerful neutrino reactions take place, and second, by heat conduction through the internal stellar layers towards the surface, and further, by thermal emission of photons from the surface. The neutrino cooling dominates at the initial cooling stage (see below), while the photon cooling dominates later, when the neutrino luminosity becomes weak (it fades faster than the photon luminosity with decreasing temperature).

From a mathematical point of view, the cooling simulation reduces to solving the heat diffusion equation within the star [58] with account for the volume (neutrino emission) and surface (photon emission) energy sinks. As a rule, one considers one-dimensional diffusion along the radial coordinate in a spherically symmetric star. In about $t \gtrsim 10^2 - 10^3$ yr, owing to the high thermal conductivity of the internal layers, a wide, almost isothermal region is formed within the entire core and the main fraction of the crust. In this case, cooling simulations are considerably simplified, being reduced to solving the global thermal-balance equation: the loss of the thermal energy (determined by the total heat capacity) is governed by the neutrino and photon luminosities of the star. This approach is described and used in Section 7.2. Accordingly the main elements of the cooling theory are: (1) NS heat capacity, (2) neutrino luminosity, (3) dependence of the photon luminosity on internal temperature (determined by the thermal conductivity of the outermost stellar layers). The first two elements are discussed in detail in this review.

The character of cooling depends on many parameters: the equation of state of internal layers, the superfluidity of nucleons in the stellar core, NS mass, magnetic field, the chemical composition of the surface layers, etc. Confronting the cooling theory with observations enables one, in principle, to constrain these parameters. In this review we discuss the constraints on the critical temperatures of neutron and proton superfluidities in NS cores.

While simulating NS cooling one calculates *cooling curves*, the dependence of the effective stellar surface temperature T_s on stellar age t. The effective temperature defines the photon luminosity: $L_\gamma = 4\pi\mathcal{R}^2\sigma T_\mathrm{s}^4$, where σ is the Stefan–Boltzmann constant. The luminosity L_γ^∞, as detected by a distant observer with account for the effects of General Relativity, is related to the local luminosity L_γ as $L_\gamma^\infty = L_\gamma[1 - (\mathcal{R}_\mathrm{g}/\mathcal{R})]$. Here $\mathcal{R}_\mathrm{g} = 2GM/c^2$ is the gravitational NS radius. The effective temperature of thermal radiation T_s^∞, detected by a distant observer, is related to the local temperature T_s by $T_\mathrm{s}^\infty = T_\mathrm{s}\sqrt{1 - (\mathcal{R}_\mathrm{g}/\mathcal{R})}$.

Figure 2 shows typical cooling curves for (non-superfluid) NSs of different masses (from Ref. [5], with the permission of the authors). The NS models are based on an equation of state which permits direct Urca processes in the cores for $M > 1.35M_\odot$. The stars with lower mass undergo standard cooling.

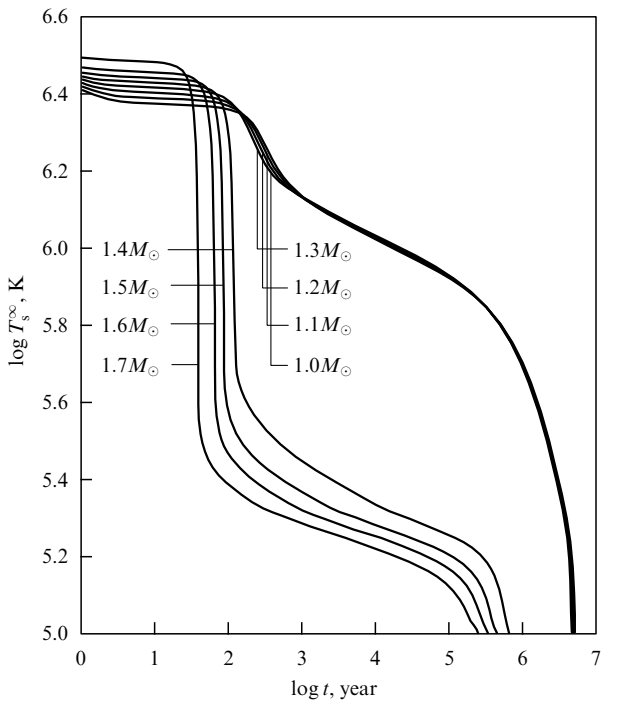

Figure 2. Redshifted surface temperature T_s^∞ versus stellar age t according to Page and Applegate [5] for non-superfluid NS models of different mass.

If the direct Urca is allowed in the stellar core, the star cools much faster than that with the standard neutrino luminosity. Typical cooling times $t \sim T/\dot{T}$ can be estimated from the thermal balance of a plasma element in the stellar core: $t \sim CT/Q_\nu$. Here, Q_ν is the neutrino emissivity, and C is the specific heat capacity. Using the heat capacity (Sect. 3.3) of an ideal degenerate gas of neutrons at $\rho = \rho_0$ and an appropriate neutrino emissivity from Sect. 2.2, one obtains (see, e.g., Refs [1, 59]): $t^{(\mathrm{D})} \sim 1\ \mathrm{min}/T_9^4$, $t^{(\mathrm{M})} \sim 1\ \mathrm{yr}/T_9^6$. It is seen that the direct Urca process decreases the internal stellar temperature to 10^9 K in $t^{(\mathrm{D})}$ min, and down to 10^8 K in several days. For the standard neutrino emissivity, the cooling time $t^{(\mathrm{M})}$ is about 1 yr and 10^6 yr, respectively.

These estimates describe the temperature variation in the stellar core at the initial cooling stage. The crust cools initially much slower since its own neutrino energy losses are relatively small. Sufficiently low thermal conductivity of the crust produces thermal insulation between the crust and the core. Thus, the core and the crust cool independently at the initial stage, and the NS surface radiation carries no information on

the thermal state of the core (the almost flat initial parts of the cooling curves in Fig. 2).

The cooling wave from the rapidly cooling core reaches the stellar surface in 10 – 1000 yr (see, e.g., Refs [60, 61]), and the surface temperature T_s falls sharply (Fig. 2). In the course of the enhanced cooling T_s drops by almost an order of magnitude in several years, which decreases the photon luminosity by a factor of $\sim 10^4$. For the standard cooling, the temperature fall is not so significant and lasts $\sim 10^2$ yr.

After the thermal relaxation in the NS interior is over the neutrino luminosity from the core remains higher than the photon surface luminosity. However, at this stage the core controls the surface temperature. This is the second relatively flat part of the cooling curve. The internal temperature exceeds the surface temperature by more than an order of magnitude; the main temperature gradient takes place in the outermost layers of the outer crust.

Finally, a rather old star appears to be at the *photon* cooling stage. The neutrino luminosity becomes much smaller than the photon one, and the cooling curves turn out to be much steeper (Fig. 2). The change of the cooling regime is associated with the different temperature dependences of the neutrino and photon cooling rates. Let us recall that the neutrino emissivity is $Q^{(\mathrm{D})} \propto T^6$ for the direct Urca process, and $Q^{(\mathrm{Mn})} \propto T^8$ for the modified Urca process (Section 2.2). The photon luminosity falls down much more weakly with decreasing temperature, as $T^{2.2}$ [62]. Simple estimates show that the time t_ν of transition to the photon cooling stage is mainly determined by the NS heat capacity and by the temperature dependence of the neutrino energy losses; typically, $t_\nu \sim 10^5$ yr. The internal temperature of a star of age t_ν is mainly determined by the efficiency of the neutrino energy losses and by their temperature dependence.

The appearance of superfluidity in the NS core changes drastically the cooling process. This is discussed in the subsequent Sections 3 – 8. We will study systematically the effects of superfluidity on the heat capacity and neutrino luminosity of NSs. This will allow us to 'calibrate' theoretical cooling curves and use cooling NSs as 'thermometers' for measuring nucleon critical temperatures in their cores. We will see that the nucleon superfluidity can either enhance or slow down cooling (depending on parameters) and it strongly reduces the difference between the enhanced and standard cooling. We will analyse observations of thermal radiation from cooling NSs and show that the observational data are difficult to explain without assuming the existence of superfluidity in the NS cores.

3. Superfluidity and heat capacity of neutron star cores

3.1 Nucleon superfluidity

The theory of electron superconductivity in metals was developed by Bardeen, Cooper and Schrieffer (BCS) [63] in 1957. Superconductivity is explained by Cooper pairing of electrons caused by a weak attraction due to the electron–phonon interaction. The superconducting state appears with decreasing temperature as a result of the second-order phase transition; typical critical temperatures are $T_c \sim 1 - 10$ K. For $T < T_c$, the dispersion relation of electrons contains an energy gap Δ, with $T \ll T_c$ at $\Delta \sim k_B T_c$.

A year after the publication of the BCS theory Bohr, Mottelson and Pines [64] suggested that a phenomenon much like superconductivity could appear in systems of nucleons in atomic nuclei. Cooper pairing of nucleons could occur due to nuclear attraction. It was expected that the gap in the nucleon spectrum, $\Delta \sim 1$ MeV ($T_c \sim 10^{10}$ K), was many orders of magnitude larger than for electrons in metals. Later the presence of pair correlations of nucleons in atomic nuclei and the associated energy gap in the nucleon spectrum was investigated theoretically and confirmed experimentally (Nobel Prize of Bohr, Mottelson and Reynoter in 1975).

Migdal [65] was one of the first who applied the BCS theory to atomic nuclei. He noticed also that neutron superfluidity caused by nuclear forces could occur in neutron matter of the inner NS layers where critical temperatures $T_c \sim 10^{10}$ could be expected.

BCS equations which describe symmetric nuclear matter in atomic nuclei and asymmetric neutron-rich NS matter have much in common but have also some differences. For instance, pairing in atomic nuclei takes place in the singlet-state of a nucleon pair. In this case, the energy gap is isotropic, independent of the orientation of nucleon momentum. On the other hand, one can expect triplet-state pairing in NS matter (see below) which leads to the anisotropic gap.

Calculations of the energy gap in symmetric nuclear matter have been carried out since 1959, starting from the classical papers by Cooper, Mills and Sessler [66] and Migdal [65]. Without pretending to give a complete description of this activity (see, e.g., Ref. [67], for a review) let us mention the early articles [68 – 71] in which the gap in the nucleon spectrum was studied for different model potentials [72] of nucleon–nucleon interaction. It was shown by the middle of the 1960s that the gap was extremely sensitive to the repulsive part of the potential and to the effective masses of nucleons in nuclear matter. These conclusions are qualitatively correct for NSs (see below).

It is well known that the BCS theory is also used to describe superfluidity in liquid ^{3}He. The foundation of the theory was built in Ref. [66] mentioned above. Superfluidity in ^{3}He (caused by interatomic attraction) is quite different from that in nucleon matter; the critical temperature in ^{3}He at normal pressure is as small as 2.6 mK. However, there is one important similarity: pairing can occur in the triplet state of interacting particles (with orbital momentum l), which leads to an anisotropic gap. The BCS equations are similar in these cases. The first article devoted to triplet-state pairing was written by Anderson and Morel [73]. While deriving the equation for the anisotropic gap the authors overlooked the contribution from one of three triplet spin states. This inaccuracy was corrected in Ref. [74].

Let us outline the microscopic theories of superfluidity in NSs. Five years after Migdal [65], Ginzburg and Kirzhnits published a brief article [75] where they estimated the gap produced by the singlet-state pairing of neutrons at a density $\rho = 10^{13} - 10^{15}$ g cm^{-3} and obtained $\Delta \sim 5 - 20$ MeV. A very serious step was made by Wolf [76] in 1966. He showed that the singlet-state neutron pairing takes place in the inner NS crust ($\rho \lesssim \rho_0$), but disappears in the core, since the singlet-state nn-interaction becomes repulsive in high-density matter. The number density of protons in the NS core is much smaller than the number density of neutrons (Section 2.1). Accordingly the single-state pp-interaction is attractive there and leads to proton pairing.

Before the discovery of pulsars in 1967 the theory of superfluidity in NSs was developing rather slowly. A detailed review of 'pre-pulsar' articles was given by Ginzburg [77]. The

discovery of pulsars initiated a great interest in the theory. Baym, Pethick and Pines [78] analyzed the macroscopic consequences of neutron superfluidity (rotation of the superfluid component in the form of quantized vortices) and proton superfluidity — superconductivity (splitting of the internal stellar magnetic field into Abrikosov magnetic flux tubes). This paper made the foundation of the modern theory which explained pulsar glitches by the interaction of normal and superfluid components of matter inside NSs (see, e.g., Ref. [4]).

A very important contribution to the theory was made in the paper by Hoffberg et al. [79] published in 1970. The authors showed that the triplet-state $^3P_2$ interaction of neutrons at $\rho \gtrsim \rho_0$ was attractive. Thus, triplet-state neutron superfluidity with an anisotropic gap can occur in the NS core. The authors performed the first calculations of the critical temperature of the triplet-state neutron superfluidity in NSs.

The paper [79] was followed by many others, where the theory was developed and nucleon critical temperatures in NSs were calculated. Superfluidities of various types have been considered using different model potentials of the nucleon–nucleon interaction. Some authors have made use of the potentials renormalized with account for polarization properties of matter on the basis of various many-body theories. A comparative analysis of different approaches has been done, for instance, in Refs [80 – 83, 67]. A detailed review was written by Takatsuka and Tamagaki [84] not long ago. Many articles have been devoted to the triplet-state superfluidity of neutrons in the NS cores (see, e.g., Refs [79, 81, 83 – 93]). Let us mention model calculations [94] of the triplet-state neutron pairing in magnetized NS cores. According to these calculations, the magnetic field $B \gtrsim 10^{16}$ G makes the triplet-state superfluidity with the nodes at the Fermi-surface energetically preferable to the familiar triplet-state superfluidity without nodes (Section 3.2). Singlet-state proton superfluidity in the NS cores has been considered thoroughly by many authors (e.g., Refs [67, 80, 83, 84, 89, 93, 95 – 98]). In Ref. [99] singlet-state proton superfluidity in the NS cores was studied and maximum densities at which this superfluidity disappears were estimated. Let us mention also Refs [100, 101], where the possibility of neutron–proton Cooper pairing in uniform nucleon matter was analyzed. This pairing is possible in symmetric nuclear matter but does not occur in NSs due to the large difference of neutron and proton Fermi momenta. Many articles (e.g., Refs [67, 79, 80, 82 – 84, 97, 98, 102 – 110]) have considered the singlet-state pairing of free neutrons in the inner NS crust. Nucleons within atomic nuclei in the inner crust can also suffer pairing which is, however, weaker than for free neutrons (see, e.g., Refs [104, 109 – 112]).

Although we will not consider exotic models of NS cores (Section 2.1), let us mention that superfluidity is possible in these models as well. For instance, Takatsuka and Tamagaki [84] reviewed calculations of neutron and proton superfluid gaps in pion condensed matter. They also obtained new results in this field [91 – 93]. The same authors [113] studied the nucleon superfluidity in the presence of kaon condensation. The pion or kaon condensates mix strongly neutron and proton states which may induce triplet-state pairing of quasiprotons. Some authors have discussed superfluidity in quark matter (e.g., Refs [30, 33, 114, 115]). If hyperons appear in npe-matter, they can also be in a superfluid state [116]. Electrons and muons, which interact via Coulomb forces, can, in principle, be superfluid as well. However, the corresponding critical temperatures are too low to be of practical interest. For instance, according to an estimate by Ginzburg [77] the critical temperature of degenerate electrons at $\rho \gtrsim 100$ g cm^{-3} does not exceed 1 K, while the internal temperature of a cooling NS of age $t \lesssim 10^6$ does not fall below 10^6 K (Sect. 7).

Let us summarize the properties of nucleon superfluidity in the cores and crusts of NSs with the standard (npe) composition.

(1) Singlet-state neutron superfluidity exists in the inner NS crust and disappears at the density $\rho \sim \rho_0$, at which an effective neutron–neutron singlet-state attraction transforms into repulsion. The density dependence of the critical temperature T_{cn} on ρ is maximum at a subnuclear density. The maximum values of T_{cn} range from 10^8 to 10^{11}, for different models of dense matter.

(2) Triplet-state neutron superfluidity appears in the NS core at $\rho \gtrsim \rho_0$ owing to an effective attraction between neutrons in the triplet state. The density dependence of the appropriate critical temperature, as a rule, is maximum at supranuclear density. The maximum values of T_{cn} vary from 10^8 to 10^{10} for different microscopic models.

(3) Protons in NS cores can suffer singlet-state pairing. The dependence $T_{cp}(\rho)$ has usually maximum at a supranuclear density, and the maximum values of T_{cp} range from 10^8 to 10^{10} for different models of matter.

(4) The critical temperature is very sensitive to the strength of the repulsive core of the nucleon–nucleon interaction (see, e.g., Refs [86, 102, 84]). T_c increases strongly with core softening, i.e., with increasing attraction between nucleons. Even a weak additional attraction (e.g., due to the inclusion of coupling between the $^3P_2$ and $^3F_2$ states for the triplet-state pairing of neutrons: see Refs [87, 84]) may increase T_c by several orders of magnitude. Generally, the superfluidity is stronger for a softer equation of state.

(5) The critical temperature falls rapidly with decreasing effective mass of nucleons in dense matter (see, e.g., Refs [84, 86, 95]), i.e., with decreasing density of state of nucleons at the Fermi surface. If the effective mass is sufficiently low ($m_N^* \lesssim 0{,}5 m_N$) the superfluidity may entirely disappear.

(6) The critical temperature depends strongly on the method of description of many-body (in-medium) effects. For instance, the in-medium effects for neutrons in the NS crusts decrease T_{cn} typically by several times (e.g., Refs [82, 84, 103, 107]).

For illustration, in Fig. 3 we present the critical temperature of the triplet-state neutron superfluidity and the singlet-state proton superfluidity obtained by different authors.

The HGRR curve has been calculated by Hoffberg et al. [79] for neutron superfluidity using the Tabakin [117] model of the nucleon–nucleon potential which reproduces quite well experimental phases of nucleon scattering at energies $\leqslant 320$ keV. The in-medium effects have been neglected in Ref. [79]; the effective neutron mass has been set equal to its bare mass. The TT-curve has been calculated by Takatsuka and Tamagaki [86] for the neutron superfluidity under the same assumptions but using the one-pion-exchange model of nucleon interaction (OPEG ^{3}O – 1) with a somewhat harder core. This lowers T_{cn}. The solid AO-curve was obtained by Amundsen and Ostgaard [81] for the neutron superfluidity using a similar one-pion-exchange approach (OPEG), but the effective neutron mass was determined self-consistently and appeared to be lower than the bare neutron mass. This additionally lowers T_{cn}. The BCLL-curve is a result of recent

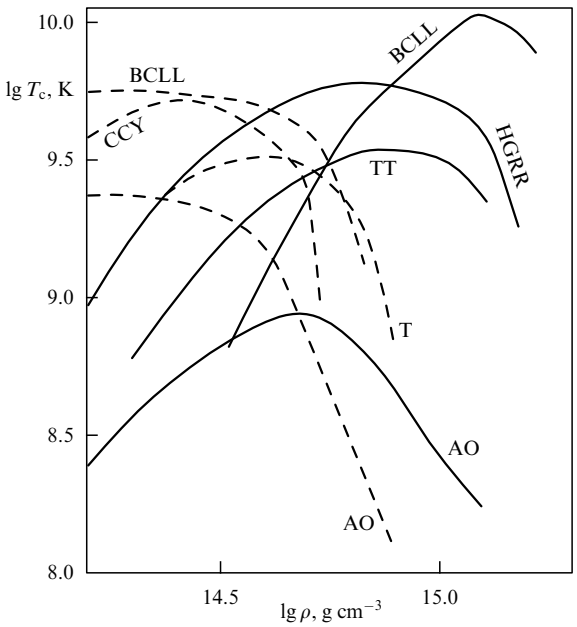

Figure 3. Critical temperatures of triplet-state neutron superfluidity (solid lines) and singlet-state proton superfluidity (dashed lined) versus density according to different authors: HGRR — [79], TT — [86], CCY — [95], T — [96], AO — [80, 81], BCLL — [83].

calculations by Baldo et al. [83] using an empirical nucleon potential (Argonne v_{14}) which reproduces accurately laboratory data on nucleon scattering. The potential and neutron mass have not been renormalized to account for the in-medium effects. As a result, the values of T_{cn} are high again.

The dashed CCY curve shows the results by Chao et al. [95] for proton superfluidity using the simplified Serber potential which describes satisfactorily the experimental phases of singlet-state nucleon–nucleon scattering. The effective proton mass has been determined self-consistently. The T curve presents the results by Takatsuka [96] obtained under the same assumption but using a more realistic OPEG potential. The dashed AO curve was calculated by Amundsen and Ostgaard [80] using the same one-pion-exchange approach but another method of evaluation of the effective proton mass which leads to noticeably different critical temperatures T_{cp}. Finally, the dashed BCLL curve was derived by Baldo et al. [83] under the same assumptions as the solid BCLL curve. A neglect of polarization effects leads to the high critical temperature T_{cp}.

Let us emphasize the large scatter of T_{cn} and T_{cp}. For instance, the BCLL curves [83] mentioned above give very high critical temperatures in matter of supranuclear density while, for instance, the calculations by Takatsuka and Tamagaki [96] indicate a significant decrease of the critical temperatures at densities of several ρ_0, at which the direct Urca process is open. Under these conditions, while analyzing the effects of superfluidity, we will not use any specific microscopic results but will treat T_{cn} and T_{cp} as free parameters.

3.2 Energy gaps and critical temperatures

Thus, the cases of the $^1S_0$ or $^3P_2$ pairing in the NS cores are of special interest. The $^3P_2$ pairing in npe matter occurs mainly in the system of neutrons. While studying this pairing one should take into account the states with different projections m_J of the total pair momentum onto the quantization axis: $|m_J| = 0, 1, 2$. The actual (energetically favorable) state may be a superposition of states with different m_J (see, e.g., Refs [81, 83]). Owing to uncertainties of microscopic theories this state is still unknown; it depends possibly on density and temperature. In simulations of NS cooling, one usually considers the triplet-state pairing with $m_J = 0$ (excluding the recent paper [118]). Below we will consider the $^3P_2$ superfluidities with $m_J = 0$ and $|m_J| = 2$, since their effects on the heat capacity and NS neutrino luminosity are qualitatively different.

For certainty, we will analyze the BCS superfluidity for an ensemble of almost free (quasi-)nucleons. The superfluidity types $^1S_0$, $^3P_2$ ($m_J = 0$) and $^3P_2$ ($|m_J| = 2$) under study will be denoted by A, B and C, respectively (Table 1). The critical temperatures will be treated as free parameters.

Table 1. Three superfluidity types.

Superfluidity type		λ	$F(\vartheta)$	$k_B T_c/\Delta(0)$
A	$^1S_0$	1	1	0.5669
B	$^3P_2(m_J = 0)$	1/2	$1+3\cos^2\vartheta$	0.8416
C	$^3P_2(\|m_J\| = 2)$	3/2	$\sin^2\vartheta$	0.4926

The superfluidity onset is accompanied by the appearance of the energy gap δ in momentum dependence of the nucleon energy $\varepsilon(\mathbf{p})$. Near the Fermi surface ($|p - p_F| \ll p_F$) one has (e.g., Ref. [119])

$$\varepsilon = \mu - \sqrt{\delta^2 + \eta^2},\ p < p_F;\ \varepsilon = \mu + \sqrt{\delta^2 + \eta^2},\ p \geqslant p_F\,. \tag{6}$$

Here, $\eta = v_F(p - p_F)$, v_F and p_F are the nucleon Fermi velocity and momentum, respectively, μ is the chemical potential; it is assumed that $\delta \ll \mu$. In the cases of study, $\delta^2 = \Delta^2(T)F(\vartheta)$, where $\Delta(T)$ is an amplitude, which determines temperature dependence of the gap, $F(\vartheta)$ describes the dependence of δ on the angle ϑ between the quantization axis and particle momentum $\mathbf{p}$. The quantities Δ and F are determined by the superfluidity type (Table 1). In case A the gap is isotropic, $\delta = \Delta$. In cases B and C the gap is anisotropic (depends on ϑ). Let us notice that in case C the gap vanishes at the Fermi-sphere poles at any temperature (since $F(0) = F(\pi) = 0$), i.e., the superfluidity does not affect the nucleons which move along the quantization axis.

The gap amplitude $\Delta(T)$ is determined by the BCS equation (see, e.g., the textbook [119] or Ref. [85]) which can be written as

$$\ln\left[\frac{\Delta_0}{\Delta(T)}\right] = 2\lambda \int \frac{d\Omega}{4\pi} \int_0^\infty \frac{dx}{z} f F(\vartheta)\,, \tag{7}$$

where $\Delta_0 = \Delta(0)$, $d\Omega$ is a solid angle element in the direction of $\mathbf{p}$, $f = (1 + \exp z)^{-1}$ is the Fermi–Dirac distribution, λ is a numerical coefficient (Table 1),

$$z = \frac{\varepsilon - \mu}{k_B T} = \mathrm{sign}(x)\sqrt{x^2 + y^2},\quad x = \frac{\eta}{k_B T},\quad y = \frac{\delta}{k_B T}\,. \tag{8}$$

Using Eqn (7) one can easily obtain the values of $k_B T_c/\Delta_0$ presented in Table 1. It is convenient to introduce the variables

$$v = \frac{\Delta(T)}{k_B T},\quad \tau = \frac{T}{T_c}\,. \tag{9}$$

The dimensionless gap amplitude v describes the temperature dependence of the gap. It is determined by the superfluidity type and the dimensionless temperature τ. In case A the amplitude v corresponds to the isotropic gap, in case B it corresponds to the minimum and in case C to the maximum gap at the Fermi surface. In this notation, the dimensionless gap y has the form:

$$y_{\rm A} = v_{\rm A}, \quad y_{\rm B} = v_{\rm B}\sqrt{1+3\cos^2\vartheta}, \quad y_{\rm C} = v_{\rm C}\sin\vartheta\,. \qquad (10)$$

Using Eqn (7) one can obtain the asymptotes of the gap amplitude near the critical temperature and in the limit of the so called strong superfluidity ($T \ll T_{\rm c}$). For instance, at $T \to T_{\rm c}$, $T < T_{\rm c}$ ($\tau \to 1$) we have (see, e.g., Refs [119, 120]): $v = \beta\sqrt{1-\tau}$, where $\beta_{\rm A} = 3.063$, $\beta_{\rm B} = 1.977$, $\beta_{\rm C} = 3.425$. For $T \ll T_{\rm c}$ we obtain $v = \Delta_0/(k_{\rm B}T_{\rm c}\,\tau)$. Levenfish and Yakovlev [121, 120] calculated $v = v(\tau)$ for intermediate τ and proposed analytic fits of the numerical data:

$$v_{\rm A} = \sqrt{1-\tau}\left(1.456 - \frac{0.157}{\sqrt{\tau}} + \frac{1.764}{\tau}\right),$$

$$v_{\rm B} = \sqrt{1-\tau}\left(0.7893 + \frac{1.188}{\tau}\right),$$

$$v_{\rm C} = \frac{\sqrt{1-\tau^4}}{\tau}\left(2.030 - 0.4903\tau^4 + 0.1727\tau^8\right). \qquad (11)$$

These fits will be useful for evaluating the heat capacity and neutrino luminosity in the superfluid NS cores.

The analytic fits presented here and below reproduce the numerical data with mean errors of about 1–2%, while the maximum error does not exceed 5%. This fit accuracy is more than sufficient for implications to NS cooling. Our fits also reproduce various asymptotes of the quantities under study.

Notice that for the triplet-state superfluidity with $|m_J| = 1$ or for a triplet-state superfluidity described by superposition of states with different $|m_J|$, the anisotropic gap δ depends not only on ϑ, but also on the azimuthal angle ϕ of nucleon momentum $\mathbf{p}$. A study of the effects of such superfluidity on the heat capacity and neutrino luminosity is complicated and has not been performed yet.

3.3 Heat capacity of superfluid neutron star cores

Consider the npe matter of the NS cores. The specific (per unit volume) heat capacity is equal to the sum of partial heat capacities of all particle species j: $C = \sum_j C_j$, where $j = {\rm n, p, e}$. Since the particles are strongly degenerate, the heat capacities at constant volume and pressure are nearly the same [119] and we make no difference between them. A partial heat capacity is determined by the standard thermodynamic formula [119]:

$$C_j = \frac{2}{(2\pi\hbar)^3}\int {\rm d}\mathbf{p}_j(\varepsilon_j - \mu_j)\frac{{\rm d}f_j}{{\rm d}T}\,, \qquad (12)$$

where ε_j and $\mathbf{p}_j$ stand for the particle energy and momentum, respectively, μ_j is the chemical potential, and f_j is the Fermi-Dirac distribution.

In our case, the electrons constitute an almost ideal, strongly degenerate, ultra-relativistic gas. Accordingly,

$$C_{\rm e} = \frac{m_{\rm e}^* p_{\rm F_e} k_{\rm B}^2 T}{3\hbar^3} \approx 5.67\times10^{19}\left(\frac{n_{\rm e}}{n_0}\right)^{2/3} T_9\ ({\rm erg\ cm^{-3}\ K^{-1}})\,, \qquad (13)$$

where $m_{\rm e}^* = \mu_{\rm e}/c^2 \approx p_{\rm F_e}/c$, $p_{\rm F_e}$ and $n_{\rm e}$ denote, respectively, the electron Fermi momentum and number density, $n_0 = 0.16\ {\rm fm^{-3}}$ is the standard nucleon number density in atomic nuclei. In the presence of muons, one should add their partial heat capacity C_μ to the total heat capacity; $C_{\rm e}$ is similar to C_μ with the only difference that muons may be non-relativistic.

Neutrons and protons ($j = {\rm N} = {\rm n}$ and p) in the NS cores constitute a non-relativistic, strongly non-ideal Fermi-liquid (Section 2.1). The partial heat capacity (12) of normal nucleons is:

$$C_{\rm N_0} = \frac{m_{\rm N}^* p_{\rm F_N} k_{\rm B}^2 T}{3\hbar^3} \approx 1.61\times10^{20}\frac{m_{\rm N}^*}{m_{\rm N}}\left(\frac{n_{\rm N}}{n_0}\right)^{1/3} T_9\ ({\rm erg\ cm^{-3}\ K^{-1}})\,. \qquad (14)$$

Here $p_{\rm F_N}$ is the nucleon Fermi momentum determined by the nucleon number density $n_{\rm N}$, and $m_{\rm N}^*$ is the effective mass of the (quasi-)nucleon in dense matter. Notice that the main contribution to the heat capacity comes from nucleons with energies near the Fermi level, $|\varepsilon_{\rm N} - \mu_{\rm N}| \lesssim k_{\rm B}T$, which can participate in processes of energy exchange $\sim k_{\rm B}T$.

For $T < T_{\rm c}$, Eqn (12) should include the energy gap (6). Generally, the nucleon heat capacity can be written as

$$C_{\rm N} = C_{\rm N_0} R(T)\,, \qquad (15)$$

where $C_{\rm N_0}$ is the partial heat capacity of normal nucleons (14), and the factor R describes the variation of the heat capacity by the superfluidity. R depends on the superfluidity type and on the dimensionless temperature τ. Clearly, $R(T) = 1$ for $T > T_{\rm c}$ ($\tau > 1$).

A general expression for R is obtained from Eqn (12) by introducing the dispersion relation (6), dimensionless variables (8) and by taking into account Eqn (14):

$$R = \frac{3}{2\pi^3}\int {\rm d}\Omega\int_0^\infty {\rm d}x\, zT\frac{{\rm d}f(z)}{{\rm d}T}\,. \qquad (16)$$

Notice that the Fermi–Dirac distribution f depends on T directly as well as functionally, through the dispersion relation (6). Therefore, ${\rm d}f/{\rm d}T$ contains the derivative of the gap amplitude $\Delta(T)$ with respect to T.

The heat capacity of superfluid Fermi-systems is well known in the physical literature (especially for the singlet-state pairing) but not in the astrophysics of NSs. The heat capacity $C_{\rm A}(T)$ for case A has been calculated by Mühlschlegel [122] and is described in textbooks [119]. Maxwell [123] proposed a fit of $C_{\rm A}(T)$ in the temperature range $0.2\,T_{\rm c} \leqslant T \leqslant T_{\rm c}$. Anderson and Morel [73] derived an asymptote of $C_{\rm C}$ at $T \ll T_{\rm c}$ for superfluidity of type C. Simple expressions for $R_{\rm A}$, $R_{\rm B}$ and $R_{\rm C}$ convenient for evaluating the nucleon heat capacity in the NS cores were obtained in Ref. [120] and are given below.

When the temperature falls below the critical value, the heat capacity suffers a jump produced by latent heat release at the phase transition. In case A the jump is given by $R_{\rm A}(T_{\rm c}) = 2.426$ [119], while in cases B and C the jump is $R_{\rm B}(T_{\rm c}) = R_{\rm C}(T_{\rm c}) = 2.188$. These jumps affect NS cooling (Section 7.2).

The energy gap in the nucleon spectrum strongly reduces the heat capacity for temperatures much below the critical one ($T \ll T_{\rm c}$, $v \to \infty$). Let us recall, that the main contribu-

tion into the heat capacity in non-superfluid matter would come from nucleons with energies $|\varepsilon-\mu| \lesssim k_{\rm B}T$. However, in the low-temperature limit $T \gg T_{\rm c}$ for all nucleons in cases A or B and almost for all nucleons (excluding a small fraction of particles near the poles of the Fermi sphere) in case C the gap δ is much larger than $k_{\rm B}T$. Therefore, the 'heat-capacious' nucleons with energies $|\varepsilon-\mu| \lesssim k_{\rm B}T$ are either absent or almost absent, which suppresses the heat capacity. Accordingly, we have the asymptotes:

$$R_{\rm A} = \frac{3\sqrt{2}}{\pi^{3/2}}\, v^{5/2}\exp(-v) = \frac{3.149}{\tau^{5/2}}\exp\left(-\frac{1.764}{\tau}\right),$$

$$R_{\rm B} = \frac{\sqrt{3}}{\pi}\, v^{2}\exp(-v) = \frac{0.7781}{\tau^{2}}\exp\left(-\frac{1.188}{\tau}\right),$$

$$R_{\rm C} = \frac{7\pi^2}{5v^2} = 3.353\tau^2\,. \qquad (17)$$

Here and hereafter we set $v = v_{\rm A}$, $v = v_{\rm B}$ or $v = v_{\rm C}$ in the factors R, labeled by indices A, B or C, respectively. With decreasing temperature, $R_{\rm A}$ and $R_{\rm B}$ are reduced exponentially, while $R_{\rm C}$ is reduced much slower, proportionally to T^2. The exponential reduction is associated with an exponentially small 'efficiency of excitation' of quasi-nucleons near the Fermi surface in the presence of a large gap. In the case of the heat capacity, this effect strongly reduces 'heat exchange', but, generally, all nucleon reactions (transitions) are reduced. A small exponent is absent in case C because the gap $\delta_{\rm C} = \delta_{\rm C}(T,\vartheta)$ vanishes for nucleons at the Fermi-sphere poles. The superfluidity disappears near the poles, and these nucleons have 'normal' heat capacity. However the fraction of these nucleons decreases proportionally to T^2, which leads to a power-law reduction of the heat capacity of the nucleon liquid as a whole.

The results of numerical calculations of R, as well as the asymptotes for $v \to 0$ and $v \to \infty$ are described by the simple fit expressions [120]

$$R_{\rm A} = \left(0.4186 + \sqrt{(1.007)^2 + (0.5010v)^2}\right)^{2.5} \times \exp\left(1.456 - \sqrt{(1.456)^2 + v^2}\right),$$

$$R_{\rm B} = \left(0.6893 + \sqrt{(0.790)^2 + (0.2824v)^2}\right)^{2} \times \exp\left(1.934 - \sqrt{(1.934)^2 + v^2}\right),$$

$$R_{\rm C} = \frac{2.188 - (9.537\times 10^{-5}v)^2 + (0.1491v)^4}{1 - (0.2846v)^2 + (0.01335v)^4 + (0.1815v)^6}\,. \qquad (18)$$

Equations (18), combined with Eqns (11), enable one to evaluate easily the factor R as a function of the dimensionless temperature τ.

The dependence of R on τ for superfluidity types A, B, C is shown in Fig. 4. The factors $R_{\rm A}$ and $R_{\rm B}$ as functions of the dimensionless gap amplitude v are close to each other which is illustrated in Fig. 5.

In simulations of NS cooling before the publication of articles [121, 120] as far as we know, one considered the superfluidity of A or B type and used the simplified factors of the form $R^* = \exp(-u)$, where $u_{\rm A} = \delta_{\rm A}/(k_{\rm B}T) = 1.764/\tau$, $u_{\rm B} = \delta_{\rm max}/(k_{\rm B}T) = 2.376/\tau$, $\delta_{\rm max} = 2\delta_{\rm B}(0)$ is the maximum

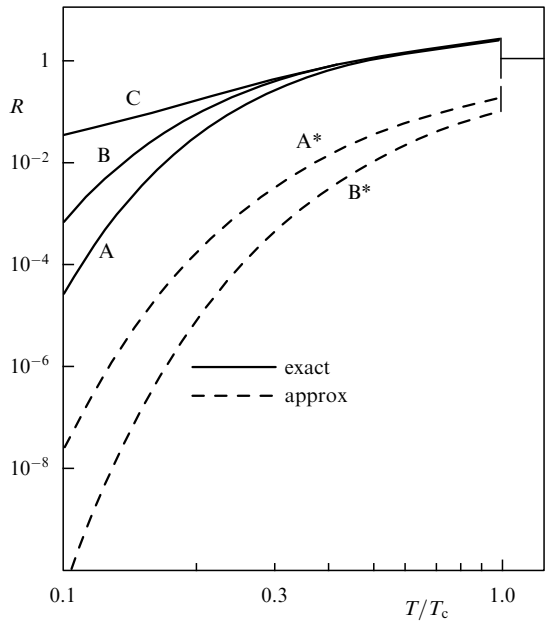

Figure 4. Factors R, which describe the variation of the heat capacity by superfluidity, versus $T/T_{\rm c}$. The letters near the curves show the superfluidity type. The dashed curves A* and B* present simplified factors R^* for superfluidities A and B, which were commonly used in applications earlier (see text).

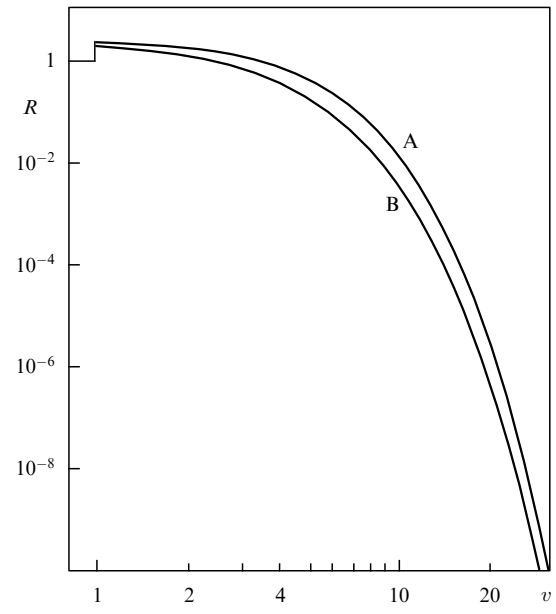

Figure 5. Factors $R_{\rm A}$ (curve A) and $R_{\rm B}$ (curve B), as in Fig. 4, but versus the dimensionless gap amplitude v.

energy gap $\delta_{\rm B}(0,\vartheta)$ as a function of ϑ at $T = 0$. These factors were introduced from physical considerations (see, e.g., Ref. [5]) based on the suggestion made in Ref. [123]. As seen from Fig. 4, the simplified factors do not reproduce the heat capacity jump at $T = T_{\rm c}$ and strongly overestimate reduction of the heat capacity at $T \ll T_{\rm c}$. Indeed, the correct asymptotes in the limit $T \ll T_{\rm c}$ contain large pre-exponents omitted in the simplified expressions. In addition, the factors $R_{\rm B}$ and $R^*_{\rm B}$ differ by exponent arguments. Instead of the correct argument $v_{\rm B} = \delta_{\rm min}/(k_{\rm B}T)$ [see Eqn (17)] the simplified factor

contains the argument $v_{\rm B}^* = \delta_{\max}/(k_{\rm B}T) = 2\delta_{\min}/(k_{\rm B}T)$, which is twice larger. As a result, for instance, at $T = 0.1\,T_{\rm c}$ the exact factor $R_{\rm A}$ exceeds the simplified factor $R_{\rm A}^*$ by about three orders of magnitude, while the exact factor $R_{\rm B}$ exceeds $R_{\rm B}^*$ by seven orders of magnitude.

Although the local heat capacities of particles are determined by a given equation of state, the relative contribution of n, p and e to the total heat capacity of a non-superfluid NS core does not depend strongly on the equation of state [124]. The neutron heat capacity is about 3/4 of the total, the proton heat capacity is about 1/4 of the total, and the electron contribution is only about 5%. Therefore, a strong superfluidity of n (with normal p) reduces the NS heat capacity by a factor of 4. In the opposite case (strong proton superfluidity and normal neutrons) the total heat capacity is reduced only by $\sim 25\,\%$. If neutrons and protons are strongly superfluid at once, only $\sim 5\,\%$ of the heat capacity of the normal core survives. In Section 7.2 we will see that the asymmetry of the nucleon composition of the NS cores affects the NS cooling.

4. Reduction of direct Urca process by nucleon superfluidity

4.1 Direct Urca process in non-superfluid matter

The neutrino cooling of a NS with the standard nuclear composition is determined by the direct Urca process (4) involving neutrons and protons; the process is allowed [19] for many realistic equations of state in the inner NS core. In the outer core, the process is forbidden by momentum conservation of reacting particles (Section 2.2).

The process (4) consists of the direct and inverse reactions. Under the beta-equilibrium condition, their rates are equal, and it is sufficient to calculate the neutrino emissivity in the first reaction and double the result. The total emissivity will be labeled by the superscript (D); in a normal (non-superfluid) matter, it is given by [19] ($\hbar = c = k_{\rm B} = 1$):

$$Q^{(\rm D)} = 2\int\left[\prod_{j=1}^{2}\frac{{\rm d}^3p_j}{(2\pi)^3}\right]\frac{{\rm d}^3p_{\rm e}}{2\varepsilon_{\rm e}(2\pi)^3}\frac{{\rm d}^3p_\nu}{2\varepsilon_\nu(2\pi)^3} \times (2\pi)^4\delta(E_{\rm f}-E_{\rm i})\delta(\mathbf{P}_{\rm f}-\mathbf{P}_{\rm i})\varepsilon_\nu\mathcal{L}\sum_{\rm spins}|M|^2\Theta\,, \qquad (19)$$

where $\mathbf{p}_j$ is the nucleon momentum ($j = 1$ corresponds to neutron and $j = 2$ to proton), $\mathbf{p}_{\rm e}$ and $\varepsilon_{\rm e}$ are the electron momentum and energy, respectively, $\mathbf{p}_\nu$ and ε_ν are the antineutrino momentum and energy, the delta function $\delta(E_{\rm f}-E_{\rm i})$ describes energy conservation, and $\delta(\mathbf{P}_{\rm f}-\mathbf{P}_{\rm i})$ describes the conservation of momentum of particles in the initial (i) and final (f) states. Furthermore, $\mathcal{L}$ stands for the product of Fermi–Dirac distributions or corresponding blocking factors of nucleons and electron, and $|M|^2$ is the squared reaction amplitude. Summation is over initial and final spin states. The step function Θ forbids the reaction in matter of not too high density (Section 2.2): $\Theta = 1$ if $p_{\rm F_n}$, $p_{\rm F_p}$, $p_{\rm F_e}$ satisfy the 'triangle condition' and $\Theta = 0$ otherwise.

Nucleons and electrons in the NS core are strongly degenerate and the main contribution to the integral (19) comes from narrow regions of momentum space near the corresponding Fermi surfaces. Thus one can set $p = p_{\rm F}$ in all smooth functions under the integral. For non-relativistic nucleons, the quantity $\sum_{\rm spins}|M|^2$ is independent of particle momenta and can be taken out of the integral. The remaining integral is evaluated by the standard method of decomposition of integration over directions and magnitudes of particle momenta. Introducing the dimensionless variables in accordance with Eqn (8), the neutrino emissivity (19) can be written as [125]

$$Q^{(\rm D)} = \frac{4}{(2\pi)^8}T^6AIS\overline{|M|^2}\Theta\,, \qquad (20)$$

$$A = \left[\prod_{j=1}^{4}\int{\rm d}\Omega_j\right]\delta\left(\sum_{j=1}^{4}\mathbf{p}_j\right), \qquad (21)$$

$$I = \int_0^\infty {\rm d}x_\nu\, x_\nu^3\left[\prod_{j=1}^{3}\int_{-\infty}^{+\infty}{\rm d}x_j\, f_j\right]\delta\left(\sum_{j=1}^{3}x_j - x_\nu\right), \qquad (22)$$

$$S = \prod_{j=1}^{3}p_{{\rm F}j}m_j^*\,. \qquad (23)$$

The quantity A contains integrals over orientations of particle momenta ($j = 1$, 2, 3, and 4 corresponds to n, p, e and $\bar\nu_{\rm e}$, respectively); ${\rm d}\Omega_j$ is the solid angle element in the direction of $\mathbf{p}_j$. All vector lengths $\mathbf{p}_j$ in the delta-function must be set equal to the corresponding Fermi momenta. The quantity I, given by Eqn (22), includes integration over the dimensionless energies of the neutrino $x_\nu = p_\nu/T = \varepsilon_\nu/T$ and other particles $x_j = v_{{\rm F}j}(p - p_{{\rm F}j})/T$ [see Eqn (8)]; $f_j = [\exp(x_j)+1]^{-1}$ is the Fermi–Dirac distribution. For particles $j = 2$ and 3, we have transformed $[1 - f(x)] \to f(x)$ by replacing $x \to -x$. Finally, S contains products of the density states at the Fermi surfaces of n, p and e; m_j^* is an effective particle mass, with $m_{\rm e}^* = \mu_{\rm e}/c^2$. As shown, for instance, in Ref. [20], the quantity $\overline{|M|^2}$, summed over the spins of final particles and averaged over the spin of the initial neutron and over the directions of electron and neutrino momenta is $G_{\rm F}^2\cos^2\theta_{\rm C}\,(f_{\rm v}^2 + 3g_{\rm a}^2)$, where $G_{\rm F} = 1.436\times 10^{-49}$ erg cm^3 is the Fermi constant of weak interaction; $f_{\rm v} = 1$ and $g_{\rm a} = 1.26$ are, respectively, the vector and axial-vector constants for the reaction under study, and $\theta_{\rm C}$ is the Cabibbo angle ($\sin\theta_{\rm C} = 0.231$).

In the absence of superfluidity, the integrals A and I are standard (e.g., Ref. [1]): $A_0 = 32\pi^3/(p_{\rm F_n}p_{\rm F_p}p_{\rm F_e})$ and $I_0 = 457\pi^6/5040$. Thus, the neutrino emissivity of the direct Urca process in non-superfluid matter (in the standard physical units) is [20]:

$$Q_0^{(\rm D)} = \frac{457\pi}{10080}G_{\rm F}^2\cos^2\theta_{\rm C}(f_{\rm v}^2+3g_{\rm a}^2)\frac{m_{\rm n}^*m_{\rm p}^*m_{\rm e}^*}{\hbar^{10}c^3}(k_{\rm B}T)^6\Theta \approx 4.00\times10^{27}\left(\frac{n_{\rm e}}{n_0}\right)^{1/3}\frac{m_{\rm n}^*m_{\rm p}^*}{m_{\rm n}^2}T_9^6\Theta\ ({\rm erg\ cm^{-3}\ s^{-1}})\,. \qquad (24)$$

Here, as before, $n_0 = 0.16$ fm^{-3}.

If muons are available in dense matter, then the muon direct Urca process is allowed. The emissivity of this process is given by Eqn (24) with $m_{\rm e}^*$ replaced by m_μ^*. A similar formula is valid for the direct Urca processes involving hyperons. Notice that $f_{\rm v}$ and $g_{\rm a}$ can be renormalized under the action of in-medium effects. Exact calculation of these effects is complicated. Here and below, for certainty, we will use non-renormalized values. Notice also that the direct Urca process is affected by the strong magnetic field, $B \gtrsim 10^{16}$ G [126].

4.2 Direct Urca process in superfluid matter

The main contribution to neutrino generation in non-superfluid matter comes from nucleons with energies $|\varepsilon-\mu| \lesssim k_{\rm B}T$. The nucleon spectrum in superfluid matter contains an energy gap which suppresses the reaction. The essence of suppression is the same as in the case of suppression of heat capacity by strong superfluidity (Section 3.3). In contrast to the heat capacity, even a weak superfluidity usually suppresses the neutrino reactions (excluding the neutrino emission due to Cooper pairing of nucleons, Sections 2.2, 6.1).

The expression for the neutrino emissivity in the direct Urca process can be generalized to the case of superfluid matter by introducing the energy gap into the $\varepsilon(\mathbf{p}_j)$ dependence [see Eqn (6)] for nucleons. Let protons ($j=2$) suffer Cooper pairing of type A, while neutrons ($j=1$) suffer pairing of types A, B or C. In order to incorporate superfluidity in Eqn (22) it is sufficient to replace $x_j \to z_j$ [see Eqn (8)] and introduce averaging over orientations of $\mathbf{p}_1$. Then the emissivity can be written as

$$Q^{(\rm D)} = Q_0^{(\rm D)} R^{(\rm D)},\ R^{(\rm D)}(v_1,v_2) = \frac{I}{I_0}$$

$$= \int \frac{{\rm d}\Omega}{4\pi} J(y_1,y_2) = \int_0^{\pi/2} {\rm d}\vartheta \sin\vartheta\, J(y_1,y_2)\,, \qquad (25)$$

where $y_2 \equiv v_2$, y_1 is given by Eqn (10),

$$J(y_1,y_2) = \frac{1}{I_0}\int_0^{+\infty} {\rm d}x_\nu\, x_\nu^3 \int_{-\infty}^{+\infty} {\rm d}x_1 f(z_1)$$

$$\times \int_{-\infty}^{+\infty} {\rm d}x_2\, f(z_2) \int_{-\infty}^{+\infty} {\rm d}x_{\rm e}\, f(x_{\rm e}) \delta(x_\nu - z_1 - z_2 - x_{\rm e})\,, \qquad (26)$$

${\rm d}\Omega$ is the solid angle element along $\mathbf{p}_1$, ϑ is the angle between $\mathbf{p}_1$ and the quantization axis; $Q_0^{(\rm D)}$ is the emissivity (24) in non-superfluid matter; and $R^{(\rm D)}$ is the factor which describes the superfluid suppression of the reaction. One formally has $R^{(\rm D)}=1$ for normal nucleons, while $R^{(\rm D)}<1$ in the presence of superfluidity. The integrals (25) and (26) have been calculated in Refs [121, 125] for different combinations of neutron and proton superfluidities. The results are discussed below.

4.3 Superfluidity of neutrons or protons

Consideration of the cases of superfluid neutrons or protons is similar. For instance, let neutrons be superfluid. Then we can set $z_2 = x_2$ in Eqns (25) and (26), and $R^{(\rm D)}$ will depend on one argument $v_1 = v$ and on the superfluidity type. For $\tau = T/T_{\rm c} \geqslant 1$, as mentioned above, $R^{(\rm D)}=1$. For strong superfluidity ($\tau \ll 1$, $v \gg 1$) the neutrino emission is greatly suppressed ($R^{(\rm D)} \ll 1$). The asymptotes of $R^{(\rm D)}$ in the cases of strong superfluidity of types A, B and C read:

$$R_{\rm A}^{(\rm D)} = \frac{252}{457\pi^6}\sqrt{\frac{\pi}{2}}\, v^{5.5}\exp(-v) = \frac{0.0163}{\tau^{5.5}}\exp\left(-\frac{1.764}{\tau}\right),$$

$$R_{\rm B}^{(\rm D)} = \frac{126}{457\pi^5\sqrt{3}}\, v^5\exp(-v) = \frac{0.00123}{\tau^5}\exp\left(-\frac{1.188}{\tau}\right),$$

$$R_{\rm C}^{(\rm D)} = \frac{6029\pi^2}{5484 v^2} = 2.634\tau^2\,. \qquad (27)$$

The asymptotes of $R_{\rm A}^{(\rm D)}$ and $R_{\rm B}^{(\rm D)}$ are seen to be exponential while the asymptote of $R_{\rm C}^{(\rm D)}$ is power-law. The latter circumstance is associated with the disappearance of the gap at some ϑ. Comparing these with the results of Section 3.3, we see that these asymptotes are similar to the asymptotes of the nucleon heat capacity in the limit of strong superfluidity.

The asymptotes (27) and numerical values of the integrals (25) and (26) for intermediate v can be fitted by:

$$R_{\rm A}^{(\rm D)} = \left[0.2312 + \sqrt{(0.7688)^2 + (0.1438v)^2}\right]^{5.5}$$

$$\times \exp\left(3.427 - \sqrt{(3.427)^2 + v^2}\right),$$

$$R_{\rm B}^{(\rm D)} = \left[0.2546 + \sqrt{(0.7454)^2 + (0.1284v)^2}\right]^{5}$$

$$\times \exp\left(2.701 - \sqrt{(2.701)^2 + v^2}\right),$$

$$R_{\rm C}^{(\rm D)} = \frac{0.5 + (0.09226v)^2}{1 + (0.1821v)^2 + (0.16736v)^4}$$

$$+ \frac{1}{2}\exp\left(1 - \sqrt{1 + (0.4129v)^2}\right). \qquad (28)$$

Equations (28), with account for Eqns (11), enable one to calculate $R^{(\rm D)}$ for any τ. The results are presented in Fig. 6.

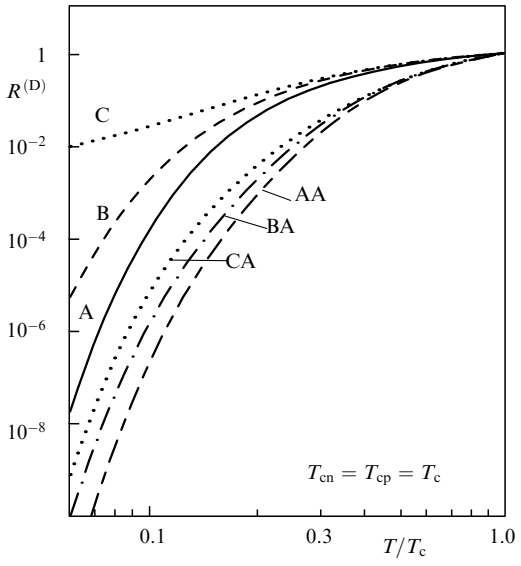

Figure 6. Superfluid reduction factors of the direct Urca process versus $\tau = T/T_{\rm c}$. The letters near the curves indicate the superfluidity type (see Table 1): A, B and C mean superfluidity of neutrons or protons, while AA, BA and CA mean superfluidity of neutrons and protons.

In simulations of NS cooling prior to publication of the above results [121, 125] one usually used (e.g., Ref. [5]) simplified factors of reduction of the direct Urca process by the superfluidity of type A or B. These factors were proposed in Ref. [123] from simple (and inadequate) consideration. Comparison of the accurate and simplified factors shows that the latter factors strongly overestimate the direct Urca reduction. For instance, for $T = 0.1\,T_{\rm c}$ the accurate factor $R_{\rm A}^{(\rm D)}$ appears to be about four orders of magnitude larger than

the simplified one, and the accurate factor $R_{\rm B}^{\rm (D)}$ is more than seven orders of magnitude larger. The difference has the same nature as the difference of accurate and simplified heat-capacity factors discussed in Section 3.3.

4.4 Superfluidity of neutrons and protons

Let us consider the reduction of the direct Urca process by the combined actions of superfluidities of neutrons and protons of types (AA), (BA) and (CA). In these cases, the reduction factor $R^{\rm (D)}$ depends on two arguments, $v_1 = v_{\rm n}$ and $v_2 = v_{\rm p}$.

Calculation of $R^{\rm (D)}$ in the presence of the neutron and proton superfluidities is complicated; let us consider the factor $R_{\rm AA}^{\rm (D)}$ as an example. According to Eqns (10) and (25), for the singlet-state pairing $R_{\rm AA}^{\rm (D)}(v_1, v_2) = J(v_1, v_2) = J(v_2, v_1)$, where $y_1 = v_1$, $y_2 = v_2$. Clearly, $R_{\rm AA}^{\rm (D)}(0,0) = 1$. If both superfluidities are strong ($v_1 \gg 1$ and $v_2 \gg 1$) and $v_2 - v_1 \gg \sqrt{v_2}$, the asymptote of the reduction factor is:

$$R_{\rm AA}^{\rm (D)} = J(v_1, v_2) = \frac{1}{I_0}\left(\frac{\pi}{2} v_2\right)^{1/2} \exp(-v_2) K\,, \tag{29}$$

$$K = \frac{s}{120}(6v_2^4 + 83 v_2^2 v_1^2 + 16 v_1^4) - \frac{1}{8} v_2 v_1^2 (3v_1^2 + 4v_2^2) \ln\left(\frac{v_2 + s}{v_1}\right), \tag{30}$$

where $s = (v_2^2 - v_1^2)^{1/2}$. In the limit $v_1 \ll v_2$ Eqn (30) gives $K = v_2^5/20$, which corresponds to the asymptote (27) of $R_{\rm A}^{\rm (D)}$. In another limit $\sqrt{v_2} \ll v_2 - v_1 \ll v_2$ we obtain $K = (2/315) s^9/v_2^4$. The asymptote (30) fails in the range $|v_2 - v_1| \lesssim \sqrt{v_2}$. One can show [125] that $v_1 = v_2$ for $K \sim \sqrt{v_2}$.

Let us also present the fit expression which reproduces the asymptote (29) and numerical values of $R_{\rm AA}^{\rm (D)}$ calculated over a wide range of arguments ($(v_1^2 + v_2^2)^{1/2} \lesssim 50$):

$$R_{\rm AA}^{\rm (D)} = J(v_1, v_2) = \frac{u}{u + 0.9163} S + D\,. \tag{31}$$

In this case

$$S = \frac{1}{I_0}\left(K_0 + K_1 + 0.42232 K_2\right)\left(\frac{\pi}{2}\right)^{1/2} p_{\rm s}^{1/4} \exp(-\sqrt{p_{\rm e}}\,),$$

$$K_0 = \frac{\sqrt{p-q}}{120}(6p^2 + 83pq + 16q^2) - \sqrt{p}\;\frac{q}{8}(4p + 3q)\ln\left(\frac{\sqrt{p} + \sqrt{p-q}}{\sqrt{q}}\right),$$

$$K_1 = \frac{\pi^2\sqrt{p-q}}{6}(p + 2q) - \frac{\pi^2}{2} q\sqrt{p}\ln\left(\frac{\sqrt{p} + \sqrt{p-q}}{\sqrt{q}}\right),$$

$$K_2 = \frac{7\pi^4}{60}\sqrt{p-q},$$

$$2p = u + 12.421 + \sqrt{w^2 + 16.350u + 45.171}\,,$$

$$2q = u + 12.421 - \sqrt{w^2 + 16.350u + 45.171}\,,$$

$$2p_{\rm s} = u + \sqrt{w^2 + 5524.8u + 6.7737}\,,$$

$$2p_{\rm e} = u + 0.43847 + \sqrt{w^2 + 8.3680u + 491.32}\,,$$

$$D = 1.52(u_1 u_2)^{3/2}(u_1^2 + u_2^2)\exp(-u_1 - u_2)\,,$$

$$u_1 = 1.8091 + \sqrt{v_1^2 + (2.2476)^2}\,,$$

$$u_2 = 1.8091 + \sqrt{v_2^2 + (2.2476)^2}\,, \tag{32}$$

with $u = v_1^2 + v_2^2$ and $w = v_2^2 - v_1^2$. For $v_2 = 0$, the factor $R_{\rm AA}^{\rm (D)}(v_1, 0)$ agrees with the factor $R_{\rm A}^{\rm (D)}(v_1)$ given by Eqn (28).

Figure 7 shows lines of $R_{\rm AA}^{\rm (D)} = $ const versus $\tau_1 = T/T_{\rm c1}$ and $\tau_2 = T/T_{\rm c2}$. The lines exhibit superfluid reduction of the direct Urca for any T, $T_{\rm c1}$ and $T_{\rm c2}$. The behavior of $R_{\rm AA}^{\rm (D)}$ at $\tau_1^2 + \tau_2^2 \ll 1$ (both superfluidities are strong) is of special interest. In this case one can obtain an approximate relationship [19, 125]

$$R_{12}^{\rm (D)} \sim \min\left(R_1^{\rm (D)}, R_2^{\rm (D)}\right), \tag{33}$$

where $R_1^{\rm (D)}$ and $R_2^{\rm (D)}$ are the reduction factors for superfluidities of one type. According to (33), the factor $R_{12}^{\rm (D)}$ is mainly determined by a stronger superfluidity (1 or 2). The presence of the second, weaker superfluidity naturally reduces $R_{12}^{\rm (D)}$, but not to a great extent. This is confirmed by the asymptote (29). A transition from the regime in which $R_{12}^{\rm (D)} \sim R_1^{\rm (D)}$ to the regime in which $R_{12}^{\rm (D)} \sim R_2^{\rm (D)}$ takes place in the region $v_2 \sim v_1$, where the asymptote $R_{12}^{\rm (D)}$ requires special consideration.

Using Eqn (25), it is not difficult to evaluate $R^{\rm (D)}$ for the cases (BA) and (CA), in which the protons suffer singlet-state pairing while the neutrons suffer triplet-state pairing. The evaluation is reduced to a one-dimensional integration in Eqn (25) of the quantity $J(y_1, y_2)$, fitted by Eqns (31) and (32). The results of calculations of $R_{\rm BA}^{\rm (D)}$ and $R_{\rm CA}^{\rm (D)}$ for any T, $T_{\rm c1}$ and $T_{\rm c2}$ are shown in Fig. 7. The dependence of $R_{\rm BA}^{\rm (D)}$ and $R_{\rm CA}^{\rm (D)}$ on τ_1 and τ_2 is similar to the dependence of $R_{\rm AA}^{\rm (D)}$, shown in the same figure, but now $R^{\rm (D)}(\tau_1, \tau_2) \neq R^{\rm (D)}(\tau_2, \tau_1)$. The approximate expression (33) in these cases is valid as well as confirmed by the asymptotes [125]. Since the superfluidity of type C reduces the neutrino emission much more weakly than that of type A or B, the transition from one dominating superfluidity to the other in case (CA) for $v_1 \gg 1$ takes place at $v_2 \sim \ln v_1$. Moreover, for $v_1 \gtrsim v_2 \gg 1$ the factor $R_{\rm CA}^{\rm (D)}$ appears to be much larger than $R_{\rm AA}^{\rm (D)}$ or $R_{\rm BA}^{\rm (D)}$ (Fig. 6).

For not very strong superfluidities (BA) ($(v_1^2 + v_2^2)^{1/2} \lesssim 5$ or $[(1-\tau_2)/0.65]^4 + [(1-\tau_1)/0.76]^4 \lesssim 1$), the reduction factor is fitted by

$$R_{\rm BA}^{\rm (D)} = \frac{10^4 - 2.839 v_2^4 - 5.022 v_1^4}{10^4 + 757.0 v_2^2 + 1494 v_1^2 + 211.1 v_2^2 v_1^2 + 0.4832 v_2^4 v_1^4}\,. \tag{34}$$

In the case of not too strong superfluidities (CA) ($(v_1^2 + v_2^2)^{1/2} \lesssim 10$ or $[(1-\tau_2)/0.825]^6 + [(1-\tau_1)/0.8]^6 \lesssim 1$) $R_{\rm CA}^{\rm (D)}$ is fitted by the expression:

$$R_{\rm CA}^{\rm (D)} = 10^4 (10^4 + 793.9 v_2^2 + 457.3 v_1^2 + 66.07 v_2^2 v_1^2 + 2.093 v_1^4 + 0.3112 v_2^6 + 1.068 v_2^4 v_1^2 + 0.01536 v_2^4 v_1^4 + 0.006312 v_2^6 v_1^2)^{-1}\,. \tag{35}$$

If $v_1 = 0$ or $v_2 = 0$, the above fits agree with Eqns (28). The tables of $R_{\rm BA}^{\rm (D)}$ and $R_{\rm CA}^{\rm (D)}$, as well as the asymptotes of these factors in the limit of strong superfluidity are given in Ref. [125].

Before publication of the above results [121, 125], as far as we know, simulation of the enhanced NS cooling with account of the superfluidity of neutrons and protons was carried out in the only paper [127]. The authors assumed the simplified reduction factor $R_{12}^{\rm (D)} = R_1^{\rm (D)} R_2^{\rm (D)}$. The actual

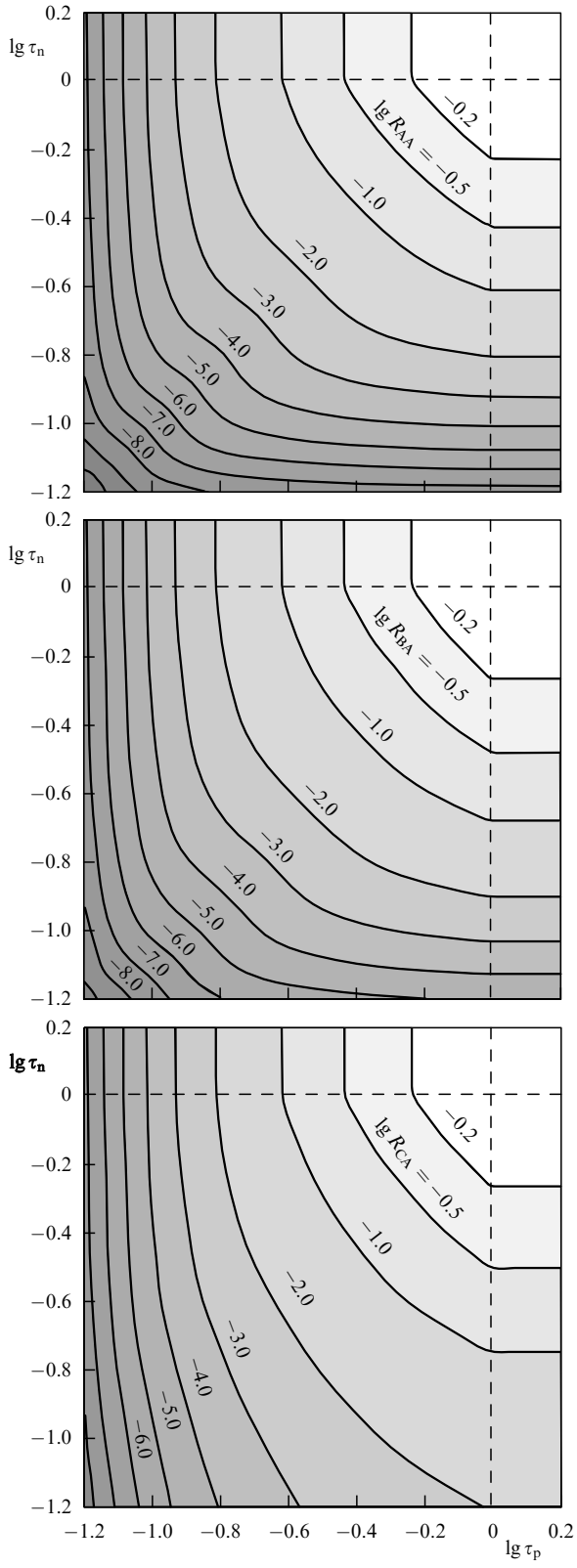

Figure 7. Lines of constant reduction factors $R^{(D)}$ for the direct Urca in the presence of neutron and proton superfluidities (AA), (BA) and (CA). The curves are labeled by the values lg $R^{(D)}$. In the region $\tau_n \geqslant 1$ and $\tau_p \geqslant 1$ neutrons and protons are normal and $R^{(D)} = 1$. In the region $\tau_n < 1$, $\tau_p \geqslant 1$, where only neutrons are superfluid, and in the region $\tau_n \geqslant 1$, $\tau_p < 1$, where only protons are superfluid, $R^{(D)}$ depends on the only parameter (Section 4.3). In the region $\tau_n < 1$, $\tau_p < 1$ both, neutron and protons, are superfluid at once.

factor, Eqn (33), is quite different, i.e., the simplified factor strongly overestimates the effect of superfluidity of neutrons and protons.

In 1992 Prakash et al. [20] showed that practically all equations of state in the inner NS cores, which predict appearance of hyperons, open the direct Urca reactions involving hyperons:

$$B_1 \to B_2 + l + \bar{\nu}\,, \qquad B_2 + l \to B_1 + \nu\,, \tag{36}$$

where B_1 and B_2 are baryons (nucleons, Λ-, Σ- or Ξ-hyperons, Δ^--resonance), and l is a lepton (electron or μ-meson). The hyperonic processes (36) do not conserve strangeness; the neutrino emissivities in these processes are somewhat lower than in the nucleon direct Urca process (4). The emissivities are given by expressions similar to Eqn (24), but with different numerical coefficients [20].

Hyperons, like nucleons, may be in a superfluid state [116]. Their superfluidity is most likely to be of singlet-state type due to their relatively small number density. The reduction factors for the direct Urca processes involving hyperons are similar to those for the nucleon direct Urca.

5. Modified Urca process and neutrino bremsstrahlung due to nucleon–nucleon scattering

5.1 Two branches of the modified Urca process

In this section we will analyze the *standard* neutrino energy loss rates in the processes (1) – (3) (Section 2.2). In the absence of superfluidity, these processes were studied by Bahcall and Wolf [22, 23], Flowers et al. [128], Friman and Maxwell [12], as well as by Maxwell [129]. The latter author also considered the processes involving hyperons. The most detailed article seems to be that by Friman and Maxwell [12], where, however, the proton branch of the modified Urca-process was neglected. The proton branch was analyzed and the superfluid reduction factors for the standard process were calculated in Ref. [130]. Below we will mainly follow the consideration of this paper.

The main standard neutrino energy loss mechanism in non-superfluid matter is the modified Urca process. It will be labeled by superscripts (MN), where N = n indicates the neutron branch (1) of the process, while N = p indicates the proton branch (2). Both branches consist of direct and inverse reactions and are described by similar Feynman diagrams. If beta-equilibrium is established, the rates of the direct and inverse branches are equal; it is sufficient to calculate the rate of any reaction and double the result. The general expressions for the neutron and proton branches of the modified Urca process can be written as ($\hbar = c = k_B = 1$):

$$Q^{(MN)} = 2\int\left[\prod_{j=1}^{4}\frac{d^3p_j}{(2\pi)^3}\right]\frac{d^3p_e}{2\varepsilon_e(2\pi)^3}\frac{d^3p_\nu}{2\varepsilon_\nu(2\pi)^3}\varepsilon_\nu(2\pi)^4$$
$$\times\,\delta(E_f - E_i)\delta(\mathbf{P}_f - \mathbf{P}_i)\frac{\mathcal{L}}{2}\sum_{\text{spins}}|M|^2\,, \tag{37}$$

where $\mathbf{p}_j$ is the nucleon momentum ($j = 1, 2, 3, 4$), $\mathbf{p}_e$ and ε_e are, respectively, the electron momentum and energy; while $\mathbf{p}_\nu$ and ε_ν are, respectively, the neutrino momentum and energy. The delta function $\delta(E_f - E_i)$ describes energy conservation, and $\delta(\mathbf{P}_f - \mathbf{P}_i)$ describes momentum conservation; the subscripts i and f refer to the initial and final particle states, respectively. Furthermore, $\mathcal{L}$ means the product of the

Fermi–Dirac functions or corresponding blocking factors for nucleons and electron; $|M|^2$ is the squared reaction amplitude, the sum is over all particle spins. The factor 2 in the denominator before the summation sign is introduced to avoid double counting of the same collisions of identical particles.

Introducing dimensionless variables, one can write [130] the emissivity (37) in a form similar to the direct Urca emissivity [see Eqn (20) and explanations afterwards]:

$$Q^{(\mathrm{MN})} = \frac{1}{4(2\pi)^{14}}\, T^8 AIS \sum_{\text{spins}} |M|^2 , \tag{38}$$

$$A = 4\pi \left[\prod_{j=1}^{5} \int \mathrm{d}\Omega_j\right] \delta\left(\sum_{j=1}^{5} \mathbf{p}_j\right) , \tag{39}$$

$$I = \int_0^\infty \mathrm{d}x_\nu\, x_\nu^3 \left[\prod_{j=1}^{5} \int_{-\infty}^{+\infty} \mathrm{d}x_j\, f_j\right] \delta\left(\sum_{j=1}^{5} x_j - x_\nu\right) , \tag{40}$$

$$S = \prod_{j=1}^{5} p_{\mathrm{F}_j}\, m_j^* . \tag{41}$$

The quantity A contains integrals over orientations of particle momenta ($j = 5$ corresponds to electron); all lengths of the momenta $\mathbf{p}_j$ of nucleons and electron in the delta function should be set equal to the Fermi momenta. The typical neutrino momentum $p_\nu \sim T$ is much smaller than the momenta p_F of other particles. Thus, it can be neglected in momentum conservation; the integration over orientations of the neutrino momentum in A immediately yields 4π. The quantity I, given by Eqn (40), includes integrals over dimensionless energies of neutrinos $x_\nu = p_\nu/T = \varepsilon_\nu/T$ and other particles $x_j = v_{\mathrm{F}_j}(p - p_{\mathrm{F}_j})/T$ [see Eqn (8)]; $f_j = [\exp(x_j) + 1]^{-1}$. Finally, the quantity S is the product of density of states of the particle species $1 \leqslant j \leqslant 5$ (with effective masses m_j^*) at the Fermi surfaces.

Owing to the similarity of the Feynman diagrams for the neutron and proton branches of the modified Urca process, (1) and (2), the reaction amplitudes M and phase integrals I are practically the same. The reactions differ by the products of the density of states S and by the angular integrals A.

In non-superfluid matter, one has $I = I_0 = 1151\,3\,\pi^8/120960$ (see, e.g., Ref. [1]). The amplitude M for the neutron branch of the modified Urca process was calculated by Friman and Maxwell [12] using the Weinberg–Salam–Glashaw theory of electroweak interaction. The long-range (small momentum transfer) part of the nucleon–nucleon interaction was described in the one-pion-exchange approach, while the short-range (large momentum transfer) part was described in the frame of the Landau Fermi-liquid theory (e.g., Refs [14]). The squared amplitude $|M|^2$ summed over spin states is given by Eqn (39) of Ref. [12].

The angular integrals (39) for processes (1) and (2) differ due to the difference of neutron and proton Fermi momenta (Section 2.1). The proton reaction branch involves three protons with a rather small Fermi momentum and the only neutron with a larger momentum, while the neutron branch involves three neutrons with a large momentum and the only proton with a small momentum. Direct calculation of the angular integrals for these processes in the absence of superfluidity gives [1, 130]

$$A_{\mathrm{n}0} = \frac{2\pi(4\pi)^4}{p_{\mathrm{F_n}}^3}, \quad A_{\mathrm{p}0} = \frac{2\pi(4\pi)^4}{p_{\mathrm{F_p}}^2 p_{\mathrm{F_n}}} \left(1 - \frac{p_{\mathrm{F_e}}}{4p_{\mathrm{F_p}}}\right) \Theta , \tag{42}$$

where $\Theta = 1$ if the proton branch is allowed by momentum conservation, and $\Theta = 0$ otherwise. Let us recall that in the outer NS core the Fermi momenta $p_{\mathrm{F_e}}$ and $p_{\mathrm{F_p}}$ are much smaller than $p_{\mathrm{F_n}}$ (Section 2.1). Thus $\Theta = 1$ for $p_{\mathrm{F_n}} < 3p_{\mathrm{F_p}} + p_{\mathrm{F_e}}$. Notice that the expression for $A_{\mathrm{n}0}$ is obtained from Eqn (39) in the case $p_{\mathrm{F_n}} > p_{\mathrm{F_e}} + p_{\mathrm{F_p}}$. In the opposite case of $p_{\mathrm{F_n}} \leqslant p_{\mathrm{F_e}} + p_{\mathrm{F_p}}$, $A_{\mathrm{n}0}$ is given by Eqn (13) of Ref. [130] but in this case the direct Urca process dominates and the modified Urca processes are insignificant.

Using the above expressions for I_0 and $A_{\mathrm{n}0}$, Friman and Maxwell [12] calculated the neutrino emissivity in the neutron branch of the modified Urca process (in the standard physical units):

$$Q_0^{(\mathrm{Mn})} = \frac{11513}{30240}\, \frac{G_\mathrm{F}^2 g_\mathrm{a}^2 m_\mathrm{n}^{*3} m_\mathrm{p}^*}{2\pi} \left(\frac{f^\pi}{m_\pi}\right)^4 \frac{p_{\mathrm{F_e}} (k_\mathrm{B} T)^8}{\hbar^{10} c^8}\, \alpha_\mathrm{n} \beta_\mathrm{n}$$

$$\approx 8.55 \times 10^{21} \left(\frac{m_\mathrm{n}^*}{m_\mathrm{n}}\right)^3 \left(\frac{m_\mathrm{p}^*}{m_\mathrm{p}}\right) \left(\frac{n_\mathrm{e}}{n_0}\right)^{1/3} T_9^8 \alpha_\mathrm{n} \beta_\mathrm{n}\ (\mathrm{erg\ cm^{-3}\ s^{-1}}) , \tag{43}$$

$g_\mathrm{a} = 1.26$ is the axial-vector constant of weak hadron current, $f^\pi \approx 1$ is the πN-interaction constant in the p-state in the one-pion-exchange approximation, and m_π is the pion mass ($\pi^\pm$). The factor α_n describes the momentum dependence of the squared reaction amplitude in the Born approximation, and β_n contains different corrections. According to Eqn (62) of Ref. [12], $\alpha_\mathrm{n} \approx 1.76 - 0.63\,(n_0/n_\mathrm{n})^{2/3}$, where n_n is the number density of neutrons. In the final Eqn (65c) of Ref. [12] for $Q_0^{(\mathrm{Mn})}$, the authors used the value $\alpha_\mathrm{n} = 1.13$, calculated for $\rho = \rho_0$, and set $\beta_\mathrm{n} = 0.68$ (to account for the correlation effects).

The expression for the neutrino emissivity in the proton reaction was derived in Ref. [130]

$$Q_0^{(\mathrm{Mp})} = \frac{11513}{30240}\, \frac{G_\mathrm{F}^2 g_\mathrm{a}^2 m_\mathrm{p}^{*3} m_\mathrm{n}^*}{2\pi} \left(\frac{f^\pi}{m_\pi}\right)^4 \frac{p_{\mathrm{F_e}} (k_\mathrm{B} T)^8}{\hbar^{10} c^8}$$

$$\times\, \alpha_\mathrm{p} \beta_\mathrm{p} \left(1 - \frac{p_{\mathrm{F_e}}}{4p_{\mathrm{F_p}}}\right) \Theta \approx 8.53 \times 10^{21} \left(\frac{m_\mathrm{p}^*}{m_\mathrm{p}}\right)^3 \left(\frac{m_\mathrm{n}^*}{m_\mathrm{n}}\right)$$

$$\times \left(\frac{n_\mathrm{e}}{n_0}\right)^{1/3} T_9^8 \alpha_\mathrm{p} \beta_\mathrm{p} \left(1 - \frac{p_{\mathrm{F_e}}}{4p_{\mathrm{F_p}}}\right) \Theta\ (\mathrm{erg\ cm^{-3}\,s^{-1}}) . \tag{44}$$

Taking into account all uncertainties concerned with the calculation of the reaction amplitude [12] we set $\alpha_\mathrm{p} = \alpha_\mathrm{n}$ and $\beta_\mathrm{p} = \beta_\mathrm{n}$. It is easy to see that the emissivities in the neutron (43) and proton (44) branches of the process are similar. The main difference of the proton branch is in its threshold character: the reaction is allowed for $p_{\mathrm{F_n}} < 3p_{\mathrm{F_p}} + p_{\mathrm{F_e}}$. In npe-matter, this inequality is equivalent to $p_{\mathrm{F_n}} < 4p_{\mathrm{F_e}}$, i.e., to $n_\mathrm{e} > n_\mathrm{n}/64$. The latter condition is realized almost everywhere in the NS core. It can be violated only for ultra-soft equations of state at $\rho \lesssim \rho_0$. For these equations of state, the proton branch can be forbidden in the outermost part of the NS core. Similar but much more stringent threshold conditions can be formulated for the direct Urca process (4) (Sections 2.2 and 4).

Comparing $Q_0^{(\mathrm{Mp})}$ and $Q_0^{(\mathrm{Mn})}$, we find: $Q_0^{(\mathrm{Mp})}/Q_0^{(\mathrm{Mn})} = (m_\mathrm{p}^*/m_\mathrm{n}^*)^2 [1 - p_{\mathrm{F_e}}/(4p_{\mathrm{F_p}})]$. For instance, at $m_\mathrm{n}^* = m_\mathrm{p}^*$ and $p_{\mathrm{F_e}} = p_{\mathrm{F_p}}$ we have $Q_0^{(\mathrm{Mp})} = 0.75\, Q_0^{(\mathrm{Mn})}$. Therefore the proton branch of the process is nearly as efficient as the neutron branch.

The potential efficiency of the proton branch was outlined by Itoh and Tsuneto [131] who, however, did not calculate

$Q_0^{(\mathrm{Mp})}$. Later the neutrino emissivity $Q_0^{(\mathrm{Mp})}$ was calculated by Maxwell [129] who found it negligibly small as compared to $Q_0^{(\mathrm{Mn})}$. This conclusion is erroneous due to several inaccuracies made in Ref. [129] (and analyzed in Ref. [130]). In particular, the author incorrectly neglected the electron momentum in momentum conservation law.

5.2 Modified Urca processes in superfluid matter

Nucleon superfluidity reduces the modified Urca processes (see Section 4.2). Let us analyze this reduction. We will adopt the traditional assumption (Section 3.1) that the proton superfluidity is of type A, while the neutron superfluidity is of type B. Our results will also be valid for the neutron pairing of type A (at $\rho \lesssim \rho_0$), as will be mentioned later. Reduction of the modified Urca process by the neutron pairing of type C has not been considered so far.

Superfluidity affects the nucleon dispersion relations under the integral (37) in accordance with Eqn (6). The neutrino emissivity of the neutron and proton branches of the process can be presented in the form

$$Q^{(\mathrm{Mn})} = Q_0^{(\mathrm{Mn})} R^{(\mathrm{Mn})}, \quad Q^{(\mathrm{Mp})} = Q_0^{(\mathrm{Mp})} R^{(\mathrm{Mp})}, \tag{45}$$

where $Q_0^{(\mathrm{Mn})}$ and $Q_0^{(\mathrm{Mp})}$ are the emissivities (43) and (44) in non-superfluid matter, while $R^{(\mathrm{Mn})}$ and $R^{(\mathrm{Mp})}$ are the factors, which describe superfluid reduction of the reactions ($R^{(\mathrm{MN})} \leqslant 1$). Generally, $R^{(\mathrm{MN})} = J_{\mathrm{N}}/(I_{\mathrm{N}0} A_{\mathrm{N}0})$, where

$$J_{\mathrm{N}} = 4\pi \int \prod_{j=1}^{5} \mathrm{d}\Omega_j \int_0^{\infty} \mathrm{d}x_\nu \, x_\nu^3 \left[\prod_{j=1}^{5} \int_{-\infty}^{+\infty} \mathrm{d}x_j \, f(z_j) \right] \times \delta\left(x_\nu - \sum_{j=1}^{5} z_j \right) \delta\left(\sum_{j=1}^{5} \mathbf{p}_j \right), \tag{46}$$

$f(z) = 1/(\exp z + 1)$ for nucleons ($j \leqslant 4$) is defined by Eqn (8); one should set $z_5 = x_5 = x_{\mathrm{e}}$ for an electron.

Equation (46) enables one to calculate the reduction factors $R^{(\mathrm{Mn})}$ and $R^{(\mathrm{Mp})}$ as a function of T, T_{cn} and T_{cp}. Below we present the results [130] for the proton superfluidity of type A and normal neutrons as well as for the neutron superfluidity of type B and normal protons. The behavior of $R^{(\mathrm{Mn})}$ and $R^{(\mathrm{Mp})}$ in the presence of the joint superfluidity of nucleons is described in Section 5.4.

5.2.1 Singlet-state proton pairing. Since the singlet-state gap is isotropic the angular and energy integrations in Eqn (46) are decomposed, and the angular integration remains the same as in non-superfluid matter.

Just as in the case of the direct Urca process, the reduction factors of the neutron and proton branches of the modified Urca process, $R_{\mathrm{pA}}^{(\mathrm{Mn})}$ and $R_{\mathrm{pA}}^{(\mathrm{Mp})}$, can be expressed in terms of the dimensionless energy gap $v_{\mathrm{p}} = v_{\mathrm{A}}$ [see Eqn (11); here and hereafter the subscripts in $R^{(\mathrm{MN})}$ indicate the superfluid particle species and superfluidity type]. Clearly, $R_{\mathrm{pA}}^{(\mathrm{Mn})} = 1$ and $R_{\mathrm{pA}}^{(\mathrm{Mp})} = 1$ for $T \geqslant T_{\mathrm{cp}}$ ($v_{\mathrm{A}} = 0$). In the case of strong superfluidity ($T \ll T_{\mathrm{cp}}$, $v_{\mathrm{A}} \to \infty$), the asymptotes of both factors are [130]

$$R_{\mathrm{pA}}^{(\mathrm{Mn})} = \frac{72\sqrt{2\pi}}{11513\pi^8} v_{\mathrm{A}}^{7.5} \exp(-v_{\mathrm{A}}) = \frac{1.166 \times 10^{-4}}{\tau_{\mathrm{p}}^{7.5}} \exp\left(-\frac{1.764}{\tau_{\mathrm{p}}} \right), \tag{47}$$

$$R_{\mathrm{pA}}^{(\mathrm{Mp})} = \frac{120960}{11513\pi^8} \xi v_{\mathrm{A}}^7 \exp(-2v_{\mathrm{A}}) = \frac{0.00764}{\tau_{\mathrm{p}}^7} \exp\left(-\frac{3.528}{\tau_{\mathrm{p}}} \right), \tag{48}$$

$$\xi = \frac{3\pi}{320} \left[339\sqrt{3} - \frac{885}{2} \ln(\sqrt{3}+2) \right] \approx 0.130, \tag{49}$$

where $\tau_{\mathrm{p}} = T/T_{\mathrm{cp}}$.

Yakovlev and Levenfish [130] calculated $R_{\mathrm{pA}}^{(\mathrm{Mn})}$ and $R_{\mathrm{pA}}^{(\mathrm{Mp})}$ for intermediate v_{A} and fitted them by the analytic expressions, which also reproduced the asymptotes in the limit of $v \to \infty$ and obeyed the condition $R^{(\mathrm{MN})}(0) = 1$:

$$R_{\mathrm{pA}}^{(\mathrm{Mn})} = \frac{a^{7.5} + b^{5.5}}{2} \exp\left(3.4370 - \sqrt{(3.4370)^2 + v_{\mathrm{A}}^2} \right), \tag{50}$$

$$a = 0.1477 + \sqrt{(0.8523)^2 + (0.1175 v_{\mathrm{A}})^2},$$

$$b = 0.1477 + \sqrt{(0.8523)^2 + (0.1297 v_{\mathrm{A}})^2};$$

$$R_{\mathrm{pA}}^{(\mathrm{Mp})} = \left[0.2414 + \sqrt{(0.7586)^2 + (0.1318 v_{\mathrm{A}})^2} \right]^7 \times \exp\left(5.339 - \sqrt{(5.339)^2 + (2v_{\mathrm{A}})^2} \right). \tag{51}$$

Equations (50) and (51), together with Eqns (11), fully determine the dependence of $R_{\mathrm{pA}}^{(\mathrm{Mn})}$ and $R_{\mathrm{pA}}^{(\mathrm{Mp})}$ on $\tau_{\mathrm{p}} = T/T_{\mathrm{cp}}$.

The above results [130] are also valid for the singlet-state superfluidity of neutrons. Evidently, in that case one should set $v_{\mathrm{n}} = v_{\mathrm{A}}$ and

$$R_{\mathrm{nA}}^{(\mathrm{Mp})}(v_{\mathrm{A}}) = R_{\mathrm{pA}}^{(\mathrm{Mn})}(v_{\mathrm{A}}), \quad R_{\mathrm{nA}}^{(\mathrm{Mn})}(v_{\mathrm{A}}) = R_{\mathrm{pA}}^{(\mathrm{Mp})}(v_{\mathrm{A}}). \tag{52}$$

Then Eqn (50) describes reduction of the proton branch of the process and Eqn (51) describes reduction of the neutron branch.

Wolf [76] (Fig. 2 of his article) as well as Itoh and Tsuneto [131] were the first who considered the reduction factor $R_{\mathrm{nA}}^{(\mathrm{Mn})}$ of the neutron branch of the modified Urca process by the singlet-state neutron superfluidity; this factor is analogous to the factor $R_{\mathrm{pA}}^{(\mathrm{Mp})}$. Notice that the latter authors analyzed only the asymptote (48). In both articles the same asymptote (48) was obtained but with different numerical factors ξ. Wolf [76] got $\xi = 0.123$, while Itoh and Tsuneto [131] obtained $\xi = \pi/15 \approx 0.209$. Recently $R_{\mathrm{nA}}^{(\mathrm{Mn})}$ has been calculated independently in Ref. [132] under the artificial assumption that the superfluid gap is temperature independent. These results are described by the factor $R_{\mathrm{nA}}^{(\mathrm{Mn})}(v_{\mathrm{A}})$ presented above with $v_{\mathrm{A}} = 1.764/\tau$.

5.2.2 Triplet-state neutron pairing. In this case the neutron gap is anisotropic. The proton branch of the modified Urca process is analyzed easily since only one superfluid particle is involved. The expression for the reduction factor $R_{\mathrm{nB}}^{(\mathrm{Mp})}$ reduces to a one-dimensional integral over the angle ϑ_{n} (between neutron momentum and quantization axis) of the factor $R_{\mathrm{pA}}^{(\mathrm{Mn})}(v)$ fitted by expression (50). The argument v_{A} in the latter expression should be formally replaced by y_{B} in accordance with Eqn (10) (Section 3.2). It is evident that $R_{\mathrm{nB}}^{(\mathrm{Mp})}(v) = 1$ for $v = v_{\mathrm{B}} = 0$. In the limit $v_{\mathrm{B}} \to \infty$ one can use the asymptote (47) in the integrand. Then for $T \ll T_{\mathrm{cn}}$ ($v_{\mathrm{B}} \gg 1$) according to Ref. [130]

$$R_{\rm nB}^{\rm (Mp)} = \frac{72}{11513\pi^7\sqrt{3}} v_{\rm B}^7 \exp(-v_{\rm B})$$

$$= \frac{3.99\times10^{-6}}{\tau_{\rm n}^7}\exp\left(-\frac{1.188}{\tau_{\rm n}}\right), \qquad (53)$$

where $\tau_{\rm n} = T/T_{\rm cn}$. In Ref. [130] $R_{\rm nB}^{\rm (Mp)}$ was calculated for intermediate values of $v_{\rm B}$ and the results were fitted by the analytic expression:

$$R_{\rm nB}^{\rm (Mp)} = \frac{a^7+b^5}{2}\exp\left(2.398-\sqrt{(2.398)^2+v_{\rm B}^2}\right),$$

$$a = 0.1612+\sqrt{(0.8388)^2+(0.1117v_{\rm B})^2},$$

$$b = 0.1612+\sqrt{(0.8388)^2+(0.1274v_{\rm B})^2}. \qquad (54)$$

Exact calculation of the reduction factor $R_{\rm nB}^{\rm (Mn)}$ of the neutron branch of the modified Urca process by the triplet-state neutron superfluidity for intermediate values of $v_{\rm B}$ is complicated; an approximate expression will be given in Section 5.4. Here we present only the asymptote of $R_{\rm nB}^{\rm (Mn)}$ in the limit $\tau_{\rm n} \ll 1$ [130]

$$R_{\rm nB}^{\rm (Mn)} = \frac{120960}{11513\pi^8}\,\frac{2}{3\sqrt{3}}\,\xi v_{\rm B}^6\exp(-2v_{\rm B})$$

$$= \frac{1.56\times10^{-4}}{\tau_{\rm n}^6}\exp\left(-\frac{2.376}{\tau_{\rm n}}\right). \qquad (55)$$

In this case, as for the proton reaction involving superfluid protons (48), the effect of superfluidity appears to be very strong: the exponent argument in $R_{\rm nB}^{\rm (Mn)}$ contains the doubled gap (three neutrons which participate in the reaction belong to superfluid component of matter).

The dependence of the reduction factors $R_{\rm pA}^{\rm (Mn)}$, $R_{\rm pA}^{\rm (Mp)}$, $R_{\rm nB}^{\rm (Mp)}$, and $R_{\rm nB}^{\rm (Mn)}$ on the dimensionless temperature τ and dimensionless gap parameter v is plotted in Figs 8 and 9. For comparison, we also present the reduction factors of the direct Urca process, $R_{\rm A}^{\rm (D)}$ and $R_{\rm B}^{\rm (D)}$. Let us mention that in the case of the strong neutron superfluidity ($T \ll T_{\rm cn}$) and normal protons the proton branch of the modified Urca process becomes much more efficient than the neutron branch. However in this case the main neutrino emission comes from the neutrino bremsstrahlung due to pp-scattering, which is not affected by the neutron superfluidity.

5.3 Neutrino bremsstrahlung due to nucleon–nucleon scattering in superfluid matter

Let us consider the effect of superfluidity on generation of neutrino pairs in nn-, np- and pp-scattering (3); these processes are often referred to as *neutrino nucleon–nucleon bremsstrahlung*. In non-superfluid matter, the neutrino bremsstrahlung is about two orders of magnitude less efficient than the modified Urca process. Corresponding neutrino emissivities (in the standard physical units) are [12, 130]

$$Q_0^{\rm (nn)} = \frac{41}{14175}\,\frac{G_{\rm F}^2 g_{\rm a}^2 m_{\rm n}^{*4}}{2\pi\hbar^{10}c^8}\left(\frac{f^\pi}{m_\pi}\right)^4 p_{\rm Fn}\alpha_{\rm nn}\beta_{\rm nn}(k_{\rm B}T)^8\mathcal{N}_\nu$$

$$\approx 7.4\times10^{19}\left(\frac{m_{\rm n}^*}{m_{\rm n}}\right)^4\left(\frac{n_{\rm n}}{n_0}\right)^{1/3}\alpha_{\rm nn}\beta_{\rm nn}\mathcal{N}_\nu T_9^8\ ({\rm erg\,cm^{-3}\,s^{-1}}), \qquad (56)$$

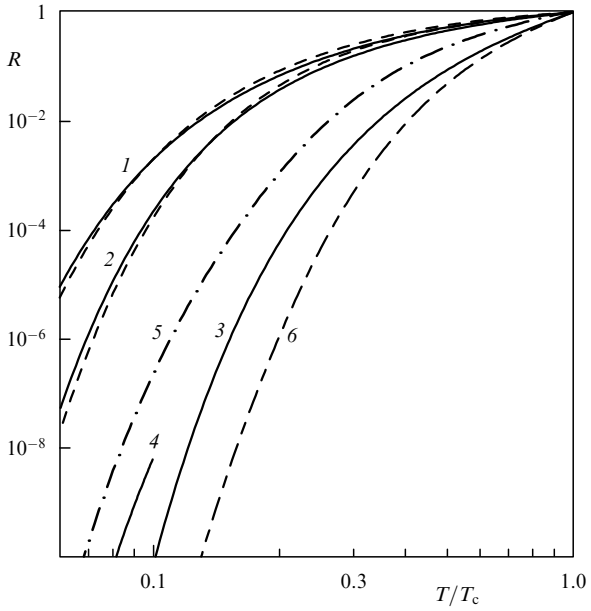

Figure 8. Reduction factors of various neutrino emission processes by superfluidity of neutrons or protons versus $T/T_{\rm c}$. Curves *1* show the reduction of the p-branch of the modified Urca process (solid line) and the direct Urca process (dashed line) by neutron superfluidity of type B. Curves *2* correspond to reduction of the n-branch of the modified Urca (solid line) and the direct Urca (dashed line) by proton superfluidity of type A. Dot-and-dash lines 5, 6 and the solid line 3 refer to the np, pp-scattering and p-branch of the modified Urca processes, respectively, for the same superfluidity. Solid line 4 is the asymptote of the reduction factor for the n-branch of the modified Urca process due to n superfluidity of type B.

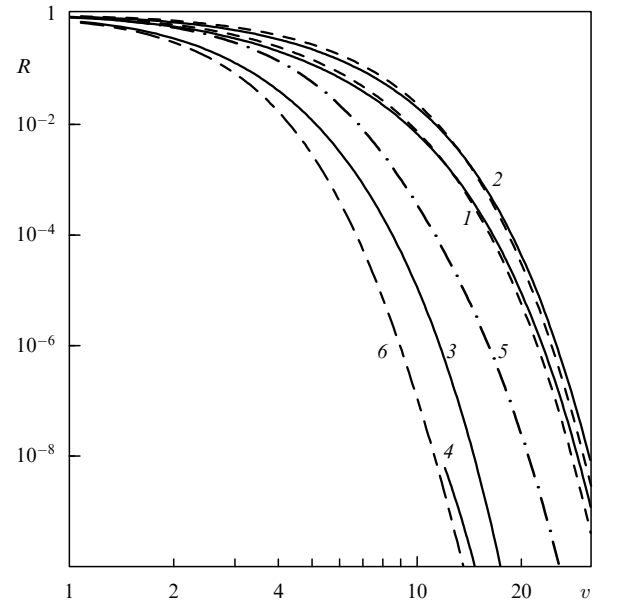

Figure 9. Same as in Fig. 8, but versus the dimensionless gap parameter.

$$Q_0^{\rm (np)} = \frac{82}{14175}\,\frac{G_{\rm F}^2 g_{\rm a}^2 m_{\rm n}^{*2} m_{\rm p}^{*2}}{2\pi\hbar^{10}c^8}\left(\frac{f^\pi}{m_\pi}\right)^4 p_{\rm Fe}\alpha_{\rm np}\beta_{\rm np}(k_{\rm B}T)^8\mathcal{N}_\nu$$

$$\approx 1.5\times10^{20}\left(\frac{m_{\rm n}^*}{m_{\rm n}}\,\frac{m_{\rm p}^*}{m_{\rm p}}\right)^2\left(\frac{n_{\rm e}}{n_0}\right)^{1/3}\alpha_{\rm np}\beta_{\rm np}\mathcal{N}_\nu T_9^8\ ({\rm erg\,cm^{-3}\,s^{-1}}), \qquad (57)$$

$$Q_0^{(\mathrm{pp})} = \frac{41}{14175}\,\frac{G_\mathrm{F}^2 g_\mathrm{a}^2 m_\mathrm{p}^{*4}}{2\pi\hbar^{10}c^8}\left(\frac{f^\pi}{m_\pi}\right)^4 p_{\mathrm{Fp}}\alpha_{\mathrm{pp}}\beta_{\mathrm{pp}}(k_\mathrm{B}T)^8\mathcal{N}_\nu$$

$$\approx 7.4\times 10^{19}\left(\frac{m_\mathrm{p}^*}{m_\mathrm{p}}\right)^4\left(\frac{n_\mathrm{p}}{n_0}\right)^{1/3}\alpha_{\mathrm{pp}}\beta_{\mathrm{pp}}\mathcal{N}_\nu T_9^8\ (\mathrm{erg\,cm^{-3}\,s^{-1}})\,, \tag{58}$$

where m_π is the π^0 mass, and $\mathcal{N}_\nu$ is the number of neutrino flavors. α_{NN} and β_{NN} have the same meaning as in Eqns (43) and (44); they are slowly varying functions of the nucleon Fermi momenta, i.e., density. Friman and Maxwell [12] assumed the factors α_{NN} to be equal to their values at $\rho=\rho_0$: $\alpha_{\mathrm{nn}}=0.59$, $\alpha_{\mathrm{np}}=1.06$, $\alpha_{\mathrm{pp}}=0.11$, and the correction factors (line $d=0.7$ fm in their Table 1) β_{NN} to be $\beta_{\mathrm{nn}}=0.56$, $\beta_{\mathrm{np}}=0.66$. They did not calculate β_{pp}. The presented values of β_{nn} and β_{np} indicate that it is reasonable to set $\beta_{\mathrm{pp}}\approx 0.7$. Hereafter we will use $\mathcal{N}_\nu=3$ in Eqns (56)–(58) while Friman and Maxwell [12] took into account two neutrino flavors.

In analogy with the Urca processes let us introduce the factors $R^{(\mathrm{NN})}$, which describe superfluid reduction of the neutrino bremsstrahlung due to NN scattering:

$$Q^{(\mathrm{NN})} = Q_0^{(\mathrm{NN})} R^{(\mathrm{NN})}\,. \tag{59}$$

Consider a singlet-state pairing A of neutrons or protons. Then the modification of the dispersion relation by superfluidity affects only the phase integral. For non-superfluid matter, the latter integral is given by Eqn (46) in Ref. [12] [cf. with Eqn (40)]:

$$I_{\mathrm{NN}}^{(0)} = \int_0^\infty \mathrm{d}x_\nu\, x_\nu^4\left[\prod_{j=1}^4\int_{-\infty}^{+\infty}\mathrm{d}x_j\, f(x_j)\right] \times\delta\left(\sum_{j=1}^4 x_j - x_\nu\right) = \frac{164\pi^8}{945}\,, \tag{60}$$

where in this case $x_\nu=\varepsilon_\nu/T$ determines the total energy ε_ν of a neutrino pair. Accordingly the reduction factors take the form:

$$R^{(\mathrm{NN})} = \frac{945}{164\pi^8}\int_0^\infty \mathrm{d}x_\nu\, x_\nu^4\left[\prod_{j=1}^4\int_{-\infty}^{+\infty}\mathrm{d}x_j\, f(z_j)\right]\delta\left(\sum_{j=1}^4 z_j - x_\nu\right), \tag{61}$$

where the dimensionless quantity z_j is defined in Eqn (8). It is clear that $R^{(\mathrm{NN})}=1$ for $\tau\geqslant 1$.

In the case of singlet-state proton pairing the reduction factors for the np and pp processes, $R_{\mathrm{pA}}^{(\mathrm{np})}$ and $R_{\mathrm{pA}}^{(\mathrm{pp})}$, are reduced to two dimensional integrals which can be calculated numerically [130]. In the limit of strong superfluidity ($\tau_\mathrm{p}\ll 1$, $v_\mathrm{A}\to\infty$) the asymptotes of these factors are:

$$R_{\mathrm{pA}}^{(\mathrm{np})} = \frac{945}{164\pi^8}\,\xi_1 v_\mathrm{A}\exp(-v_\mathrm{A}) = \frac{0.910}{\tau_\mathrm{p}}\exp\left(-\frac{1.764}{\tau_\mathrm{p}}\right), \tag{62}$$

$$R_{\mathrm{pA}}^{(\mathrm{pp})} = \frac{8505}{41\pi^6}\,v_\mathrm{A}^2\exp(-2v_\mathrm{A}) = \frac{0.671}{\tau_\mathrm{p}^2}\exp\left(-\frac{3.528}{\tau_\mathrm{p}}\right), \tag{63}$$

where $\xi_1\approx 849$. The asymptotes (62) and (63), as well as the numerical values of $R_{\mathrm{pA}}^{(\mathrm{np})}$ and $R_{\mathrm{pA}}^{(\mathrm{pp})}$ calculated for intermediate values of v_A can be fitted by the expressions:

$$R_{\mathrm{pA}}^{(\mathrm{np})} = \frac{1}{2.732}\left[a\exp\left(1.306-\sqrt{(1.306)^2+v_\mathrm{A}^2}\right) + 1.732\,b^7\exp\left(3.303-\sqrt{(3.303)^2+4v_\mathrm{A}^2}\right)\right],$$

$$a = 0.9982+\sqrt{(0.0018)^2+(0.3815v_\mathrm{A})^2}\,,$$

$$b = 0.3949+\sqrt{(0.6051)^2+(0.2666v_\mathrm{A})^2}\,; \tag{64}$$

$$R_{\mathrm{pA}}^{(\mathrm{pp})} = \frac{1}{2}\left[c^2\exp\left(4.228-\sqrt{(4.228)^2+(2v_\mathrm{A})^2}\right) + d^{7.5}\exp\left(7.762-\sqrt{(7.762)^2+(3v_\mathrm{A})^2}\right)\right],$$

$$c = 0.1747+\sqrt{(0.8253)^2+(0.07933v_\mathrm{A})^2}\,,$$

$$d = 0.7333+\sqrt{(0.2667)^2+(0.1678v_\mathrm{A})^2}\,. \tag{65}$$

For singlet-state neutron pairing, we evidently have

$$R_{\mathrm{nA}}^{(\mathrm{np})}(v_\mathrm{A}) = R_{\mathrm{pA}}^{(\mathrm{np})}(v_\mathrm{A}),\ R_{\mathrm{nA}}^{(\mathrm{nn})}(v_\mathrm{A}) = R_{\mathrm{pA}}^{(\mathrm{pp})}(v_\mathrm{A})\,. \tag{66}$$

The reduction factors considered above are shown in Fig. 8 versus T/T_c and in Fig. 9 versus dimensionless gap parameter v.

Summarizing the results of Sections 5.2 and 5.3 we note that the exponent argument in the asymptote of a reduction factor contains a single gap if one or two reacting particles belong to the superfluid component of matter. By the number of reacting particles we mean the total number of particles (in the initial and final states of a bremsstrahlung process, in the initial and final state of direct or inverse reaction of an Urca process) belonging to the superfluid component. The gap in the exponent argument is doubled if three or four superfluid particles are involved, etc. As seen from Fig. 9, the factor $R_{\mathrm{pA}}^{(\mathrm{np})}$ (two superfluid particles) falls with increasing superfluidity strength (with increasing v) much more rapidly than the factors $R_{\mathrm{pA}}^{(\mathrm{Mn})}$ or $R_{\mathrm{nB}}^{(\mathrm{Mp})}$ (one superfluid particle). Accordingly, $R_{\mathrm{pA}}^{(\mathrm{pp})}$ (four superfluid particles) falls faster than $R_{\mathrm{pA}}^{(\mathrm{Mp})}$ (three superfluid particles). Let us stress that we are discussing the neutrino reactions considered in Sections 4 and 5. The formulated rule is invalid for neutrino emission due to Cooper pairing of nucleons (Section 6.1).

5.4 Neutrino reactions in the presence of neutron and proton superfluidity

If neutrons and protons are superfluid simultaneously, calculations of multi-dimensional integrals (46) and (61), which determine the reduction of the standard neutrino reactions, become very complicated. However, if a very high accuracy is not required, one can avoid calculation by noticing that the reduction factors for the processes involving one superfluid particle ($R_\mathrm{A}^{(\mathrm{D})}$, $R_{\mathrm{pA}}^{(\mathrm{Mn})}$, $R_\mathrm{B}^{(\mathrm{D})}$ and $R_{\mathrm{nB}}^{(\mathrm{Mp})}$) are close to one another as functions of the dimensionless parameter v (Fig. 9). This enabled Levenfish and Yakovlev [133] to formulate approximate *similarity criteria* for different reduction factors. Using these criteria we constructed the approximate reduction factors for the proton and neutron branches of the modified Urca process in the presence of neutron and

proton superfluidity:

$$R_{\rm BA}^{\rm (Mp)}(v_{\rm n},v_{\rm p}) \approx \frac{R_{\rm BA}^{\rm (D)}(v_{\rm n},2v_{\rm p})}{R_{\rm B}^{\rm (D)}(v_{\rm n})}\,R_{\rm nB}^{\rm (Mp)}(v_{\rm n}), \tag{67}$$

$$R_{\rm BA}^{\rm (Mn)}(v_{\rm n},v_{\rm p}) \approx \frac{R_{\rm BA}^{\rm (D)}(2v_{\rm n},v_{\rm p})}{R_{\rm A}^{\rm (D)}(v_{\rm p})}\,R_{\rm pA}^{\rm (Mn)}(v_{\rm p})\,. \tag{68}$$

We expect that these factors, as functions of the corresponding parameters v (corrected due to the number of superfluid particles) do not differ strongly from the reduction factor $R_{\rm BA}^{\rm (D)}(v_{\rm n},v_{\rm p})$ for the direct Urca process. If the protons are normal ($v_{\rm p}=0$), then the expression for $R_{\rm BA}^{\rm (Mp)}(v_{\rm p},v_{\rm n})$ becomes exact; if the neutrons are normal ($v_{\rm n}=0$), the factor $R_{\rm BA}^{\rm (Mn)}(v_{\rm n},v_{\rm p})$ is exact. In addition, the approximate factors satisfy a relationship analogous to Eqn (33).

One can also expect similarity of the reduction factors for other neutrino reactions. For instance, the reduction of the neutron branch of the modified Urca process, $R_{\rm nB}^{\rm (Mn)}$, by a moderate neutron superfluidity ($v \lesssim 10$) should not deviate strongly from the reduction of the proton branch of the modified Urca process, $R_{\rm pA}^{\rm (Mp)}$, by the proton superfluidity:

$$R_{\rm nB}^{\rm (Mn)} \approx R_{\rm pA}^{\rm (Mp)}(v_{\rm n})\,. \tag{69}$$

The approximate reduction factor $R_{\rm nB}^{\rm (nn)}$ for the nn scattering in the presence of neutron superfluidity and the approximate reduction factor $R_{\rm BA}^{\rm (np)}$ of the np scattering by the neutron and proton superfluidities can be written as

$$R_{\rm nB}^{\rm (nn)} \approx R_{\rm pA}^{\rm (pp)}(v_{\rm n})\,, \tag{70}$$

$$R_{\rm BA}^{\rm (np)} \approx \frac{R_{\rm BA}^{\rm (D)}(v_{\rm n},v_{\rm p})}{R_{\rm A}^{\rm (D)}(v_{\rm p})}\,R_{\rm pA}^{\rm (np)}(v_{\rm p})\,. \tag{71}$$

In the absence of the neutron superfluidity, Eqn (71) becomes exact.

The modified Urca and neutrino bremsstrahlung processes can involve hyperons. After minor modifications, the above reduction factors can be valid for these reactions as well.

6. Neutrino emission due to Cooper pairing of nucleons

6.1 Neutrino emissivity produced by nucleon pairing

In contrast to the neutrino emission processes considered in Sections 4 and 5, this process is allowed only in the presence of superfluidity (Section 2.2): the superfluidity distorts the nucleon dispersion relation near the Fermi surface and opens the reaction (5). Actually the process consists in the emission of a neutrino pair by a nucleon whose dispersion relation contains an energy gap; however, in theoretical studies, it is convenient to use the formalism of quasi-particles and treat it [51] as the annihilation of two quasi-nucleons $\tilde{\rm N}$ into a neutrino pair:

$$\tilde{\rm N}+\tilde{\rm N} \to \nu+\bar{\nu}\,. \tag{72}$$

The reaction goes via weak neutral currents and produces neutrinos of all flavors. Following Ref. [56] we will outline the derivation of the neutrino emissivity due to singlet-state or triplet-state pairing of non-relativistic nucleons. The reaction is described by the Hamiltonian ($\hbar=c=k_{\rm B}=1$)

$$\hat{H} = -\frac{G_{\rm F}}{2\sqrt{2}}\,(c_{\rm v}J_0 l_0 - c_{\rm a}\mathbf{J}\mathbf{l})\,, \tag{73}$$

where $G_{\rm F}$ is the Fermi constant, and $c_{\rm v}$ and $c_{\rm a}$ are, respectively, the vector and axial-vector constants of neutral hadron currents. For neutron currents, we have (see, e.g., Ref. [134]) $c_{\rm v}=1$, $c_{\rm a}=g_{\rm a}=1.26$, while for proton currents $c_{\rm v}=4\sin^2\Theta_{\rm W}-1\approx -0.08$, $c_{\rm a}=-g_{\rm a}$, where $\Theta_{\rm W}$ is the Weinberg angle, $\sin^2\Theta_{\rm W}=0.23$. The strong difference of $c_{\rm v}$ for neutrons and protons comes from different quark structure of these particles. Furthermore,

$$J^\mu = \left(J^0,\mathbf{J}\right) = \left(\hat{\Psi}^+\hat{\Psi},\,\hat{\Psi}^+\boldsymbol{\sigma}\hat{\Psi}\right),\quad l^\mu = \overline{\psi}_{\rm v}\gamma^\mu(1+\gamma^5)\psi_{\rm v} \tag{74}$$

are 4-vectors of neutral currents of quasi-nucleons and neutrinos ($\mu=0,\ 1,\ 2,\ 3$) respectively; $\psi_{\rm v}$ is the neutrino wave function, upper bar denotes Dirac conjugate; γ^μ and γ^5 are Dirac gamma-matrices, $\boldsymbol{\sigma}$ is a vector Pauli matrix; $\hat{\Psi}$ is a second-quantized quasi-nucleon wave function. The function $\hat{\Psi}$ is derived using the Bogolyubov transformation. Its description for the singlet-state and triplet-state pairing is given, for instance, in Refs [119] and [85]. In both cases

$$\hat{\Psi} = \sum_{\mathbf{p}\sigma\eta}\chi_\sigma\Big[\exp(-{\rm i}\epsilon t+{\rm i}\mathbf{p}\mathbf{r})U_{\sigma\eta}(\mathbf{p})\hat{\alpha}_{\mathbf{p}\eta} + \exp({\rm i}\epsilon t-{\rm i}\mathbf{p}\mathbf{r})V_{\sigma\eta}(-\mathbf{p})\hat{\alpha}^+_{\mathbf{p}\eta}\Big]\,, \tag{75}$$

where $\mathbf{p}$ and $\epsilon=\sqrt{v_{\rm F}^2(p-p_{\rm F})^2+\delta_{\mathbf{p}}^2}$ are, respectively, the quasiparticle momentum and energy (with respect to the Fermi level). A basic spinor χ_σ describes a nucleon state with fixed spin projection ($\sigma=\pm1$) onto the quantization axis (axis z); η enumerates quasi-nucleon spin states; $\delta_{\mathbf{p}}$ is the energy gap in the quasi-particle spectrum, $v_{\rm F}$ is the Fermi velocity, $\hat{\alpha}^+_{\mathbf{p}\eta}$ and $\hat{\alpha}_{\mathbf{p}\eta}$ are, respectively, creation and annihilation operators for a quasiparticle in a $\hat{\alpha}_{\mathbf{p}\eta}$ state; $\hat{U}(\mathbf{p})$ and $\hat{V}(\mathbf{p})$ are the operators of the Bogolyubov transformation. For $|p-p_{\rm F}|\ll p_{\rm F}$, their matrix elements obey the relationships $U_{\sigma\eta}(\mathbf{p})=u_{\mathbf{p}}\delta_{\sigma\eta}$ and $\sum_{\sigma\eta}|V_{\sigma\eta}(\mathbf{p})|^2=2\,v_{\mathbf{p}}^2$, where

$$u_{\mathbf{p}} = \left[\frac{1}{2}\left(1+\frac{v_{\rm F}(p-p_{\rm F})}{\epsilon}\right)\right]^{1/2},$$

$$v_{\mathbf{p}} = \left[\frac{1}{2}\left(1-\frac{v_{\rm F}(p-p_{\rm F})}{\epsilon}\right)\right]^{1/2}. \tag{76}$$

For a singlet-state pairing, the gap $\delta_{\mathbf{p}}$ is isotropic, and the quantities $u_{\mathbf{p}}$ and $v_{\mathbf{p}}$ depend only on $p=|\mathbf{p}|$. For a triplet-state pairing, the quantities $\delta_{\mathbf{p}}$, $u_{\mathbf{p}}$ and $v_{\mathbf{p}}$ also depend on the orientation of $\mathbf{p}$.

Let $q_{\rm v}=(\omega_{\rm v},\mathbf{q}_{\rm v})$ and $q'_{\rm v}=(\omega'_{\rm v},\mathbf{q}'_{\rm v})$ be 4-momenta of a neutrino and antineutrino, respectively, while $p=(\epsilon,\mathbf{p})$ and $p'=(\epsilon',\mathbf{p}')$ be 4-momenta of annihilating quasi-nucleons. Using the Golden Rule of quantum mechanics, we can present the neutrino emissivity due to Cooper pairing (CP) as:

$$Q^{(\mathrm{CP})} = \left(\frac{G_\mathrm{F}}{2\sqrt{2}}\right)^2 \frac{1}{2}\mathcal{N}_\nu \int \frac{\mathrm{d}\mathbf{p}}{(2\pi)^3}\,\frac{\mathrm{d}\mathbf{p}'}{(2\pi)^3}\, f(\epsilon)\, f(\epsilon') \times \int \frac{\mathrm{d}\mathbf{q}_\nu}{2\omega_\nu(2\pi)^3}\,\frac{\mathrm{d}\mathbf{q}'_\nu}{2\omega'_\nu(2\pi)^3}\left[c_\mathrm{v}^2 I_{00}|l_0|^2 + c_\mathrm{a}^2 I_{ik} l_i l_k^*\right] \times (2\pi)^4 \delta^{(4)}(p + p' - q_\nu - q'_\nu)(\omega_\nu + \omega'_\nu)\,, \qquad (77)$$

where $\mathcal{N}_\nu = 3$ is the number of neutrino flavors, and the factor $1/2$ before $\mathcal{N}_\nu$ excludes double counting of the same quasi-nucleon collisions. The integral is taken over the range $(q_\nu + q'_\nu)^2 > 0$, where the process is open kinematically; $f(\epsilon) = 1/[\exp(\epsilon/T) + 1]$, $i, k = 1, 2, 3$;

$$I_{00} = \sum_{\eta\eta'} |\langle B|\hat{\Psi}^+\hat{\Psi}|A\rangle|^2,$$

$$I_{ik} = \sum_{\eta\eta'} \langle B|\hat{\Psi}^+\sigma_i\hat{\Psi}|A\rangle\langle B|\hat{\Psi}^+\sigma_k\hat{\Psi}|A\rangle^*\,. \qquad (78)$$

Here $|A\rangle$ stands for the initial state of the quasi-particle system in which one-particle states $(\mathbf{p}, \eta)$ and $(\mathbf{p}', \eta')$ are occupied, and $|B\rangle$ stands for the final state of the system in which the indicated one-particle states are empty.

The integral (77) is simplified by the standard technique, as described in Ref. [56]. The transformations take into account that nucleons are non-relativistic and strongly degenerate as well as the fact that the process is open kinematically in a small domain of phase space where the quasi-nucleon momenta $\mathbf{p}$ and $\mathbf{p}'$ are almost parallel. The latter circumstance allows one to take the smooth functions $I_{00}(\mathbf{p}, \mathbf{p}')$ and $I_{ik}(\mathbf{p}, \mathbf{p}')$ out of the integral over $\mathrm{d}\mathbf{p}'$ putting $\mathbf{p}' = -\mathbf{p}$. After a number of transformations the final expression for the neutrino emissivity can be written (in the standard physical units) as [55, 56]

$$Q^{(\mathrm{CP})} = \frac{4G_\mathrm{F}^2 m_\mathrm{N}^* p_\mathrm{F}}{15\pi^5\hbar^{10}c^6}(k_\mathrm{B}T)^7\mathcal{N}_\nu a F = 1.170\times 10^{21}\left(\frac{m_\mathrm{N}^*}{m_\mathrm{N}}\right)\left(\frac{p_\mathrm{F}}{m_\mathrm{N}c}\right) T_9^7 \mathcal{N}_\nu a F\ (\mathrm{erg\,cm^{-3}\,s^{-1}})\,, \qquad (79)$$

where $T_9 = T/(10^9\ \mathrm{K})$, a is a numerical factor (see below), and the function F, in our standard notation (8), is given by the integral

$$F = \frac{1}{4\pi}\int \mathrm{d}\Omega\, y^2 \int_0^\infty \frac{z^4\,\mathrm{d}x}{(\exp z + 1)^2}\,. \qquad (80)$$

The singlet-state gap $\delta_\mathbf{p}$ is isotropic; thus, integration over $\mathrm{d}\Omega$ is trivial and gives 4π. In the triplet-state case, the function F contains averaging over positions of a quasi-nucleon on the Fermi-surface. While using Eqn (79), one can take into account that $p_\mathrm{F}/(m_\mathrm{N}c) \approx 0.353(n_\mathrm{N}/n_0)^{1/3}$, where n_N is the number density of nucleons N, and $n_0 = 0.16\ \mathrm{fm}^{-3}$ as earlier.

The emissivity $Q^{(\mathrm{CP})}$ depends on the superfluidity type through the factor a and the function F. For singlet-state neutron pairing, a is determined by the only vector constant c_v: $a_\mathrm{nA} = c_\mathrm{v}^2 = 1$. If we used a similar expression for the singlet-state pairing of protons, we would obtain a very small factor $a_\mathrm{pA} = 0.0064$, which indicates the weakness of the process. Under these conditions, one should take into account the relativistic correction to a, produced by the axial-vector proton current. Calculating and adding this correction for the singlet-state pairing of protons, Kaminker et al. [135] obtained

$$a_\mathrm{pA} = c_\mathrm{v}^2 + c_\mathrm{a}^2\left(\frac{v_{\mathrm{F_p}}}{c}\right)^2\left[\left(\frac{m_\mathrm{p}^*}{m_\mathrm{p}}\right)^2 + \frac{11}{42}\right] = 0.0064 + 1.59\left(\frac{v_{\mathrm{F_p}}}{c}\right)^2\left[\left(\frac{m_\mathrm{p}^*}{m_\mathrm{p}}\right)^2 + \frac{11}{42}\right], \qquad (81)$$

where $v_{\mathrm{F_p}}/c = (p_{\mathrm{F_p}}/m_\mathrm{p}c)(m_\mathrm{p}/m_\mathrm{p}^*)$. The relativistic correction appears to be about 10 – 50 times larger than the main non-relativistic term. This noticeably enhances the neutrino emission due to singlet-state proton pairing although it remains much weaker than the emission due to the neutron pairing.

In the case of triplet-state pairing a is determined by both the vector and axial-vector constants of neutral hadron currents: $a = a_\mathrm{NB} = a_\mathrm{NC} = c_\mathrm{v}^2 + 2c_\mathrm{a}^2$ [56]. For the neutron pairing, we obtain $a_\mathrm{nB} = a_\mathrm{nC} = 4.17$. Notice that in the case of triplet-state pairing of protons which is thought to be hardly possible in NS cores we would obtain $a_\mathrm{pB} = a_\mathrm{pC} = 3.18$. Under such exotic conditions, the neutrino emission due to proton pairing would be almost as efficient as the emission due to neutron pairing.

The result for the singlet-state pairing of neutrons, presented above, coincides with that obtained in the pioneering article by Flowers et al. [51] (for two neutrino flavors, $\mathcal{N}_\nu = 2$). Similar expressions obtained in Refs [49, 52] for $\mathcal{N}_\nu = 1$ contain an extra factor $(1 + 3g_\mathrm{a}^2)$. In addition, the expression for $Q^{(\mathrm{CP})}$ in Refs [49, 52] contains a misprint: π^2 in the denominator instead of π^5 (although the numerical estimate of $Q^{(\mathrm{CP})}$ is obtained with the correct factor π^5). The cases of singlet-state proton pairing and triplet-state neutron pairing were analyzed in Refs [55, 56, 135] for the first time.

Let us mention that the values of c_v, c_a and a can be renormalized in dense NS matter under in-medium effects. The renormalization is a difficult task. It will be neglected below.

The function F, given by Eqn (80), depends on the only variable v, the gap parameter [see Eqn (9)]. Using Eqn (80) one can easily obtain the asymptote of this function and calculate its dependence on $\tau = T/T_\mathrm{c}$ for superfluidity of types A, B and C in analogy with the calculations presented in Sections 3 – 5. This has been done in Refs [55, 56].

In a small vicinity of $T \approx T_\mathrm{c}$, in which $v \ll 1$ and $\tau \to 1$, we have:

$$F_\mathrm{A}(v) = 0.602v^2 = 5.65(1-\tau),$$
$$F_\mathrm{B}(v) = 1.204v^2 = 4.71(1-\tau),$$
$$F_\mathrm{C}(v) = 0.4013v^2 = 4.71(1-\tau)\,. \qquad (82)$$

For the low temperatures $T \ll T_\mathrm{c}$ the parameter $v \gg 1$, and the asymptotes of $F(v)$ are

$$F_\mathrm{A}(v) = \frac{\sqrt{\pi}}{2}v^{13/2}\exp(-2v) = \frac{35.5}{\tau^{13/2}}\exp\left(-\frac{3.528}{\tau}\right),$$
$$F_\mathrm{B}(v) = \frac{\pi}{4\sqrt{3}}v^6\exp(-2v) = \frac{1.27}{\tau^6}\exp\left(-\frac{2.376}{\tau}\right),$$
$$F_\mathrm{C}(v) = \frac{50.03}{v^2} = 12.1\tau^2\,. \qquad (83)$$

Let us stress that the neutrino emission due to nucleon pairing differs from other neutrino reactions: first, it has a temperature threshold (is allowed only for $T < T_c$); second, its emissivity is a nonmonotonic function of temperature. The emissivity grows rapidly with decreasing T just after superfluidity but then reaches maximum and decreases. According to Eqn (83), a strong superfluidity reduces considerably the emissivity just as it reduces the heat capacity or direct Urca process: the reduction is exponential if the gap is nodeless (cases A and B) and it is power-law otherwise (case C); see Sections 3 and 4.

The asymptotes (82) and (83), as well as the numerical values of $F(v)$ for intermediate v, are fitted by the simple expressions [55, 56]

$$F_{\rm A}(v) = (0.602v^2 + 0.5942v^4 + 0.288v^6) \times \left(0.5547 + \sqrt{(0.4453)^2 + 0.0113v^2}\right)^{1/2} \times \exp\left(-\sqrt{4v^2 + (2.245)^2} + 2.245\right),$$

$$F_{\rm B}(v) = \frac{1.204v^2 + 3.733v^4 + 0.3191v^6}{1 + 0.3511v^2} \times \left(0.7591 + \sqrt{(0.2409)^2 + 0.3145v^2}\right)^2 \times \exp\left(-\sqrt{4v^2 + (0.4616)^2} + 0.4616\right),$$

$$F_{\rm C}(v) = \frac{0.4013v^2 - 0.043v^4 + 0.002172v^6}{1 - 0.2018v^2 + 0.02601v^4 - 0.001477v^6 + 0.0000434v^8}. \quad (84)$$

Equations (79) and (84) enable one to calculate easily the neutrino emissivity $Q^{(\rm CP)}$ due to Cooper pairing of nucleons for superfluidity of types A, B and C. Similar expressions describe neutrino emissivity due to pairing of hyperons. The required values of a are listed in Ref. [56].

Figure 10 (from Ref. [56]) shows the temperature dependence of the emissivity $Q^{(\rm CP)}$ due to neutron pairing in the NS core for $\rho = 2 \times 10^{14}$ g cm^{-3}. The adopted equation of state of matter is described in Section 7.2. The effective nucleon masses are set equal to $m_{\rm N}^* = 0.7\,m_{\rm N}$, and the critical temperature is $T_{\rm cn} = 10^9$ K. The density chosen is typical for transition between single-state pairing and triple-state pairing (Section 3.1). Thus, different models of nucleon–nucleon interaction may lead to a different neutron superfluidity type. We present the curves for the three superfluidity types considered above.

When the temperature falls below $T_{\rm cn}$ the neutrino emissivity produced by Cooper pairing strongly increases. The main neutrino energy release takes place in the temperature interval $0.2T_{\rm cn} \lesssim T \lesssim 0.96\,T_{\rm cn}$, with the maximum at $T \approx 0.4\,T_{\rm cn}$. The emissivity may be sufficiently high, comparable with or even larger than the emissivity of the modified Urca process in non-superfluid matter (Section 4). Under certain conditions, neutrino emission due to pairing of neutrons may be significant in the inner NS crust [55, 45]. The reaction may be noticeable even in the presence of the direct Urca process in the inner NS core if the direct Urca is partly suppressed by the proton superfluidity (see below).

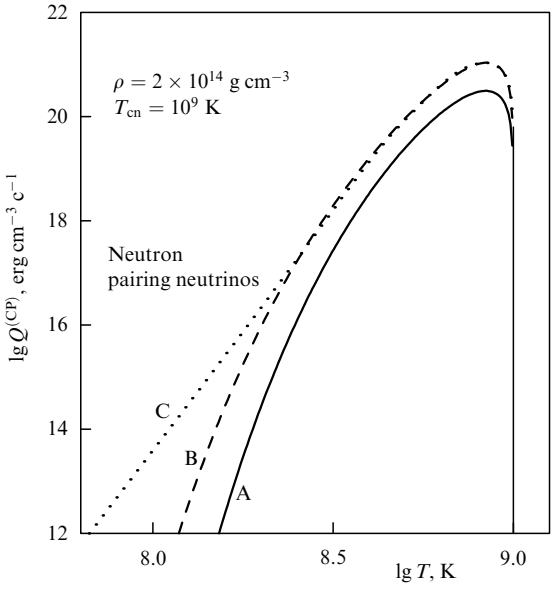

Figure 10. Temperature dependence of the neutrino emissivity due to Cooper pairing of neutrons for $\rho = 2 \times 10^{14}$ g cm^{-3} and $T_{\rm c} = 10^9$ K for superfluidity types A (solid line), B (dashes) and C (dots).

6.2 Summary of Sections 3–6

Let us summarize the results of Sections 3–6. For illustration, we use the same equation of state of matter (neutrons, protons and electrons) in the NS core as in our cooling simulations (Section 7.2), and set $m_{\rm N}^* = 0.7\,m_{\rm N}$. Let us adopt that the neutron pairing is of type B, while the proton pairing is of type A.

Figure 11 illustrates the effect of superfluidity on the heat capacity for $\rho = 2\rho_0$, $T_{\rm cn} = 4 \times 10^9$ K and $T_{\rm cp} = 6 \times 10^8$ K. In the absence of superfluidity, the main contribution to the heat capacity comes from neutrons. The heat capacities of protons and electrons are lower than that of neutrons by a

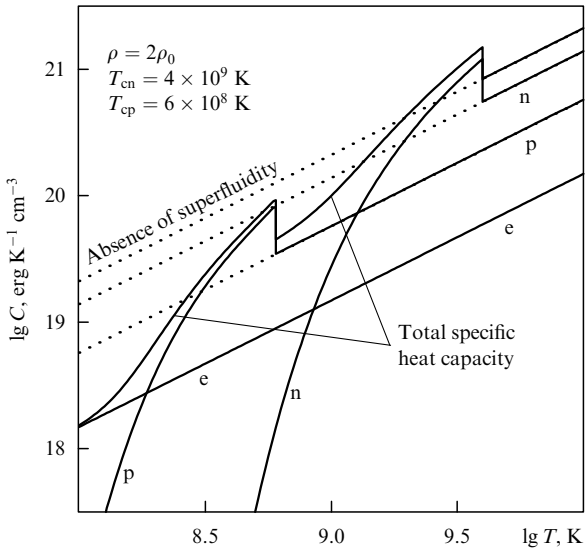

Figure 11. Temperature dependence of the total and partial (n, p, e) specific heat capacities at $\rho = 2\,\rho_0$ for neutron superfluidity of type B with $T_{\rm cn} = 4 \times 10^9$ and proton superfluidity of type A with $T_{\rm cp} = 6 \times 10^8$ K. The dotted lines show corresponding heat capacities in non-superfluid matter.

factor of 2.5 and 9, respectively. After superfluidity appears with decreasing temperature, the relative contributions of different particles change. The jumps of the total and neutron heat capacities with the fall of temperature below $T = T_{cn}$ are associated with latent heat release produced by pairing of neutrons. However for $T \lesssim 10^9$ K the neutron superfluidity becomes strong and reduces greatly the partial heat capacity. The main contribution to the heat capacity now comes from protons. When the temperature falls below T_{cp}, the proton heat capacity jumps up due to the appearance of proton superfluidity. For $T \lesssim 2 \times 10^8$ K the latter superfluidity, in turn, becomes strong and reduces exponentially the proton heat capacity. As a result, at lower temperatures the total heat capacity is determined by electrons and does not depend on nucleon superfluidity. Examining Fig. 11, it is easy to predict the relative contributions of different particles to the heat capacity for any relationships between T, T_{cn} and T_{cp}.

The effect of superfluidity on neutrino reactions is more complicated. For instance, Fig. 12 shows the neutrino emissivities in different reactions for $T_{cn} = 8 \times 10^8$ K and $T_{cp} = 4 \times 10^9$ K. The top panel corresponds to $\rho = 2\rho_0$. The direct Urca process is forbidden at this density (being allowed at $\rho_{cr} = 4.64\,\rho_0 = 1.30 \times 10^{15}$ g cm^{-3}, for a given equation of state). In the absence of neutron superfluidity ($T > T_{cn}$) the dominant mechanism is the modified Urca process. If, however, the temperature decreases from $T = T_{cn}$ to $T \approx 10^{8.9}$ K the total neutrino emissivity increases by about two orders of magnitude due to Cooper pairing of neutrons. Therefore, sometimes the appearance of superfluidity accelerates NS cooling instead of slowing it.

The bottom panel of Fig. 12 corresponds to denser matter, $\rho = 5\rho_0$, where the powerful direct Urca process is switched on. In this case, the neutrino emissivity is actually determined by two processes, the direct Urca and Cooper pairing of nucleons. The direct Urca dominates at $T \gtrsim 3 \times 10^8$ K. With further decrease of T, the direct Urca and the reactions considered in Sections 4 and 5 are reduced so strongly, that the Cooper pairing becomes dominant.

It is well known that the neutrino emission from a non-superfluid NS core is mainly determined by a single, most powerful neutrino emission mechanism: the direct Urca for the enhanced cooling, or the modified Urca for the standard cooling. However, as seen from Fig. 12, this 'simplicity' is violated in superfluid NS cores. Different neutrino mechanisms can dominate at different cooling stages depending on T, T_{cn}, T_{cp}, and ρ.

Figure 13 shows which neutrino mechanisms dominate for different T_{cn} and T_{cp}. In addition to the neutrino processes considered above we have included one more process, neutrino bremsstrahlung due to electron–electron collisions [136]. This mechanism, as a rule, is sufficiently weak and neglected in cooling simulations. The three left diagrams of Fig 13 illustrate the case of standard cooling at $\rho = 2\,\rho_0$ for three internal stellar temperatures: 10^8, 3×10^8 and 10^9 K; the three on the right correspond to enhanced cooling at $\rho = 5\,\rho_0$ for the same T. The chosen values of T cover the region most interesting in practice. Our calculations show that the topology of the figures varies only slightly with ρ as long as ρ does not cross the threshold value $\rho = \rho_{cr}$. Therefore, the presented figures reflect adequately the efficiency of all neutrino processes in the core of a cooling NS. One can see that, in the presence of superfluidity, many different mechanisms can dominate in certain parameter ranges.

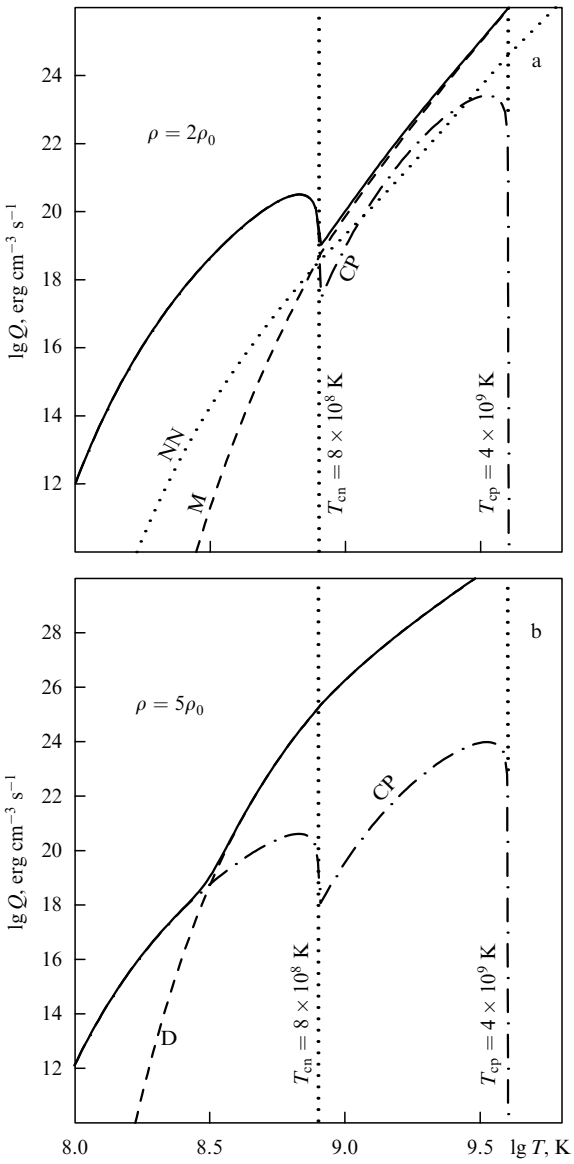

Figure 12. Temperature dependence of the neutrino emissivity in different reactions for neutron superfluidity of type B with $T_{cn} = 8 \times 10^8$ K and proton superfluidity of type A with $T_{cp} = 4 \times 10^9$ K at $\rho = 2\,\rho_0$ [standard neutrino reactions, panel (a)] and $\rho = 5\,\rho_0$ [direct Urca is allowed, panel (b)]. The dot-and-dash line shows the emissivity due to Cooper pairing of neutrons plus protons; the solid line presents the total emissivity. Panel (a): the dashed line gives the total emissivity in two branches of the modified Urca process; the dotted line exhibits the total bremsstrahlung emissivity due to nn, np and pp scattering. Panel (b): the dashed line corresponds to the direct Urca process.

Notice that if the direct Urca process is open, the modified Urca process is always insignificant and may be neglected. In the presence of neutron superfluidity alone, the neutrino bremsstrahlung due to pp collisions becomes the main mechanism at $T \ll T_{cn}$ being independent of the neutron superfluidity. In the presence of proton superfluidity alone, the neutrino bremsstrahlung due to nn collisions dominates at $T \ll T_{cp}$. The Cooper pairing of neutrons exceeds the standard neutrino energy losses for $T \lesssim 10^9$ K and for not too strong neutron superfluidity ($0.12 \lesssim T/T_{cn} \lesssim 0.96$). This parameter range is very interesting for applications. The neutrino emission due to Cooper pairing of neutrons is also significant at early cooling stages, when $T \gtrsim 10^9$ K, but in a

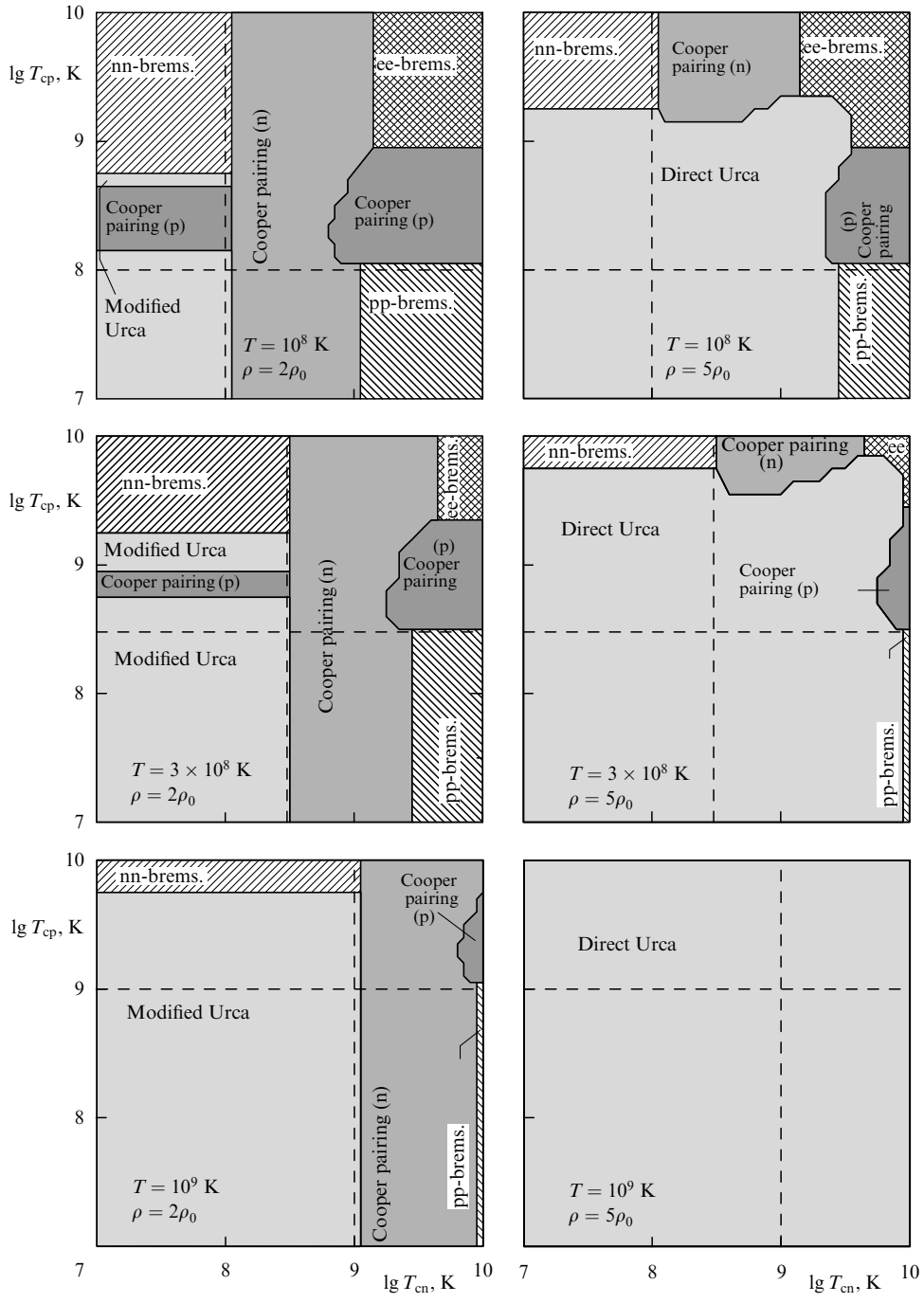

Figure 13. Regions of T_{cn} (superfluidity of type B) and T_{cp} (type A), in which different neutrino reactions dominate at $T = 10^9$, 3×10^8 and 10^8 K in matter of density $\rho = 2\rho_0$ (standard cooling) and $\rho = 5\rho_0$ (enhanced cooling).

narrower temperature range near $T \approx 0.4\,T_{cn}$, or in the presence of proton superfluidity. Although the neutrino production due to proton pairing is much weaker, it can also dominate. The neutrino emission due to pairing of neutrons and protons can dominate in the enhanced NS cooling as well provided the nucleons of one species are strongly superfluid while the others are moderately superfluid. Very strong superfluidities of neutrons and protons (upper right corners of the figures) switch off all neutrino processes involving nucleons. As a result, the neutrino bremsstrahlung due to electron–electron collisions, which is practically unaffected by superfluidity, becomes dominant. It is difficult to expect that this weak process is important under other conditions.

7. Cooling of neutron stars

7.1 Review of articles on neutron star cooling

7.1.1 Overall review. The theory of NS cooling has been developing over more than 30 years. The first articles appeared even before the discovery of NSs. Their authors tried to prove that not too old NSs may emit sufficiently powerful thermal X-ray radiation which could serve to discover NSs. The first estimates of the thermal emission from cooling NSs were most probably done by R. Stabler [137] in 1960. In 1964 Chiu [138] repeated these estimates and theoretically proved the possibility of discovering NSs from

their thermal emission. First, simplified calculations of the NS cooling were done by Morton [139], Chiu and Salpeter [46] and also by Bahcall and Wolf [23] after the discovery of X-ray sources in the Crab nebula and Scorpion constellation in the balloon experiments by Bowyer et al. [140].

The foundation of the strict cooling theory was laid in the fundamental paper by Tsuruta and Cameron [141] who explicitly formulated the main elements of the theory — the relationship between the internal and surface NS temperatures, the neutrino and photon cooling stages, etc. Later the theory was developed in many papers.

In the 1970s and 1980s, the main attention was paid to the equation of state and nuclear composition of the NS cores (including the possible appearance of exotic particles), to neutrino reactions and to the relationship between the internal and surface temperatures of NSs (particularly in the presence of strong magnetic fields). The achievements of the theory in the middle of the 1970s were reviewed by Tsuruta [142]. A splash of theoretical activity at the beginning of the 1980s was concerned with the launch of the *Einstein* space observatory (Section 8.1). The articles of the 'Einstein series' were also reviewed by Tsuruta [143 – 145]. The launch of the *ROSAT* observatory in 1990 (Section 8.1) initiated a new rise of theoretical activity which is still being continued. Recent articles are mainly focused on the mechanisms of NS reheating at the late evolutionary stages (see below) and the effects of superfluidity in NS cores. Let us mention a recent review by Tsuruta [146]. New microscopic theories of dense matter are appearing ever complicating cooling models; many problems are still unsolved.

Let us outline some aspects of the theory.

The first articles were devoted to the standard cooling (produced by the neutrino reactions from the 'standard' collection, Section 5). Enhanced cooling has been simulated since the end of the 1970s. It has been assumed in many articles that the enhanced neutrino luminosity is associated with the exotic composition of the NS cores containing pion condensates of quark plasma; see, e.g., Refs [30, 142, 147 – 153]. By the end of the 1980s a new cooling agent was put forward, kaon condensate [30, 154, 155]. New models of dense matter with highly polarized pion degrees of freedom [48 – 50] have also been proposed. According to these models the neutrino luminosity is strongly enhanced due to virtual excitation of the pion field even if the density of matter does not exceed the critical density of actual pion condensation. Modern cooling theories of stars with quark cores, or pion or kaon condensates have been described, for instance, in Refs [21, 30].

A new stage of the theory of enhanced cooling was opened by Lattimer et al. [19] who showed that the direct Urca process can be allowed in the NS cores with the standard nuclear composition for many realistic equations of state. The process initiates rapid NS cooling [5, 30, 124, 127, 133, 156 – 158] without invoking 'exotic' hypotheses (Section 2.2). A detailed description of the 'non-exotic' standard and enhanced cooling theories was given by Pethick [21].

The effect of the NS magnetic field on the relationship between the internal and surface stellar temperatures has been taken into account starting from the articles by Tsuruta and coauthors [159 – 161]. These articles were the first where a representative set of neutrino reactions in the NS crust and core was included (plasmon decay, annihilation of electron-positron pairs, photon decay, electron bremsstrahlung due to scattering off nuclei, the neutron branch of the modified Urca process). A detailed study of the relationship between the internal and surface temperatures in a NS with the magnetic field normal to the surface was carried out by Van Riper [162]. He also analysed in detail [163] the effect of such magnetic fields on NS cooling. Page [164] as well as Shibanov and Yakovlev [165] considered the cooling of a NS with a dipole magnetic field and showed that the dipole field affected the cooling much more weakly, and in a qualitatively different way, than a purely radial magnetic field.

Let us mention also a recent series of articles by Heyl and coauthors [166 – 171] devoted to the cooling of NSs with superstrong magnetic fields $10^{14} - 10^{16}$ G (the so called 'magnetars', see Section 8.1.1). These fields may strongly reduce the thermal insulation of the NS envelope, making the magnetar's surface much hotter at the early cooling stage, than the surface of an 'ordinary' NS. Let us stress that the microscopic properties of matter in superstrong magnetic fields (equation of state, thermal conductivity) are poorly known, so that the results by Heyl and coauthors can be regarded as very preliminary.

The cooling can also be affected noticeably [53, 155, 172 – 174] by the presence of a thin (of mass $\lesssim 10^{-8} M_{\odot}$) envelope of light elements (H, He) at the surface of a non-magnetized or weakly magnetized NS. Owing to the higher electron thermal conductivity of plasma composed of light elements, the NS surface appears to be significantly warmer at the early cooling stages.

An important contribution to the theory was made in the PhD thesis by Malone [175]. He was the first who calculated the standard NS cooling beyond the approximation of isothermal internal layers. This allowed him to describe the thermal relaxation of the internal layers in the first 100 – 1000 years of NS life. Analogous nonisothermal calculations of the cooling enhanced by the presence of a pion condensate were done in the PhD thesis of Richardson [176]. The results of both theses were published in one paper [150]. Later the thermal relaxation of the internal layers in a young NS was studied in a series of articles by Nomoto and Tsuruta [60, 177 – 180] as well as by Lattimer et al. [61]. The thermal relaxation is accompanied by propagation of a cooling wave from the internal layers to the surface. In principle, the appearance of the cooling wave at the surface can be observed in young NSs. The moment of appearance depends on the equation of state in the central stellar region [61].

In 1980 Glen and Sutherland [147] and a year later Van Riper and Lamb [148] included the effects of General Relativity into the equations of NS thermal evolution (in addition to the equations of hydrostatic equilibrium as had been done before). In this connection let us mention a recent paper [181] where the first two-dimensional cooling calculations of a rotating NS were carried out with an exact account of the general relativistic effects produced by rotation.

A new direction of study was opened by Alpar et al. [182] and Shibazaki and Lamb [183] at the end of 1980s. The authors took into account possible reheating at late cooling stages (NS age $t \gtrsim 10^4$ yr) due to viscous dissipation of rotational energy inside a NS. The effect is caused by interaction of superfluid and normal components of matter in the inner crust of a pulsar which is spinning down under the action of magnetodipole losses. The cooling theory with viscous reheating was developed further in a number of articles (e.g., Refs [53, 151, 152, 155, 174, 184 – 187]).

The core of a cooling NS can also be reheated by the energy release associated with a weak deviation from beta-

equilibrium [188]. In addition, the reheating of the star with a non-superfluid core can be produced by Ohmic dissipation of the core magnetic field [189–192] due to the enhancement of the electric resistance across the strong magnetic field. The criticism of this effect in Ref. [193] is not convincing because, while calculating the electric resistance, the authors of Ref. [193] neglected the motion of the neutron component of matter (the inconsistency of such an approximation is clearly seen from the results of Ref. [194]). Finally, the reheating in an old NS ($t \gtrsim 10^7$ yr) can be provided by Ohmic decay of the magnetic field in the NS crust [195, 196]. Let us add that the magnetic field dissipation in the crust represents a very important process which determines the evolution of the surface magnetic field, the magnetodipole NS spindown, NS activity as a radio pulsar, etc. The dissipation process is associated with cooling since the electric resistance of the crust decreases in the course of cooling (until it reaches the minimum produced by electron scattering off charged impurities). Therefore, the dissipation rate depends on the cooling type: it is very weak for rapid cooling. On the other hand, the magnetic field decay weakens the electrodynamic spindown of the star. This means that cooling, magnetic field evolution and spindown should be considered, in principle, self-consistently as *magneto-rotational evolution* of a NS. The corresponding theory has been developed in a series of papers by Urpin and coauthors (see, e.g., papers [196–198]) and references therein) without account for the effect of superfluidity on the NS cooling.

7.1.2 Cooling of superfluid stars. The effect of nucleon superfluidity in the NS core on cooling was taken into account starting from the article by Tsuruta et al. [159]. In the first articles, as a rule, it was included in a simplified manner; it was assumed that the superfluidity completely switches off the corresponding heat capacity or neutrino emission from the very beginning of the cooling (which corresponds to infinitely large critical temperatures). Maxwell [123] was the first who studied the dependence of standard NS cooling on nucleon critical temperatures. Friman and Maxwell [12] considered a simplified NS model with a constant-density core neglecting the effects of General Relativity, but employing sufficiently realistic neutrino luminosity. For a long time, before publication of the article by Page and Applegate [5], superfluidity was not considered as a powerful cooling regulator. It was taken into account because it appeared inevitably in microscopic theories of dense matter (Section 3.1). However recent studies show that superfluidity is one of the most important factors which affect the standard and enhanced NS cooling.

Simulations of the standard cooling of NSs with superfluid cores have been performed in many papers, in particular, in Refs [30, 57, 56, 60, 123 124, 133, 142, 143, 147, 148, 150, 159, 175, 177, 180, 199]. While calculating the standard neutrino luminosity of the NS core, as a rule, one took into account the contribution of the neutron branch of the modified Urca processes and the neutrino bremsstrahlung due to nn- and np-scattering. Tsuruta et al. [159] were the first who studied the NS cooling accompanied by the singlet-state pairing of neutrons and protons. The authors of Ref. [159] described reduction of the n-branch of the modified Urca-process and the np bremsstrahlung by the asymptotic expressions obtained in Ref. [131] for the modified Urca in the limit of strong ($T \ll T_c$) singlet-state pairing of neutrons; they multiplied the nn-scattering rate by $\exp(-\Delta_n/k_BT)$. In Ref. [123] the modified Urca process was just switched off at temperatures below T_{cn} or T_{cp}. In a number of papers various authors used the simplified reduction factors proposed by Malone [175]: $\exp[-(\Delta_n + \Delta_p)/k_BT]$ for superfluidity of neutrons and proton at once; $\exp(-\Delta_N/k_BT)$ for singlet-state superfluidity of neutrons or protons (for the neutron branch of the modified Urca-process and np-bremsstrahlung). The reduction of the nn-bremsstrahlung by the neutron superfluidity was described by the expression $\exp(-2\Delta_n/k_BT)$. The accuracy of these approximations was analyzed in Sections 4 and 5. Their effect on the cooling is demonstrated in Fig. 14.

The complete set of neutrino reactions considered in Sections 4 and 5 was first used in Ref. [133]. The authors of Ref. [133] also employed a more accurate description of the effects of superfluidity on the heat capacity and neutrino luminosity (Sections 3–5), but neglected the neutrino emission due to Cooper pairing of nucleons (Section 6). The latter process has been included only in recent simulations [50, 53–57, 174]; let us mention that the authors of Refs [54–57] made use of more accurate expressions for the neutrino emissivity given in Section 6 (although neglected the relativistic correction to the neutrino emissivity due to pairing of protons).

The importance of neutrino emission due to Cooper pairing of nucleons for the standard NS cooling is illustrated in Fig. 15a. One can see that the appearance of superfluidity at the neutrino cooling stage can not only slow down the NS cooling, as thought before, but, on the contrary, strongly accelerate it (see, e.g., Ref. [56]). The acceleration can be so fast that at $t \sim 10^5 - 10^6$ yr the star can be much cooler that in the case of the enhanced neutrino energy losses. An exclusion

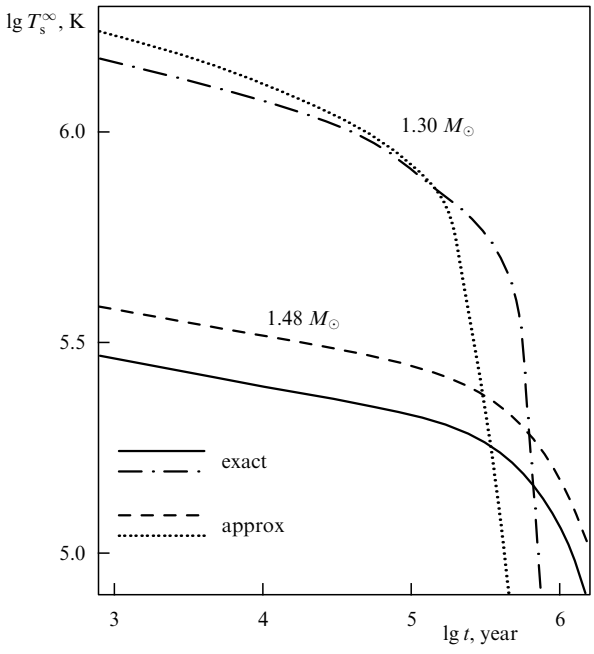

Figure 14. Cooling curves calculated using accurate (solid and dash-dotted lines) and approximate (dashed and dotted lines) description of the effects of superfluidity on the neutrino luminosity and heat capacity (see text). Solid and dashed lines correspond to the enhanced cooling of a NS ($M = 1.48\,M_\odot$) in the presence of the proton superfluidity with $T_{cp} = 10^8$ K. Dash-dotted and dotted lines refer to the standard cooling of a NS ($1.30\,M_\odot$) in the presence of neutron and proton superfluidities with $T_{cn} = 10^9$ K and $T_{cp} = 10^8$ K. The parameters of the models are given in Section 7.2.2. Neutrino emission due to nucleon pairing is neglected.

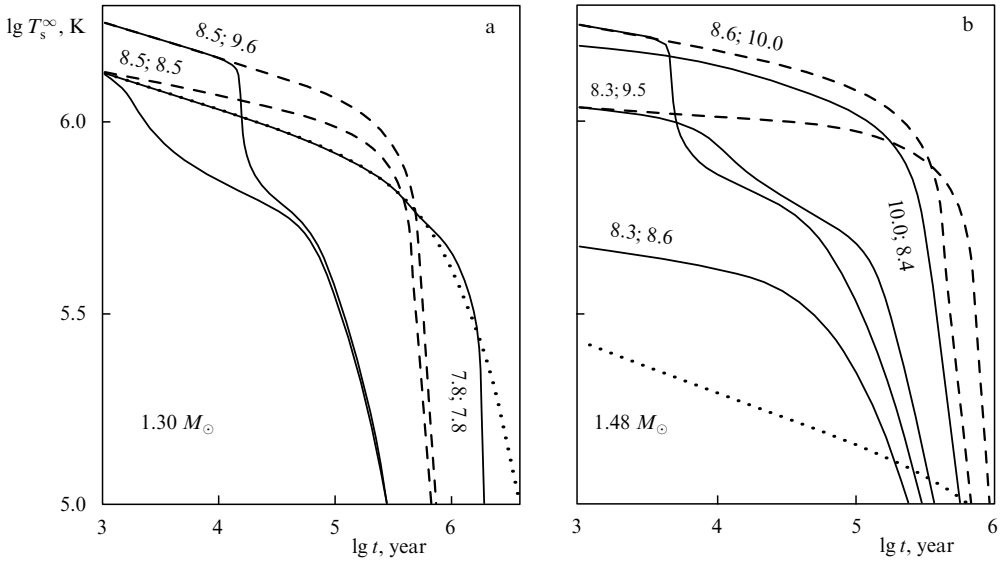

Figure 15. Standard cooling of a NS with $M = 1.30\,M_\odot$ (a) and enhanced cooling of a NS with $M = 1.48\,M_\odot$ (b) in the presence of superfluidity. The curves are labeled by the values of lg T_{cn} and lg T_{cp}. Solid lines are obtained including the neutrino emission due to pairing of nucleons while dashed lines are obtained neglecting this emission. Dotted lines show cooling of non-superfluid NSs. The parameters of the models are given in Section 7.2.2. The solid and dashed lines for lg $T_{cn} = 7.8$ and lg $T_{cp} = 7.8$ in panel (a) coincide with each other and so do the lines for lg $T_{cn} = 8.3$, lg $T_{cp} = 8.6$ and lg $T_{cn} = 10.0$, lg $T_{cp} = 8.4$ in panel (b).

is provided by superfluidity of protons alone since proton pairing does not produce intense neutrino emission. In addition, the difference between the cooling curves is small in the case of normal protons and strongly superfluid neutrons ($T_{cn} \gtrsim 10^9$ K), in which the Cooper pairing of neutrons is not a dominant process (Section 6.2).

Simulation of enhanced cooling of NSs with the standard composition of the cores was started by Page and Applegate [5]. These authors were the first who discovered an interesting feature in the cooling of NSs in which the direct Urca process was open and neutrons or protons were superfluid: after thermal relaxation was over the surface temperature of these stars fell rapidly to the value $T_s = T_s(T_i)$, appropriate to the internal temperature $T_i = \alpha T_c$, and remained almost constant during the subsequent neutrino cooling stage. Here T_c is the critical temperature of neutrons or protons in the core, and $\alpha \sim 1$ is a numerical coefficient (for instance, according to Ref. [5], $\alpha \approx 0.2$). Moreover, the temperature T_i is almost insensitive to other NS parameters [124]. The nature of this phenomenon is very simple — the star cools rapidly before the superfluidity onset, whereas the superfluidity suppresses the cooling and 'freezes' the internal temperature at the level of αT_c. This opens the possibility to study superfluidity in those NSs whose surface temperature is known from observations.

Page [124] analyzed this possibility in more detail (neglecting the Cooper-pairing neutrino emission). He showed that the measured surface temperatures of PSR 0656 + 14 [200] and Geminga [201] could be explained in the standard and enhanced cooling models. The observations of the Vela pulsar [202] are more easily explained by the enhanced cooling model, and the observations of PSR 1055 – 52 [203] by standard cooling. In all these cases one needs [124] the presence of neutron and proton superfluidities with high critical temperatures $T_c \sim 10^9$ K throughout the NS body where the main neutrino emission occurs.

Let us stress that the results and quantitative conclusions of Refs [5, 124] are considerably modified by including the effects of joint superfluidity of nucleons and Cooper-pairing neutrinos. However the principal conclusion by Page and Applegate remains the same: a NS of age $10^2 - 10^5$ yr with superfluid nucleons in its core is a 'thermometer' of this superfluidity — one can measure (constrain) the critical temperatures of neutrons T_{cn} and protons T_{cp} from the values of the surface temperature.

Aside from Refs [5, 124] the enhanced cooling of NSs with standard nuclear composition and nucleon superfluidity in the cores has been studied, for instance, in Refs [53 – 57, 127, 133, 156, 157, 174]. As in the case of standard cooling, the effect of superfluidity on the heat capacity and neutrino luminosity was described in earlier articles by approximate factors of the form $\exp(-\Delta_N/k_B T)$, but gradually the theory presented in Sections 3 – 5 has become implemented. The difference between the standard and enhanced cooling curves calculated using the accurate (Sections 3 – 5) and approximate ($\exp(-\Delta_j/k_B T)$) reduction factors is illustrated in Fig. 14. The accurate reduction factors 'freeze' the cooling at the neutrino cooling stage at a lower internal temperature T and, accordingly, at a lower surface temperature [156].

In calculations of the enhanced neutrino luminosity the contribution from Cooper pairing of nucleons (Section 6) has usually been neglected (excluding Refs [50, 53 – 57, 174]). According to Yakovlev [56] this process is especially important in the presence of proton superfluidity with $T_{cp} \gg T_{cn}$. Such superfluidity appears at the early cooling stage and suppresses the direct Urca process long before the onset of neutron pairing. Therefore, the splash of neutrino emission associated with neutron pairing is very pronounced. In this case the NS cooling does not slow down, as it would without neutrino emission due to nucleon pairing, but is strongly accelerated (Fig. 15b). Let us recall that a similar situation persists in the case of standard cooling (also see Section 7.2).

As a result, nucleon superfluidity plays the leading role for the both standard and enhanced cooling [53 – 57, 174]. Moreover, the superfluidity mixes the cooling types, since the

enhanced cooling may look like standard cooling while the standard cooling may look like enhanced (especially if the neutrino emission due to Cooper pairing is taken into account, cf. Figs 15a and 15b). In these cases, the star, independently of its cooling type, remains a good 'thermometer' for measuring the nucleon critical temperatures: even weak variations of T_{cn} or T_{cp} strongly affect the cooling curves. The only problem is to 'calibrate' properly this thermometer (Sections 3–6).

Finally, let us mention that Schaab et al. [118] have considered recently, for the first time, standard and enhanced cooling in the presence of triplet-state neutron superfluidity of type C (with the nodes of the gap at the Fermi surface). The authors based their calculations on the model of neutron pairing in strong magnetic fields [94] according to which the field $B \gtrsim 10^{16}$ G makes the pairing of type C energetically more favorable than that of type B. Let us also note the first calculations [204] of cooling of a NS with a hyperonic core taking into account the hyperon superfluidity. We mention, however, that the authors of Refs [118, 204] made use of approximate reduction factors of neutrino reactions and approximate expressions for the neutrino emissivity due to Cooper pairing of particles.

The theoretical conclusion on the leading role of superfluidity in NS cooling was made at about the same time as new observational data on the surface temperatures of some NSs appeared (Section 8). The latter data brought the problem of studying superfluidity in NS cores to reality.

7.2 Cooling simulations

In this section we illustrate the possibility of exploring nucleon superfluidity in NS cores. We will mainly follow our recent article [57]. In addition, we include in the simulations a relativistic correction to the neutrino luminosity produced by proton pairing (Section 6.1). This affects slightly the cooling curves at some values of T_{cn} and T_{cp} but does not change the main conclusions of Ref. [57].

7.2.1 Simulation scheme. Below we present the results obtained with the cooling code [54, 133, 156, 157, 205] that is based on the approximation of isothermal stellar interiors. The code was mainly developed by O Y Gnedin. The isothermal approximation is valid for a star of age $t > 10-10^3$ yr, inside which the thermal relaxation is over. The superfluidity strongly affects the surface temperature only after reaching the thermally relaxed stage. Following Ref. [147] we have assumed that the isothermal region is restricted by the condition $\rho > \rho_b = 10^{10}$ g cm^{-3}. The real boundary of the isothermal region is at lower ρ and depends on temperature: it moves to the surface in the course of cooling. The chosen value of ρ_b guarantees that the region $\rho > \rho_b$ is isothermal in a star of age $t \gtrsim 10^3$ yr. The quantity $T_i(t) = T(r,t)\exp[\Phi(r)]$ (which may be called the internal redshifted temperature) is constant over the isothermal region at any moment of time t. Here $T(r,t)$ is the local temperature, $\Phi(r)$ is the dimensionless gravitational potential, and r is the radial coordinate.

We take into account explicitly the effects of General Relativity on the NS structure and cooling. The cooling simulation in the isothermal approximation is reduced to solving the equation of thermal balance (see, e.g., Ref. [147])

$$C(T_i)\frac{dT_i}{dt} = -L_{\nu i}(T_i) - L_{\gamma i}(T_s), \tag{85}$$

$$C = \int c_V\, dV, \qquad dV = 4\pi r^2\left(1-\frac{2Gm}{rc^2}\right)^{-1/2} dr, \tag{86}$$

$$L_{\nu i} = \int Q\exp(2\Phi)\, dV, \quad L_{\gamma i} = 4\pi\mathcal{R}^2\sigma T_s^4\exp(2\Phi_b). \tag{87}$$

In this case, C is the total heat capacity of the star, c_V is the specific heat capacity, and $m = m(r)$ is the gravitational mass inside a sphere with radial coordinate r. The quantities $L_{\nu i}$ and $L_{\gamma i}$ determine the neutrino and photon NS luminosities, respectively, Q is the neutrino emissivity, Φ_b is the value of Φ at the isothermal region boundary ($\rho = \rho_b$), and σ is the Stefan–Boltzmann constant.

The photon luminosity of the star depends on the effective temperature T_s of its surface. The relationship between T_s and the temperature $T_b = T_i\exp(-\Phi_b)$ at $\rho = \rho_b$ is determined by the thermal insulation of the outer envelope ($\rho < \rho_b$), where the main temperature gradient is formed. We have not taken into account the effect of the magnetic field on the NS cooling and have used the relationship $T_s(T_b)$, obtained recently [173] for $B = 0$. We assume that the NS surface may be covered by a thin layer (of mass $\lesssim 10^{-13}\,M_\odot$) of hydrogen or helium. This amount of light elements is too small to affect the thermal insulation of the envelope and the NS cooling but it can affect the spectrum of thermal radiation. Actually, the effect of the dipole surface magnetic fields $B \lesssim 5\times10^{12}$ G on the NS cooling is rather weak [165]. Therefore, our calculations can be used, at least qualitatively, for stars with such fields. In these cases, by T_s we mean the average effective surface temperature which determines the total (nonredshifted) photon surface luminosity of the star as $L_\gamma = 4\pi\sigma\mathcal{R}^2T_s^4$.

7.2.2 Models of cooling neutron stars. For simplicity, we assume that the matter of the NS core consists of neutrons, protons and electrons (muons and hyperons are absent). We will adopt a moderately stiff equation of state proposed by Prakash et al. [206] (the version with the compression modulus $K_0 = 180$ MeV and the same simplified symmetry factor S_V that was used in Ref. [5]). The maximum NS mass, for a given equation of state, is $1.73\,M_\odot$. In order to study the enhanced and standard cooling we consider NS models of two masses. In the first case, the NS mass is $M = 1.48\,M_\odot$, the radius $\mathcal{R} = 11.44$ km, and the central density $\rho_c = 1.376\times10^{15}$ g cm^{-3}, while in the second case $M = 1.30\,M_\odot$, $\mathcal{R} = 11.87$ km, and $\rho_c = 1.07\times10^{15}$ g cm^{-3}. The adopted equation of state opens the direct Urca process at the density $\rho > \rho_{cr} = 1.30\times10^{15}$ g cm^{-3}. Therefore, the $M = 1.48\,M_\odot$ NS suffers *enhanced* cooling: the powerful direct Urca process (4) is allowed in a small central kernel of radius 2.32 km and mass $0.035\,M_\odot$ (in addition to the processes (1)–(3) and (5) throughout the core). In the $M = 1.30\,M_\odot$ NS the threshold value ρ_{cr} is not reached, and the star has the *standard* neutrino luminosity, determined by the processes (1)–(3) and (5). Notice that Levenfish and Yakovlev [133], while calculating the equation of state, set the parameter n_0 (the standard saturation nuclear-matter density) equal to 0.165 fm^{-3}. In the present calculations we set $n_0 = 0.16$ fm^{-3}. Owing to this reason the mass of the rapidly cooling NS model is somewhat different from that ($1.44\,M_\odot$) used in Ref. [133].

In order to calculate the heat capacity of the superfluid NS core and its neutrino luminosity due to the reactions (1) – (5) we have used the equations of Sections 3 – 6. The results obtained in these sections are summarized in Section 6.2. The neutrino bremsstrahlung due to ee scattering in the NS core has been neglected: we have shown that its effect on the cooling is negligible, for our NS models. We have also taken into account the neutrino luminosity of the NS crust due to bremsstrahlung of electrons which scatter off atomic nuclei (using an approximate formula proposed in Ref. [123]): $L_{\rm br} = 1.65 \times 10^{39} (M_{\rm cr}/M_\odot) \times (T_{\rm b}/10^9\ {\rm K})^6 \exp(2\Phi_{\rm b})$ erg s^{-1}, where $M_{\rm cr}$ is the crust mass. In our case, $M_{\rm cr} = 0.0120 M_\odot$ for the $M = 1.48 M_\odot$ model, and $M_{\rm cr} = 0.0153 M_\odot$ for the $M = 1.3 M_\odot$ model. The NS heat capacity has been set equal to the sum of the partial heat capacities of n, p and e in the stellar core; the contribution of the crustal heat capacity has been neglected due to the smallness of the crust mass for the chosen NS models. In the calculations of the neutrino luminosity and the heat capacity the effective masses of neutrons and protons in the NS cores have been taken as $m_{\rm N}^* = 0.7\, m_{\rm N}$.

Various microscopic theories of Cooper pairing in the NS cores give a very wide scatter of the critical temperatures of the neutron and proton superfluids, $T_{\rm cn}$ and $T_{\rm cp}$ ($\sim 10^7 - 10^{10}$ K), and various density dependences of these temperatures (Section 3.1). Thus we have made a simplified assumption that the critical temperatures $T_{\rm cn}$ and $T_{\rm cp}$ are constant throughout the NS core and may be treated as free parameters. This is the main simplification of our simulations. We assume that protons suffer $^1S_0$-state pairing (superfluidity of type A, Table 1) and neutrons suffer $^3P_2$-state pairing with zero projection of the pair moment onto the quantization axis (superfluidity of type B). We will study the cooling for different values of $T_{\rm cn}$ and $T_{\rm cp}$, and we will determine (Section 8.2.2) those values which are in better agreement with observations.

As already mentioned in Section 7.1, the difference between the enhanced and standard cooling regimes is smeared out in the presence of superfluidity. Under these conditions, the cooling regime formally indicates whether direct Urca is allowed or forbidden in the NS core.

7.2.3 Results. We have calculated about 2000 NS cooling curves. The curves describe the dependence of the effective surface stellar temperature $T_{\rm s}^\infty = T_{\rm s}\sqrt{1 - \mathcal{R}_{\rm g}/\mathcal{R}}$, as detected by a distant observer, on age t; here, $\mathcal{R}_{\rm g}$ is the gravitational NS radius. For $M = 1.30\, M_\odot$ and $M = 1.48\, M_\odot$ we have $T_{\rm s}^\infty/T_{\rm s} = 0.822$ and 0.786, respectively. The critical temperatures of neutrons and protons, $T_{\rm cn}$ and $T_{\rm cp}$, in the NS core have been varied over a wide interval from 10^6 to 10^{10} K.

Examples of the cooling curves for selected values of $T_{\rm cn}$ and $T_{\rm cp}$ were already discussed above (Figs 15a and 15b). However it is rather inconvenient to analyze the results in the form of the cooling curves. It is better to plot the values of $T_{\rm cn}$, and $T_{\rm cp}$, which lead to certain surface temperatures $T_{\rm s}^\infty$ of the NS of given age t. Figures 16 – 19 present the results in this way. For example, we have chosen the values of t, which correspond to the ages of the Geminga pulsar (3.4×10^5 yr, Figs 16 and 18) and PSR 0656 + 14 (10^5 yr, Figs 17 and 19). Observational data on these and other cooling NSs are given in Section 8.1.

Before discussing the results of calculations let us recall some relationships which determine the main features of the NS cooling. We will use these relationships for describing Figs 16 – 19.

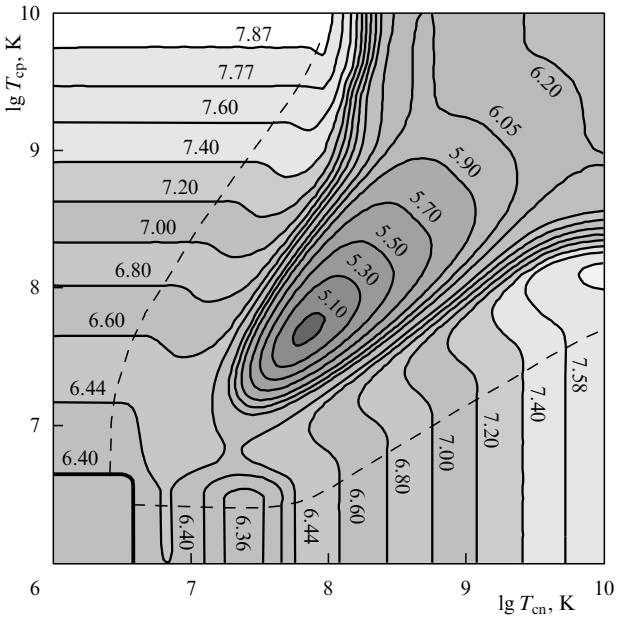

Figure 16. Lines of values of $T_{\rm cn}$ and $T_{\rm cp}$ which correspond to certain internal temperatures $T_{\rm i}$ (the values of lg $T_{\rm i}$ are given near the curves) or surface temperatures $T_{\rm s}^\infty$ (given in Table 2) of a NS with enhanced neutrino luminosity ($1.48\, M_\odot$) and Geminga's age (3.4×10^5 yr). The region of joint neutron and proton superfluidity (in the center and the upper right corner) is enclosed by the dashed lines. A small region where the superfluidity does not appear by the given age (the left lower corner) is separated by the thick solid line.

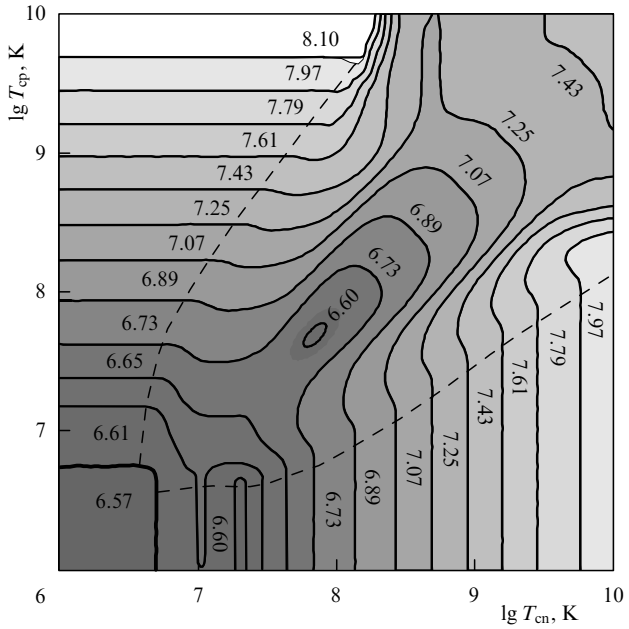

Figure 17. Same as in Fig. 16, but for a NS of the age of PSR 0656 + 14 (10^5 yr).

The effects of neutron and proton superfluidities on the heat capacity are different. In a non-superfluid NS, the heat capacities of p and n constitute $\sim 1/4$ and $\sim 3/4$ of the total heat capacity $C_{\rm tot}$, respectively. Therefore, a strong superfluidity of p reduces $C_{\rm tot}$ by $\sim 25\%$, while a strong superfluidity of n reduces it by about 4 times. When the ratio of the

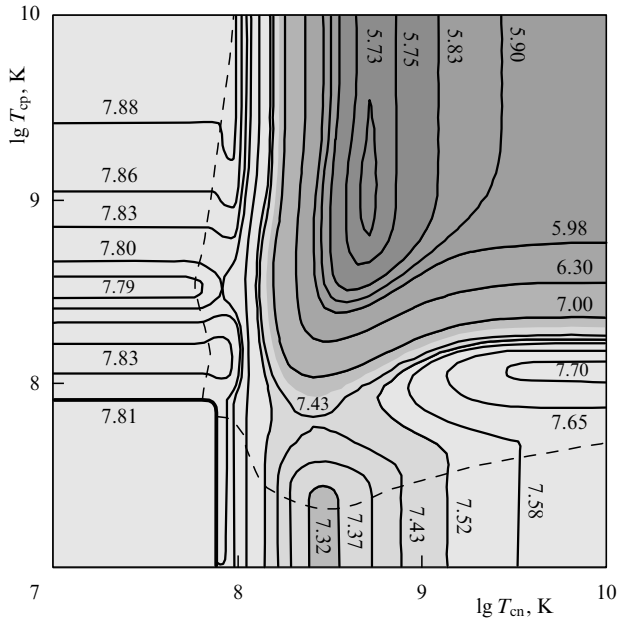

Figure 18. Isotherms of the internal temperature T_i (or the surface temperature T_s^∞, Table 2) for a NS of Geminga's age, as in Fig. 16, but for standard cooling ($1.30\,M_\odot$).

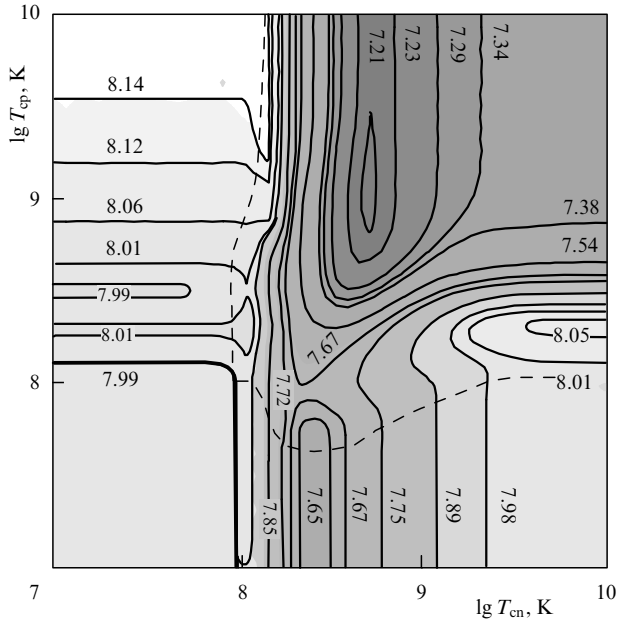

Figure 19. Same as in Fig. 18, but for a NS of the age of PSR 0656 + 14.

internal stellar temperature T_i to a critical nucleon temperature T_{cN} decreases from 0.3 to 0.1 (for instance, in the course of NS cooling), the heat capacity of nucleons N = n or p decreases by more than three orders of magnitude and becomes much lower than the heat capacity of electrons. Further reduction of the nucleon heat capacity does not change the total heat capacity. The appearance of the weak superfluidity of nucleons N almost doubles their heat capacity due to the latent heat release at the phase transition. The heat capacity of nucleons remains higher than the heat capacity of non-superfluid nucleons as long as T_i/T_{cN} decreases from 1 to 0.3, i.e., as long as the difference of temperature logarithms is $\lg T_{cN} - \lg T_i \leqslant 0.5$.

The effects of the superfluidities of n and p on the NS neutrino luminosity are also different. For the direct and modified Urca processes this difference is weak. If Cooper-pairing neutrino emission were neglected, the asymmetry of Figs 16–19 with respect to inversion of the axes $T_{cn} \rightleftarrows T_{cp}$, would be mainly explained by different contributions of n and p to the heat capacity. This can be proved by comparing Figs 16–19 with analogous figures in Ref. [133], where the neutrino emission due to Cooper pairing was neglected. Inclusion of the Cooper-pairing neutrinos greatly amplifies the asymmetry: the neutrino emission due to proton pairing is weak, while the emission due to neutron pairing dominates over the standard neutrino losses for $T_i \lesssim 10^9$ K $\lesssim T_{cn}$ and over the direct Urca process for $T_i \lesssim T_{cn} \ll T_{cp}$. The main neutrino energy release in the process takes place at $0.2 \lesssim T_i/T_{cn} \lesssim 0.96$ (as long as the difference of the temperature logarithms is $\lg T_{cn} - \lg T_i \leqslant 0.7$).

7.2.4 Enhanced cooling. Figures 16 and 17 illustrate the enhanced cooling of NSs of the ages of the Geminga and PSR 0656 + 14 pulsars.

Figure 16 shows isotherms of the internal temperature T_i of a NS of Geminga's age versus T_{cn} and T_{cp}. Since the temperature is related to the surface temperature, the same lines are isotherms of the surface temperature T_s^∞ (Table 2). Dashes exhibit the auxiliary lines which enclose the region of

Table 2. Relationship between T_i and T_s^∞ for Figs 16–19.

$M = 1.48M_\odot$		$M = 1.30M_\odot$	
lg T_i, K	lg T_s^∞, K	lg T_i, K	lg T_s^∞, K
5.10	4.53	5.73	4.8
5.30	4.61	5.75	4.79
5.50	4.68	5.83	4.82
5.70	4.76	5.90	4.85
5.90	4.84	5.98	4.88
6.05	4.91	6.30	5.02
6.20	4.98	7.00	5.37
6.36	5.05	7.21	5.48
6.40	5.07	7.23	5.49
6.44	5.09	7.29	5.53
6.57	5.16	7.32	5.54
6.60	5.17	7.34	5.55
6.61	5.18	7.38	5.57
6.65	5.20	7.43	5.60
6.73	5.24	7.52	5.65
6.80	5.28	7.54	5.66
6.89	5.32	7.58	5.69
7.00	5.38	7.65	5.72
7.07	5.42	7.67	5.74
7.20	5.49	7.70	5.75
7.25	5.52	7.75	5.78
7.40	5.60	7.79	5.80
7.43	5.62	7.80	5.81
7.60	5.71	7.81	5.81
7.61	5.72	7.83	5.82
7.77	5.81	7.85	5.84
7.79	5.82	7.86	5.84
7.87	5.86	7.88	5.85
7.97	5.92	7.89	5.86
8.10	5.99	7.98	5.91
		7.99	5.91
		8.01	5.93
		8.05	5.95
		8.06	5.95
		8.12	5.99
		8.14	6.00

joint superfluidity of nucleons. The region to the left of the upper dashed line corresponds to the superfluidity of protons and normal neutrons, while the region to the right of the lower line corresponds to the superfluidity of neutrons and normal protons. The dashed lines intersect at the isotherm of temperature $T_i = 10^{6.4}$ K, to which a non-superfluid star would cool by the moment t. This isotherm, plotted by a thick line, encloses the region where the nucleon superfluidity has not appeared by the moment t and does not affect the cooling. Notice, that owing to the effects of General Relativity, the isotherms T_i correspond to somewhat higher local temperatures of matter (see above). Thus, the isotherm $T_i = 10^{6.4}$ K is associated with values of T_{cN} which are slightly higher than T_i.

First we discuss the behavior of isotherms to the right of the lower auxiliary line. The vertical segments of the isotherms reveal that the NS cooling is governed only by the superfluidity of n. With increasing T_{cn} at $\lg T_{cn} \gtrsim 7.7$, the core temperature T_i grows which can be explained in the following way. The higher T_{cn}, the earlier the neutron superfluidity appears. Accordingly, the powerful direct Urca process is suppressed earlier, the cooling delay is longer, and the NS is hotter at a given t. For low T_{cn}, the NS cools down in a non-superfluid state almost all its life and is sufficiently cold by the age t. The neutrino luminosity of such a star is rather weak and becomes comparable to the photon luminosity. Additional neutrino energy losses due to neutron pairing at $\lg T_{cn} \gtrsim 6.6$ slightly accelerate the cooling at $6.6 \lesssim \lg T_{cn} \lesssim 6.6 + 0.7$. However, for $\lg T_{cn} \lesssim 6.6 + 0.5$ the acceleration is compensated by the latent heat release produced by the jump of the neutron heat capacity. The values 0.7 and 0.5 have been explained above.

Vertical segments of the isotherms intersect the auxiliary line at temperatures T_{cp}, at which the proton superfluidity appears. With a further increase of T_{cp}, the NS heat capacity (determined by protons for $\lg T_{cn} \gtrsim 7.4$) approximately doubles. The latent heat release increases T_i: in a strip of width 0.5 in $\lg T_{cp}$ above the lower dashed line the isotherms shift to the left. With further growth of T_{cp} the heat capacity is strongly reduced, the NS becomes cooler and the isotherms shift to the right.

In a similar fashion, exchanging the proton and neutron superfluids, we can explain the horizontal segments of the isotherms to the left of the upper auxiliary line. In this case acceleration of the NS cooling in the range $\lg T_{cp} \gtrsim 6.6$ does not appear because of the weakness of the neutrino emission produced by proton pairing. A strong proton superfluidity suppresses the heat capacity more weakly than a neutron superfluidity with the same critical temperature. Therefore, at high T_{cp} the star is warmer than for the same T_{cn} for the vertical segments of isotherms in the lower right part of the figure.

The horizontal segments of the isotherms intersect the upper auxiliary line at temperatures T_{cn} which switch on the neutron superfluidity. This superfluidity induces latent heat release and associated slight NS heating (dips on the isotherms to the right of the auxiliary line). With increasing T_{cp}, the NS heating produced by the neutron superfluidity becomes weaker and disappears (the dips vanish). The effect is mainly caused by neutrino emission due to neutron pairing which is more pronounced if the direct Urca process is strongly suppressed. At high T_{cp} the neutron pairing becomes the main neutrino emission mechanism. Since neutrino emission due to the neutron pairing is more efficient than the latent heat release the appearance of neutron superfluidity with the growth of T_{cn} does not delay the cooling but, on the contrary, accelerates it. A noticeable NS cooling via Cooper-pairing neutrinos takes place in a strip of width 0.7 (in $\lg T_{cn}$) to the right of the upper dashed line. Lower and to the right of this strip the cooling is associated with reduction of the neutron heat capacity.

Now consider the region of T_{cn}, T_{cp} between the auxiliary lines in more detail. Some increase of T_i at $\lg T_{cn} \lesssim 6.6 + 0.5$ and $\lg T_{cp} \lesssim 6.6 + 0.5$ is caused by the latent heat release at onset of superfluidity of n and p. Further growth of $T_{cn} \sim T_{cp}$ induces an initially rapid decrease and then a weak increase of T_i. The decrease is explained by exponential reduction of the heat capacity by the joint superfluidity of n and p while the weak increase is associated with reduction of the direct Urca process at the early cooling stages.

Figure 17 is analogous to Fig. 16, but corresponds to a younger NS of age 10^5 yr. Figures 16 and 17 show that one needs $T_{cp} \ll T_{cn}$ or $T_{cn} \ll T_{cp}$ to support a high surface temperature T_s^∞ (or T_i) for a longer time.

7.2.5 Standard cooling. Standard cooling of a $1.30\,M_\odot$ NS is illustrated in Figs 18 and 19 for the stars of Geminga and PSR 0656+14 ages, respectively. The isotherms are qualitatively different from those for the enhanced cooling (cf. with Figs 16 and 17): even an approximate symmetry of the neutron and proton superfluidities is absent. The asymmetry can be attributed to the weakness of the standard neutrino energy losses. First, in the absence of such a powerful cooling regulator as the direct Urca process the difference of the heat capacities of n and p (see above) is more pronounced. Second, the Cooper-pairing neutrino emission becomes more important on the background of weaker neutrino emission produced by other neutrino reactions; the Cooper-pairing emission is asymmetric itself, being more efficient for neutrons than for protons.

If the superfluidity is absent, a NS ($1.30\,M_\odot$) enters the photon cooling stage at $t_\nu \sim 1.6 \times 10^5$ yr. Thus the PSR 0656+14 pulsar appears to be at the transition stage and Geminga at the photon stage. The neutrino luminosity is already weak and the superfluidity affects the cooling mainly either through the heat capacity or through the neutrino emission due to Cooper pairing of neutrons and, to a less extent, of protons.

Consider, for instance, Fig. 18. Two dashed auxiliary lines enclose the domain of joint superfluidity of nucleons. To the left of the upper line protons are superfluid and neutrons not, while below the lower line only neutrons are superfluid. The lines intersect at the isotherm of the temperature $\lg T_i \approx 7.81$, which a non-superfluid NS would have by the age t. The superfluidity with $\lg T_{cn} \lesssim 7.9$ and $\lg T_{cp} \lesssim 7.9$ does not appear by the moment t and does not affect the cooling.

Horizontal segments of isotherms to the left of the upper dashed line show that the cooling is regulated by the proton superfluidity alone. For $\lg T_{cp} \gtrsim 7.9$ K, the superfluidity appears just before the given moment t and is weak. In the range $7.9 \lesssim \lg T_{cp} \lesssim 7.9 + 0.5$ it initiates latent heat release and a weak increase of the total heat capacity (determined mainly by normal neutrons). In the range $7.9 + 0.1 \lesssim T_{cp} \lesssim 7.9 + 0.7$ the weak increase of the heat capacity is compensated by the (also weak) increase of the neutrino emission due to pairing of protons. As a result, T_i

initially increases, and then decreases. For $\lg T_{cp} \gtrsim 8.4$, the proton heat capacity is reduced, and the total NS heat capacity decreases by $\sim 25\%$. On the other hand, for high T_{cp}, the proton superfluidity onset is shifted to the neutrino cooling stage. The cooling delay produced by the suppression of the neutrino luminosity in the neutrino era is somewhat stronger than the cooling acceleration produced by the effect of superfluidity on the heat capacity. Thus T_i continues its growth with increasing T_{cp}.

Horizontal segments of the isotherms end at temperatures $T_{cn} \sim 10^8$ K, at which the neutron superfluidity is switched on. The neutron pairing induces a splash of neutrino emission and cooling acceleration in a strip of width 0.7 (in $\lg T_{cn}$) to the right of the auxiliary line. The minimum of T_i occurs in the interval $8.5 \lesssim \lg T_{cn} \lesssim 8.7$, because at $8.0 \lesssim \lg T_{cn} \lesssim 8.0 + 0.5$ the neutrino energy losses are partly compensated by the latent heat release. The lowest temperatures T_i are realized in the case $T_{cp} \gg 10^8$ K, in which the nucleon heat capacity suffers the strongest suppression.

On vertical segments of the isotherms below the lower dashed line the cooling is regulated by the neutron superfluidity alone. With growing T_{cn} in this domain, the temperature T_i varies in the same manner as with growing T_{cp} in the domain of the purely proton superfluidity. This happens because at $\lg T_{cn} \gtrsim 7.9$ the neutrino emission due to neutron pairing is important. It speeds up the NS cooling in the range $7.9 \lesssim \lg T_{cn} \lesssim 7.9 + 0.7$ (see above). If $7.9 \lesssim \lg T_{cn} \lesssim 7.9 + 0.5$, the neutrino cooling is partly compensated by the latent heat release. Therefore the minimum of T_i occurs in the range $7.9 + 0.5 \lesssim \lg T_{cn} \lesssim 7.9 + 0.7$. It is not so deep as in the upper part of Fig. 18 since the nucleon heat capacity is now suppressed only partly.

A strong neutron superfluidity reduces the heat capacity more strongly and the neutrino luminosity more weakly than a strong proton superfluidity. Owing to the weakness of the neutrino energy losses this difference is sufficient for a NS with high T_{cn} and normal p to cool in a different way than at equally high T_{cp} and normal n. The strong neutron superfluidity delays the cooling of those NSs which would be at the neutrino cooling stage or at the neutrino-photon transition stage if they were non-superfluid. This is demonstrated in Fig. 19 (for PSR 0656+14); in the absence of superfluidity at $t = 10^5$ yr the pulsar would be at the transition stage. The strong neutron superfluidity accelerates the cooling of older NSs, e.g., of Geminga's age (Fig. 18).

The vertical segments of isotherms in Fig. 18 intersect the auxiliary line at temperatures T_{cp}, at which the proton superfluidity appears. This superfluidity leads to latent heat release and to the growth of T_i in a strip of width 0.5 in $\lg T_{cp}$ above the lower dashed line. With further growth of T_{cp} the heat capacity is strongly reduced and the cooling is accelerated. For a very strong joint superfluidity of n and p ($T_{cn} \gg 10^{7.9}$ K, $T_{cp} \gg 10^{7.9}$ K, the very right upper corner of Fig. 18), the nucleon heat capacity and the neutrino luminosity of the NS core are fully suppressed, and the cooling is governed by the electron heat capacity.

Figure 19 is analogous to Fig. 18, but corresponds to a younger NS. Its neutrino luminosity is somewhat higher and the relative contribution of nucleon-pairing neutrinos is smaller. The neutrino emission produced by pairing affects the cooling more weakly.

Comparison of the present calculations with observations will be made in the next section.

8. Thermal emission from neutron stars and superfluidity in their cores

8.1 Thermal emission from neutron stars

8.1.1 Observations of X-ray emission from neutron stars. In the very first article devoted to NSs Baade and Zwicky [207] predicted that NSs should be born hot and cool gradually emitting thermal radiation. Since NSs are compact, their radiation is weak. Modern detectors are able to register it only from the closest ($D \lesssim 1-2$ kpc) and sufficiently hot ($T_s \gtrsim 10^5 - 10^6$ K) isolated NSs. The main radiation flux for the surface temperatures T_s mentioned above is emitted in the soft X-ray and hard ultraviolet spectral ranges (0.01 – 1 keV), which are thus most favorable for observations. This radiation, however, is strongly absorbed by the Earth's atmosphere and can be detected only from balloons, rockets and space observatories.

Attempts to discover NSs from their thermal surface emission undertaken in the middle of 1960s in the first balloon experiments with X-ray detectors were not successful. NSs were discovered later, in 1967, as radio pulsars [208]. Soon afterwards they were also discovered in X-rays as X-ray pulsars, X-ray bursters and transients; however, the radiation from these objects is determined by accretion of matter onto the NSs in binary systems, but not by outflow of thermal energy from the interiors of cooling NSs. A search for intrinsic thermal radiation from NSs was continued.

In 1975 Wolff et al. [209] as well as Toor and Seward [210] attempted to detect the thermal radiation of the Crab pulsar in a balloon experiment during a lunar occultation of the pulsar. The thermal radiation was not detected but the upper limit of the surface temperature of the pulsar was established which does not differ considerably from the present upper limit.

Subsequent observations were mainly carried out in the soft X-rays with the X-ray telescopes on board the orbital observatories *Einstein* (1978 – 1981), *EXOSAT* (The European X-Ray Observatory Satellite, 1983 – 1986), *ROSAT* (The Röntgen Satellite, 1990 – 1998), *ASCA* (The Advanced Satellite for Cosmology and Astrophysics, operating since 1993) and *RXTE* (The Rossi X-ray Timing Explorer, launched in December, 1995). In these studies, various types of detectors have been used: gaseous (scintillation) photon proportional counters which possess moderate spectral resolution (from ~ 8 to 40%, depending on the detector scheme and photon energy) and rather large angular resolution ($\sim 12'' - 3'$); solid-state microchannel photodetectors with high angular resolution (down to $3''$) but giving almost no spectral information; solid-state CCD matrices with higher spectral resolution (to 3%) than the gaseous detectors, but worse angular resolution ($1'$) than the microchannel photodetectors. Temporal resolution (0.001 – 0.5 ms), in most cases, enables one to study variations of the radiation fluxes concerned, for instance, with NS rotation. By the moment of completing this review the best angular, spectral and temporal resolutions were possessed by, respectively: the microchannel X-ray detector HRI (High Resolution Imager) on board *ROSAT* ($\sim 5''$ in the energy range 0.1 – 2.5 keV), the detector SIS (Solid-state Imaging Spectrometer) on board *ASCA* (0.4 – 10 keV, $\Delta E/E \sim 2\%$ for photon energy $E \sim 6$ keV) and PCA (Proportional Counter Array) on *RXTE* (~ 1 μs in 2 – 60 keV range). X-ray detectors have high sensitivity. For instance, the *ROSAT* observatory was able to detect sources with a flux $\sim 5 \times 10^{-14}$ erg cm^{-2} s^{-1}.

Orbital observatories have led to great progress in the search for thermal NS radiation. Soft X-ray radiation has been detected from about thirty radio pulsars and from several isolated radio silent NSs. Thermal component has been identified sufficiently reliably in $\sim 20\%$ of cases [1].

A search for the thermal radiation from NS surfaces was also carried out with the ultraviolet observatory *EUVE* (The Extreme Ultra-Violet Explorer, operating since 1992) using the DS (Deep Survey) and ST (Scanning Telescope) telescopes, sensitive in the photon energy range 70 – 760 eV, with the angular resolution $\sim 30 - 45''$ (using wideband filters 40 – 190 A and 160 – 238 A). About 20 known NSs were observed [211]. Five sources were detected in the 40 – 190 A band. Two of them, PSR 0656 + 14 and Geminga, are cooling pulsars, and one, RX J1856-37, is an isolated (probably cooling) radio silent NS. For other objects, the upper limits to the ultraviolet fluxes were obtained.

Since 1978 wideband photometric observations of isolated NSs have been carried out in optics using sensitive ground-based telescopes such as ESO-NTT (The New Technology Telescope of the European South Observatory), the Keck Telescope, the 6-meter Telescope, and the orbital HST (the Hubble Space Telescope, launched in 1990). About ten radio pulsars have been identified as optical sources [212]. As a rule, the luminosity of isolated NSs in optics is several orders of magnitude weaker than in X-rays. This serves as an additional argument in identifying point-like X-ray sources as isolated NSs, especially if they are not pulsars. The point-like X-ray sources associated with accreting NSs in close binaries in pairs with normal stars (X-ray pulsars, bursters, transients) usually show higher optical fluxes due to the contribution of companions or accretion disks. Multicolor photometric observations have been carried out for several isolated NSs (PSR 0540 – 69, PSR 1509-58, PSR 0656 + 14, Crab, Vela, Geminga), while for others (PSR 1929 + 10, PSR 0950 + 08, PSR 1055 – 52, RX J185635 – 3854, RX J0720.4 – 3125) the fluxes have been measured with one or two filters only. Recently Martin et al. [213], using the 10-meter Keck Telescope, obtained the first optical spectra (with ~ 2 A resolution), of Geminga, the isolated middle-aged pulsar. Earlier the spectroscopic observations were carried out of only two young pulsars, Crab and PSR 0540 – 69, whose optical emission is non-thermal. Recently Shearer et al. [214], using the MAMA (Multiple Anode Microchannel-Plate Array) detector with high temporal resolution and the 6-meter Telescope, discovered temporal variations of the optical emission (in the B-filter) from Geminga and PSR 0656 + 14, cooling medium-aged NSs; the radiation pulsates with the NS spin periods. Earlier, pulsating optical emission had been observed only from several young pulsars (including Crab, Vela, PSR 0540 – 69) with spectra of a clearly non-thermal origin. The energy of the non-thermal emission is taken mainly from the NS spin energy.

The optical and ultraviolet observations complement the X-ray spectra with data in Rayleigh-Jeans part of the spectrum. This enables one to get more definite conclusions on the spectrum type (thermal or non-thermal) and on the parameters of the NS atmospheres. Interpretation of the thermal radiation has to be consistent with observations of the non-thermal emission from pulsars and nearby space in radio, X-rays and gamma-rays. Finally, one should use modern atmospheric models of NS radiation for a correct interpretation of observations.

8.1.2 Interpretation of observations. The discovery and interpretation of the thermal radiation from cooling NSs is a complicated problem. As mentioned above, the radiation is weak since the NSs are compact. The radiation has to be separated from the surrounding background which is especially difficult for young NSs in supernova remnants. The strong background is created by non-thermal emission of synchrotron nebulae (plerions) which are formed around young and active pulsars. The background is also produced in non-thermal processes of emission of X-ray and optical quanta in the magnetospheres of radio pulsars. The distances to NSs are known poorly (the uncertainty is often some ten percent or higher). The next difficulty is provided by interstellar gas which absorbs the soft part of the spectrum (from a fraction of keV down to optics), especially for objects which are more distant than some hundred pc or are obscured by local clumps of interstellar gas. Finally, the thermal radiation from the main part of the pulsar's surface is superimposed by the thermal radiation from the hotter ($\sim (2-3) \times 10^6$ K) polar caps heated by fluxes of energetic particles from the magnetosphere. The spectra of both thermal components and the power-law spectrum of the possible non-thermal component strongly overlap which complicates interpretation even more.

It is clear that the medium-aged radio pulsars ($\sim 10^4 - 10^6$ yr) are most favorable for studies of thermal radiation. Their surface is still rather hot, $T_s \sim 10^5 - 10^6$ K, enough to be observable but the objects are already insufficiently active to support synchrotron nebulae around them. Supernova remnants are dissolved by the given age, and the non-thermal magnetospheric processes weaken due to pulsar spin down. All these factors reduce the background and increase the chances of discovering radiation from the pulsar surface. The isolated NSs which, for some reason, do not show pulsar activity from the early stage, for instance, due to the weak magnetic field or rapid spin down are of special interest for the cooling theory. These stars should possess a lower background of non-thermal emission which simplifies detection of the thermal component (see below).

An observer who studies X-ray radiation from cooling NSs usually has a poor set of observational data in the form of photon count rates in various spectral channels of a detector; the count rates do not exceed, for instance, 1 – 10 counts per second for the brightest objects detected with PSPC (Position Sensitive Proportional Counter) on board *ROSAT*. For the majority of isolated NSs observed with *ROSAT*, the count rate is $\sim 10^{-3} - 10^{-2}$ counts per second; therefore, the exposure time should exceed ten hours to accumulate a statistically significant number of counts (e.g., 100 – 1000). Data processing and reconstruction of the real spectrum of the NS radiation is an example of a classical incorrect inverse problem which can be solved only under additional assumptions on the spectrum of the source. The spectral analysis is usually carried out by calculating the count rates in different channels by 'transmitting' a model spectral flux of the object through the response matrix of a detector; calculated values are then compared with observations. A model flux depends on NS parameters such as distance, column density of interstellar hydrogen, etc. These parameters are varied (for instance, by the χ^2 method) to obtain the best agreement with

[1] More detailed information on active and future detectors can be found, for instance, through the Internet site *http://heasarc.gsfc.nasa.gov/docs/heasarc/missions.html*.

observations. However the response matrix is usually known with some uncertainty. Its parameters vary in time and require permanent checking using calibration sources on board a space observatory or cosmic standard sources. The model spectrum may be multicomponent; for instance, it may contain contributions of thermal emission from the main part of the pulsar surface and from the hot polar caps as well as non-thermal magnetospheric emission. While fitting the spectrum one can, in principle, determine all the varying quantities: parameters of the NS thermal radiation (effective temperature, magnetic field and chemical composition of the surface), parameters of the hard radiation component (temperature and sizes of polar caps), the spectral index and intensity of the non-thermal component, the spin period, the NS radius and mass, the distance, the column density of interstellar gas, etc. Additional constraints on the variable quantities can be obtained from similar fitting of X-ray light curves.

A complete realization of the above scheme is not possible, to date, mainly because of the poor statistics of photon counts and the poor spectral resolution of the detectors. Another obstacle comes from incompleteness of the theory of magnetospheric pulsar emission and the theory of atmospheres of isolated NSs with strong magnetic fields. The non-thermal magnetospheric radiation is usually described by a power-law spectrum with an index determined from fitting. In the absence of atmosphere models, the thermal NS radiation is often described by a black body spectrum. However, the properties of radiation emerging from a NS are actually determined by a thin atmosphere with the temperature growing inside the star. The atmospheric spectrum may significantly differ from black body. This is proved by the well elaborated models of NS atmospheres with 'weak' magnetic fields $B \lesssim 10^9 - 10^{10}$ G [215, 216, 7] and hot atmospheres ($T_s > 10^6$ K) with strong fields $B \gtrsim 10^{11}$ G [6, 7]. In particular, the radiation spectra from weakly magnetized NSs covered with atmospheres of light elements (hydrogen, helium) appear to be harder for the same effective temperature T_s. For typical temperatures $T_s \sim 10^5 - 10^6$ K, the light elements are almost completely ionized; the main contribution to opacity comes from free-free transitions which are well described by the Kramers formula (the spectral opacity decreases as E^{-3} with the growth of photon energy E). This makes the atmosphere more transparent for higher-energy photons, which emerge thus from deeper and hotter layers, leading to hardening of the spectrum. In the atmospheres of heavier elements (iron), which are more difficult to ionize, the photoeffect and bound–bound transitions are most important. This leads to a weaker energy dependence of the opacity on the photon energy. The radiation spectrum becomes closer to that of black body, with a temperature corresponding to some mean depth from which the quanta emerge. In this case the almost Planckian continuum contains deep and wide photoionization jumps and absorption lines of atoms and ions of heavy elements. In contrast to the black body emission, the atmospheric radiation is anisotropic even for NSs with weak magnetic fields. The anisotropy depends on photon energy and chemical composition; the well known 'limb darkening' effect is quite pronounced. The anisotropy is greatly amplified by a strong magnetic field. In this case, the anisotropy axis is aligned along the magnetic field and the radiation beaming can be strongly asymmetric. An allowance for the anisotropy and gravitational bending of photon trajectories near the NS surface [217] is especially important for interpretation of the light curves.

To date, among the models of NS atmospheres with strong magnetic fields, $B \gtrsim 10^{10} - 10^{11}$ G, only the models of hot atmospheres ($T_s > 10^6$ K) composed of fully ionized plasma are reliable. According to these models, the radiation spectrum becomes softer than for weaker magnetic fields, but remains noticeably harder than the Planck spectrum. For lower temperatures, the magnetized atmospheres become partly ionized. The strong magnetic fields drastically distort the structure of atoms and ions and affect the spectral opacity. Detailed calculation of the opacity is complicated and has not been done yet even for the simplest case of a hydrogen plasma. The magnetic field increases the binding energies of electrons in atoms. For instance, the field $B \sim 10^{12}$ G amplifies the binding energy of the hydrogen atom to ~ 150 eV. The number density of neutral atoms becomes larger increasing the role of the photoeffect and bound–bound transitions; these processes must be calculated with allowance for thermal motion of atoms. Such calculations are complicated since the electric fields induced in an atom-comoving reference frame due to atomic motion across the magnetic field are so strong that they change the structure of atomic energy levels and probabilities of radiative transitions (the dynamic Stark-effect; see, e.g., Ref. [218]). While calculating the opacity of this partly ionized plasma it is important to take into account the effects of plasma non-ideality and pressure ionization. These calculations are being performed at present. Only models of hydrogen and iron atmospheres neglecting the dynamic Stark effect have been constructed so far [219, 220]. The dependence of the radiation spectrum on chemical composition has the same tendencies as for the atmospheres with a weak field. The spectra of the iron atmospheres are softer and closer to those of black body than the spectra of the hydrogen atmospheres. An account for the induced electric fields, which strongly broaden the photoionization jumps and other spectral features, will enable one to check the above statement.

Owing to the effects mentioned above an 'atmospheric' temperature T_s appears to be significantly lower (typically, by a factor of $1.5-3$) than a 'black body' temperature in the interpretation of the same observational data. If the validity conditions of the available atmosphere models are fulfilled, then the spectra of the thermal radiation and the NS light curves are better fitted by the atmosphere models than by the black body. The parameters inferred from atmospheric interpretation (emitting surface area, distance to the NS, column density of the interstellar gas, etc.) are, as a rule, in better agreement with the data provided by independent observations in other spectral bands (see, e.g., Refs [221, 222]). The black body interpretation often gives less realistic parameter values and meets some difficulties in explaining all the set of observational data.

Since the statistics of count rates are commonly poor and the number of adjustable parameters is large, the confidence ranges of these parameters are often too wide. To make them narrower some parameters are fixed (NS mass and radius, distance, etc.). The parameters then become more constrained. In a sense, this is an illusion if not confirmed by the results of independent observations (e.g., in other spectral bands). For instance, radio observations of non-thermal pulsar emission are very useful for the interpretation of X-ray observations. They give additional constraints on the distance from parallax measurements, on interstellar extinc-

tion from dispersion measure determination, on orientation of the NS spin and magnetic axes from polarimetric measurements, on pulsar age from measurements of the spin down rate, on the stellar mass from measurements of orbital parameters of binary systems containing NSs, etc. Additional constraints can also be obtained from optical and gamma-ray observations.

8.1.3 Observational results. As a result of a more than 30-year search for thermal radiation, X-ray radiation has been discovered or upper limits of the surface temperature have been obtained for some tens of isolated NSs [223, 224]. However, so far the discovery of the thermal component can be regarded as definite only in several cases. These cases include the four closest medium-aged radio pulsars (Vela, Geminga, PSR 0656 + 14 and PSR 1055 – 52) and three fairly young radio silent NSs in supernova remnants (1E 1207 – 52 in the remnant PKS 1209-51/52, RX J0002 + 62 near CTB-1 and RX J0822 – 4300 in Puppis A). All seven sources are reliably identified; their nature as isolated NSs is confirmed by observations of periodic pulsations (excluding 1E 1207 – 52), produced by stellar rotation, and/or the large ratio of the X-ray to optic luminosities. These NSs are listed in Table 3 in accordance with their age. For each star, we give its characteristic age (determined either from the NS spin down rate or from the morphology of a supernova remnant), the spin period, the method of interpretation of the thermal spectrum, the effective surface NS temperature $T_{\rm s}^{\infty} = T_{\rm s}\sqrt{1-(\mathcal{R}_{\rm g}/\mathcal{R})}$ (Section 7.2.3) determined by this method, and the distance to the source.

Among the 'atmospheric' interpretations presented in Table 3, those for 1E 1207 – 52, RX J0002 + 62, RX J0822 – 43 and the Vela pulsar seem to be the most reliable. The interpretation of their spectra with hydrogen–helium atmosphere models has an additional advantage: the fits of observational data with iron atmosphere models or with the black body spectrum are of lower statistical significance. Geminga and PSR 0656 + 14 are older and cooler. An important contribution to the opacity of their atmospheres comes from the effects of motion of neutral and partly ionized atoms across a strong magnetic field (see Refs [225, 226] and also Section 8.1.2). The presented interpretations have been made using simplified atmosphere models in which these effects have been neglected. The hydrogen composition of Geminga's atmosphere is additionally confirmed by a possible discovery of the proton cyclotron line in its optical spectrum [227, 213]. The 'atmospheric' temperatures of Geminga and PSR 0656 + 14 are likely to be closer to reality than the 'black body' temperatures but less reliable than for younger NSs.

Comparison of the surface temperatures of the objects from Table 3 with the simulations of NS cooling will be discussed in Section 8.2. In this discussion we will assume that the 'atmospheric' and 'black body' interpretations of observations are equally acceptable and obtain constraints on critical temperatures of nucleon superfluidity in the NS cores. Here we will outline some other observations.

The upper limits of $T_{\rm s}$ for the majority of other objects are too high to be of interest for the NS cooling theory. Let us mention only the upper limit of the surface temperature of the young Crab pulsar. Numerous attempts to detect thermal radiation from the pulsar have failed due to the powerful nonthermal radiation from the magnetosphere and supernova remnant over a wide spectral range. The most stringent upper limit $T_{\rm s}^{\infty} = 1.55 \times 10^6$ K was obtained by Becker and Aschenbach [228] from the *ROSAT* observations. Taking into account the uncertainty in distance and interstellar absorption, this upper limit does not contradict the standard cooling of the Crab pulsar (with a non-superfluid core) although for stiffer equations of state the agreement is rather questionable. Let us mention that the surface temperature of Crab can be estimated independently from observations of after-glitch relaxation. According to the theory, this relaxation depends on the internal NS temperature, and the internal temperature is related to the surface one. Such estimates are not very definite but give $T_{\rm s}^{\infty} \approx 1.6 \times 10^6$ K [229], in excellent agreement with the above upper limit.

There are about ten more potential candidates to the cooling isolated NSs among radio silent compact X-ray sources in addition to those listed in Table 3. New observations are required to confirm that these sources are cooling NSs. The two most probable candidates are the point-like X-ray objects in the young supernova remnants: 1E 1841 – 045 in the center of Kes 73 and 1E 161348 – 5055 in the center of RCW 103. Both objects have close black body temperatures, $T_{\rm s} \sim 0.7$ and ~ 0.6 keV. Such temperatures are too high for ordinary cooling NSs of supernova remnant ages, $\sim 2000 - 4000$ yr [230, 231]. However, for 1E 1841 – 045, the above age agrees with its dynamic age determined from the spin down rate (from observations of coherent pulsations of X-ray emission discovered recently), $P = 11.8$ s and $\dot{P} = 4.73 \times 10^{-11}$ s s^{-1} [232]. The standard (for radio pulsars) estimate of the magnetic field from P and $\dot{P}$ reveals the enormous field strength $B \sim 10^{15}$ G. Optical and radio emission from the objects has not been discovered. If confirmed in future observations (in accord with preliminary estimates [166]), these data can be explained by the thermal radiation from young cooling NSs with superstrong magnetic fields and with outer shells composed of light elements. The presence of a superstrong field and a shell increases the thermal conductivity of the outer layers and, as a consequence, increases the surface temperature at the early cooling stage. For the second source, 1E 161348 – 5055, this hypothesis should be treated with great care due to the recently discovered mysterious increase of luminosity for several months accompanied by an increase of the X-ray flux by an order of magnitude with an unchanged spectrum [233]. A search for pulsations with the NS spin period has not been successful so far for this object, which has been observed regularly in X-rays since 1979.

The sources of repeating soft gamma-ray emission (SGRs — *soft gamma repeaters*) possibly belong to the same family of cooling NSs with a superstrong magnetic field (called 'magnetars' [234]). However, they probably undergo a different evolutionary stage. All of them are located near supernova remnants which indicates that they are young. For two of them, SGR 1900 + 14 and SGR 1806 – 20, coherent pulsations of X-ray radiation with periods 5.16 and 7.47 s, respectively, have been discovered recently [235 – 237]. Both sources have about the same large braking index as the source in Kes 73. The estimated surface temperatures of the objects ($T_{\rm s} \lesssim 1$ keV) exceed typical temperatures of ordinary cooling NSs of their ages ($t \lesssim 1000 - 10000$ yr), if the ages are the same as the parental supernova remnants.

Let us mention one more type of source. These are the so called 'anomalous X-ray pulsars', X-ray sources with a soft thermal spectrum ($T \lesssim 1$ keV; e.g., Ref. [238]) and almost sinusoidal light curve. Typical periods of their brightness

variation are about ten seconds. The magnitude of the pulsating component of their radiation is anomalously small and more typical for the thermal radiation from the surface of a cooling NS than for an X-ray pulsar. One cannot exclude that at least some of these objects also belong to the family of cooling magnetars. No binary companions were found for these objects, and no accretion disks which would provide accreted matter for X-ray pulsars. Powerful electrodynamic radiation of a rotating NS with a superstrong magnetic field would naturally explain the rapid spin down; an increase of the thermal conductivity of the outer layers would produce a sufficiently high surface temperature. The low ages of some anomalous pulsars are also confirmed by the coincidence of their positions with the centers of supernova remnants. They are also radio silent.

Finally, let us mention two more radio silent isolated NSs. They have been discovered quite recently; first, as bright point-like sources of soft X-ray radiation in the *ROSAT* surveys, and later as weak optical objects in special observations with the ground-based Keck Telescope and the Hubble Space Telescope. These stars are not associated with supernova remnants.

One of them, RX J1856.5−3754 [239, 240] has a black body surface temperature $(8.5 \pm 1.4) \times 10^5$K [241] for the adopted values of $\mathcal{R} = 10$ km and $M = 1.4 M_\odot$, and is situated at a distance $D \lesssim 130$ pc. The radiation fluxes in the optical filters F606W (6000 A) and F300W (3000 A), detected with the Hubble Space Telescope [240], are 25.9 and 23.48 stellar magnitudes, respectively. They agree with the hypothesis on the thermal origin of the spectrum in the spectral range from optics to X-rays. The upper limit on the pulsating component is rather high (about 15%). Further accumulation of photon statistics will enable one to continue the search for periodic pulsations. On the other hand, the observed thermal radiation can be explained by accretion of interstellar gas on a cold, weakly magnetized NS which moves slowly through interstellar matter [240, 242]. In order to choose between these two hypotheses one needs to measure the parallax and proper motion of the object.

The other NS, RX J0720.4−3125, is somewhat hotter (the black body surface temperature is 79 ± 4 eV). Its X-ray flux pulsates with the period 8.39 s and modulation $\sim 12\%$ [243]. There are not very reliable indications of the spin down, $\dot{P} \sim 10^{-11} - 10^{-12}$ s s^{-1}. Optical observations with the Keck Telescope indicate the presence of an object identified with this source. The detected fluxes are 26.6 ± 0.2 and 26.9 ± 0.3 stellar magnitudes in the B and R filters, respectively [244]. For a distance to the source $D \lesssim 100$ pc, the weakness of the optical emission is in favor of the hypothesis that the object is an isolated NS. One can expect to be dealing either with a cooling NS-magnetar or with an old, weakly magnetized NS accreting matter from the interstellar medium. A choice of correct hypothesis can be made only on the basis of future observations.

Let us also mention two more radio silent NSs, RX J0806.4−4123 [245] and 1RX J130848.6 +212708 [246] discovered most recently in the *ROSAT* surveys; they are very similar to the two latter NSs. They are possibly cooling NSs [247] but the observations are still insufficient to draw final conclusions.

8.2 Theory and observations of cooling neutron stars

8.2.1 Necessity of superfluidity for interpretation of observations. The aim of this section is to confront the cooling theory of superfluid NSs (Section 7.2) with observations (Section 8.1). Table 3 presents the data on the surface temperatures of seven isolated NSs. In Fig. 20 these data (circles) are compared with the cooling curves (Section 7.2). The diagonal and horizontal shading shows the regions of the surface temperature $T_s^\infty(t)$ filled, respectively, by different standard and enhanced cooling curves calculated by varying T_{cn} and T_{cp} from 10^6 to 10^{10} K. The short-dash curves show cooling of non-superfluid stars.

The 'non-superfluid' curves are seen to be in poor agreement with observations. On the other hand, the observations can be explained by assuming superfluidity in the NS cores. This is illustrated by the standard cooling curve (the solid line). The values of T_{cn} and T_{cp} are chosen in such a way that the curve describes the maximum number of observational points at once.

According to Fig. 20, all the 'atmospheric' temperatures as well as the 'black body' temperatures of RX J0002+62, PSR 0656+14 and Geminga are located in the allowed regions of the standard and enhanced cooling of superfluid NSs. Thus our cooling calculations can be compared with the 'atmospheric' and 'black body' temperatures T_s of these sources.

The high black body surface temperatures of RX J0822−43, 1E 1207−52 (not presented in Fig. 20, but given in Table 3), Vela, and PSR 1055−52 are not explained by our

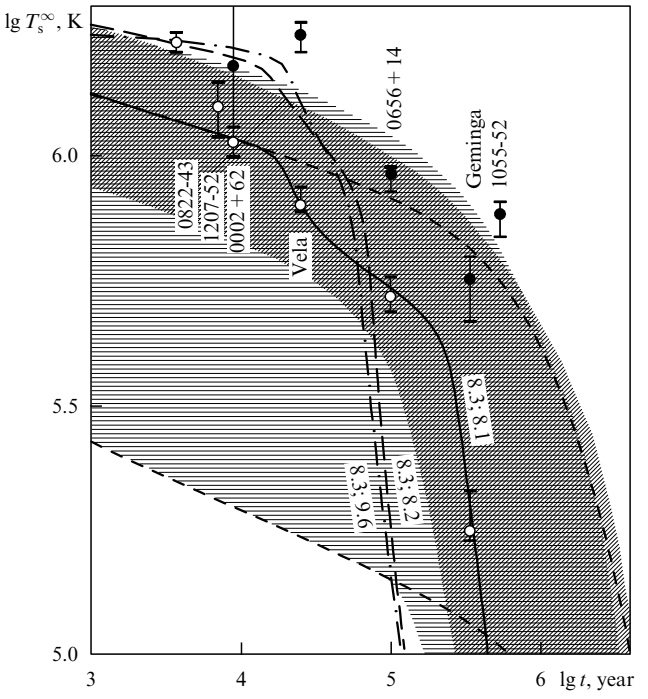

Figure 20. Observational data on the surface temperatures of NSs obtained (Table 3) in the models of black body radiation (filled circles) and hydrogen atmosphere (open circles). The shaded regions show the ranges of T_s^∞ filled by the standard (diagonal shading) and the enhanced (horizontal shading) cooling curves of NSs with different masses $1.30\,M_\odot$ and $M = 1.48\,M_\odot$ (for various T_{cn} and T_{cp}). The solid line shows the standard cooling ($1.30\,M_\odot$) for the specified values lg T_{cn} and lg T_{cp} (given near the curve). The short-dashed lines exhibit the standard (upper line) and enhanced (lower line) cooling of a non-superfluid NS. The dashed and dot-and-dashed lines show, respectively, the standard and enhanced cooling of a NS which possesses an envelope of mass $7 \times 10^{-10} M_\odot$ composed of light elements (see Section 8.2.1).

Table 3. Observational data.

Source	lg t, year	P, ms	Model *	lg T_s^∞, K	Confidence level T_s^∞, % **	Distance, kpc	References
RX J0822 – 43	3.57	75	H	$6.23^{+0.02}_{-0.02}$	95.5%	1.9 – 2.5	[252]
			bb	$6.61^{+0.05}_{-0.05}$	95.5%	2.5 – 3.5	[252]
1E 1207 – 52	3.85	—	H	$6.10^{+0.05}_{-0.06}$	90%	1.6 – 3.3	[222]
			bb	$6.49^{+0.2}_{-0.01}$	90%	11 – 13	[222]
RX J0002 + 62	3.95 ***	242 ****	H	$6.03^{+0.03}_{-0.03}$	95.5%	2.7 – 3.5	[251]
			bb	$6.18^{+0.18}_{-0.18}$	95.5%	3.1 ± 0.4	[251]
PSR 0833 – 45 (Vela)	4.4 *****	89	H	$5.90^{+0.04}_{-0.01}$	90%	0.4 ± 0.12	[221]
			bb	$6.24^{+0.03}_{-0.03}$	—	0.5	[253]
PSR 0656 + 14	5.00	385	H	$5.72^{+0.04}_{-0.02}$	—	$0.28^{+0.06}_{-0.05}$	[254]
			bb	$5.96^{+0.02}_{-0.03}$	90%	0.76	[255]
R S R 0630 + 178 (Geminga)	5.53	237	H	$5.25^{+0.08}_{-0.01}$	90%	0.008 – 0.022	[256]
			bb	$5.75^{+0.05}_{-0.08}$	90%	0.16	[257]
PSR 1055 – 52	5.73	197	bb	$5.88^{+0.03}_{-0.04}$	—	0.9	[253]

* H observations are interpreted with a hydrogen atmosphere model, bb with a black body spectrum.
** Confidence level of temperature T_s^∞ (95.5% corresponds to the 2σ level, and 90% corresponds to 1.64σ); a dash means that the level is not indicated in the cited references.
*** The mean age is taken according to Ref. [248].
**** According to Ref. [249]
***** According to Ref. [250]

models but can be explained by other models of cooling NSs, particularly, models with superfluid cores. For instance, the observations of the Vela pulsar agree with the standard cooling of a superfluid NS ($T_{cn} = 10^7$ K, $T_{cp} = 10^{10}$ K) possessing an outer envelope of mass $\sim 10^{-9} M_\odot$ composed of light elements [173]. High black body temperatures of RX J0822 – 43, 1E 1207 – 52 and PSR 1055 – 52 may indicate either the presence of some additional reheating mechanism inside these sources (Section 8.1) or the presence of superstrong ($B \gtrsim 10^{14}$ G) magnetic fields (e.g., Ref. [166]). Finally, one cannot exclude that the black body interpretation of their spectra is incorrect (Section 8.1.2).

8.2.2 Confronting calculations and observations. Let us analyze which critical temperatures of nucleon superfluidity in the NS cores, T_{cn} and T_{cp}, used in the cooling simulations (Section 7.2) agree with the observations of the NS thermal radiation (Table 3). As seen from Fig. 20, we can explain the majority of NS observations either by standard or by enhanced NS cooling assuming the presence of nucleon superfluidity. These observations include six 'atmospheric' interpretations (RX J0822 – 43, 1E 1207 – 52, RX J0002 + 62, Vela, PSR 0656 + 14, Geminga) and three 'black body' ones (RX J0002 + 62, PSR 0656 + 14, Geminga).

Let us assume that the NS atmospheres may contain light elements whose surface density is insufficient (Section 7.2) to affect the cooling. In this case, we can use both the 'black body' and 'atmospheric' interpretations of the spectra of thermal radiation. Although the values of M and $\mathcal{R}$ and, accordingly, the gravitational redshift for our models (Section 7.2.2) are somewhat different from those which were obtained (or adopted) in interpretation of the observations, the temperatures T_s^∞ from Table 3 and Fig. 20 can be compared with our cooling curves for several reasons. First, our calculations are not very sensitive to variation of a NS mass or radius (see Sect. 8.3 below). Second, the confidence regions of M and R, inferred from interpretation of observations, include, as a rule, the values we use in modeling.

For simplicity, we assume that the internal structure of the indicated NSs is the same, and, particularly, the NSs have the same mass. Then the critical temperatures of nucleons in their cores should be the same. Let us analyse the confidence regions of T_{cn} and T_{cp} constrained by the observations. Including the observations of several NSs enables us to reduce these regions.

The regions in question are plotted in Figs 21 – 23. Figure 21 corresponds to the standard and enhanced cooling of NSs (with masses $1.30\,M_\odot$ and $1.48\,M_\odot$, respectively) with a black body spectrum. Figure 22 corresponds to the enhanced cooling of the stars ($1.48\,M_\odot$) possessing hydrogen atmospheres. Finally, the standard cooling of NSs ($1.30 M_\odot$) with hydrogen atmospheres is shown in Fig. 23. In each figure, the lines of different types enclose the confidence regions of T_{cn}

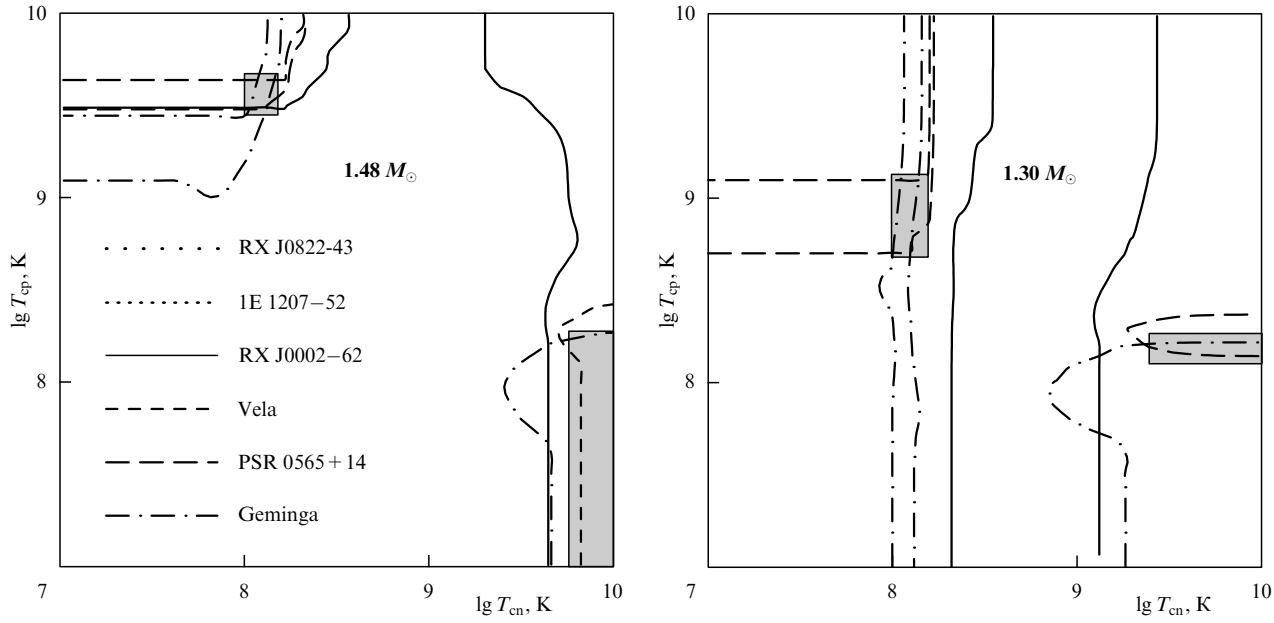

Figure 21. Confidence regions of T_{cn} and T_{cp} which correspond to the 'black body' surface temperatures (Table 3, Fig. 20) of RX J0002+62, PSR 0656+14 and Geminga in the models of enhanced (left) and standard (right) NS cooling.

and T_{cp} associated with the error bars of the observed NS surface temperatures T_s^∞ (Table 3). The correspondence of the lines to the selected NSs is displayed in Fig. 21. For the PSR 0656+14 and Geminga pulsars, the isotherms are taken from Figs 16–19. In each figure the actual overall confidence region of T_{cn} and T_{cp} lies at the overlap of the confidence regions of all objects.

Figures 21–23 show that the observations of several NSs at once can be explained either by the standard or by the enhanced cooling, adopting either black body or atmospheric interpretations of the spectra. In all the cases, there are ranges of T_{cn} and T_{cp} close or joint for all NSs; they do not contradict to the microscopic theories of nucleon superfluidity in NSs (Section 3.1).

According to the left panel of Fig. 21, by adopting the enhanced cooling and the black body interpretation of the observations we obtain two confidence regions of T_{cn} and T_{cp}; each explains the cooling of three objects at once. The first region corresponds to a moderate neutron superfluidity ($\lg T_{cn} \approx 8.1$) and a strong proton superfluidity

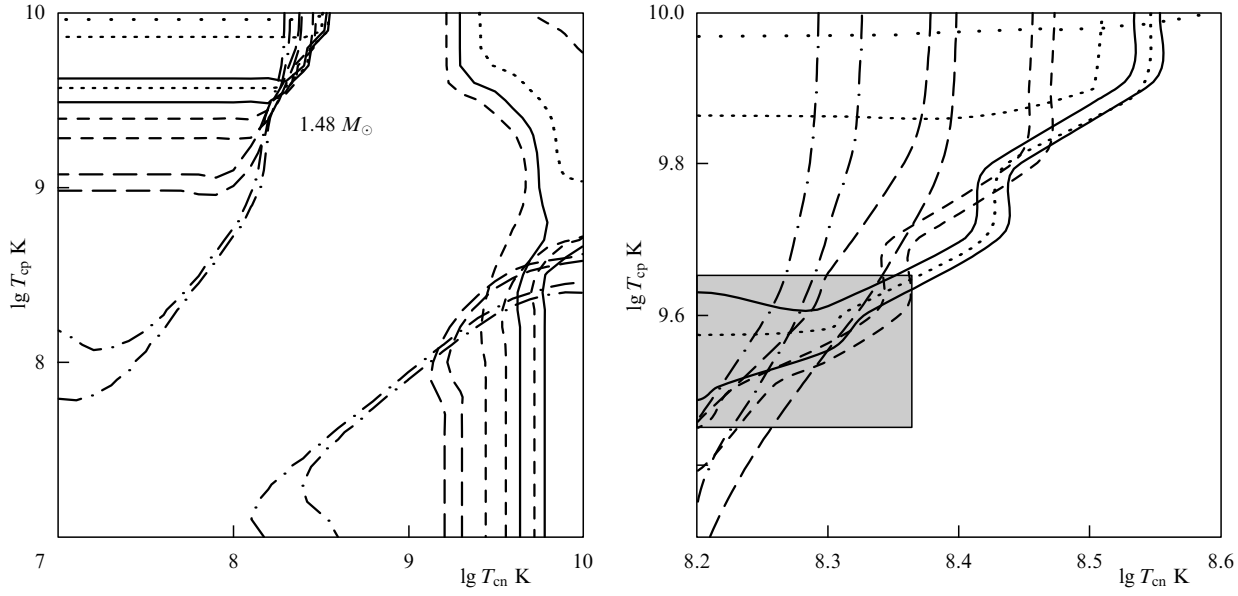

Figure 22. Same as in Fig. 21, but for the enhanced cooling and 'atmospheric' interpretation (Table 3) of spectra of thermal radiation from RX J0822–43, 1E 1207–52, RX J0002+62, Vela, PSR 0656+14 and Geminga. On the right panel, we show in more detail the region (shaded rectangle) in which the allowed values of T_{cn} and T_{cp} of the five latter objects are either close or intersect.

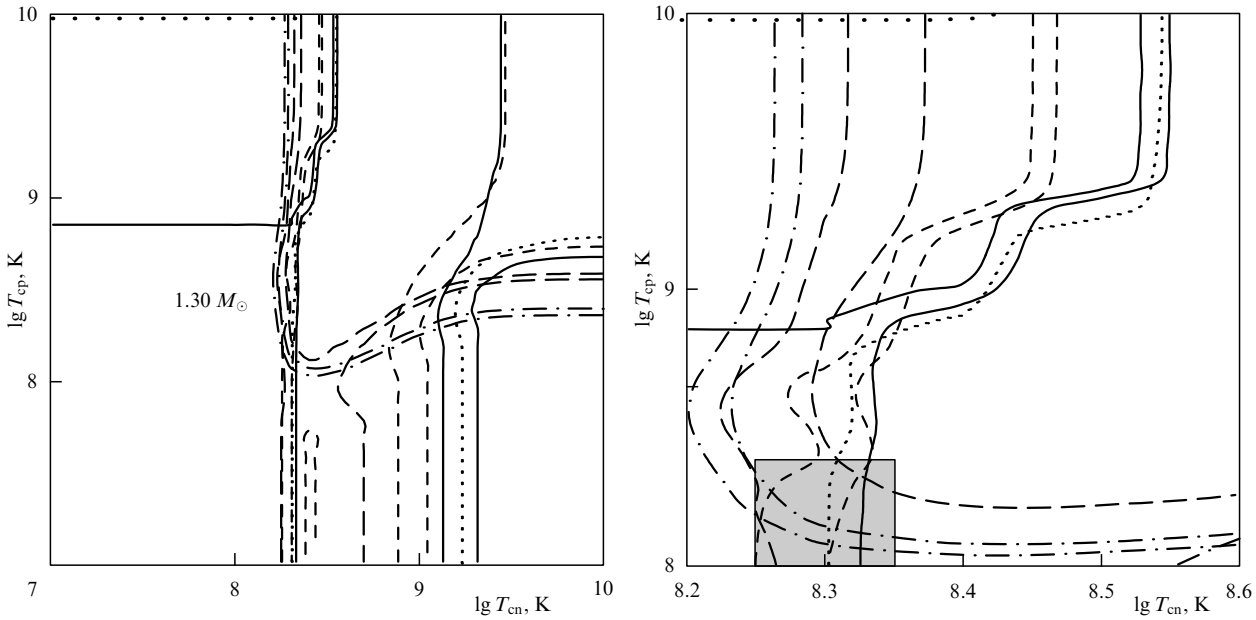

Figure 23. Same as in Fig. 22, but for the standard cooling.

($9.6 \lesssim \lg T_{cp} \lesssim 9.8$); the second, wider region corresponds to a strong neutron superfluidity ($9.75 \lesssim \lg T_{cn} \lesssim 10.0$) and a moderately weak proton superfluidity ($\lg T_{cp} < 8.3$). For the standard cooling of a NS with the black body spectrum (the right panel of Fig. 21), there are also two regions of T_{cn} and T_{cp} for the three NSs, but they are somewhat different from those for the enhanced cooling. The first region corresponds to a moderate neutron superfluidity ($8.0 \lesssim \lg T_{cn} \lesssim 8.2$) and a moderately strong proton superfluidity ($8.7 \lesssim \lg T_{cp} \lesssim 9.1$), while the second one is associated with a strong neutron superfluidity ($\lg T_{cn} > 9.3$) and a moderately weak proton one ($8.1 < \lg T_{cp} < 8.3$).

In the case of enhanced cooling and 'atmospheric' surface temperatures (Fig. 22) there is the only region of joint or very close values of T_{cn} and T_{cp} for five NSs (the shaded rectangle on the right panel). It indicates a moderate neutron ($8.2 \lesssim \lg T_{cn} \lesssim 8.35$) and strong proton ($9.45 \lesssim \lg T_{cp} \lesssim 9.65$) superfluidity. Such superfluidity ($\lg T_{cn} = 8.3$, $\lg T_{cp} = 9.6$) enables us also to describe the sixth object from the 'atmospheric' set (RX J0822 – 43), if we assume that it possesses a thermally insulating envelope of light elements with a mass of $7 \times 10^{-10} M_\odot$ (see Fig. 20). However, even in the absence of the envelope, the confidence region of T_{cn} and T_{cp} for this object is sufficiently close to the joint confidence region indicated above.

Finally, for the standard cooling and the 'atmospheric' spectrum (Fig. 23), there is again a single confidence region of T_{cp} and T_{cn}, where the critical temperatures are nearly the same for the five NSs; it corresponds to moderately strong superfluidity of n and p ($8.25 \lesssim \lg T_{cn} \lesssim 8.35$ and $8.0 \lesssim \lg T_{cp} \lesssim 8.4$, shaded rectangle). The observations of RX J0822 – 43 can also be explained by the presence of the same superfluidity ($\lg T_{cn} = 8.3$, $\lg T_{cp} = 8.2$) assuming that the object possesses an envelope of light elements of mass $7 \times 10^{-10} M_\odot$ (see Fig. 20). In the absence of the envelope, the confidence region of T_{cn} and T_{cp} is outside the joint confidence region since the error bar of T_s^∞ for this object lies at the boundary of the shaded region (filled by the cooling curves of superfluid NSs).

8.3 Discussion

As follows from the results of Section 8.2, the majority of NS observations can be explained using the adopted NS models by the standard and enhanced cooling for the 'black body' and 'atmospheric' interpretations of the spectra observed. In all these cases there are values of T_{cn} and T_{cp} close or common for all NSs which do not contradict the microscopic theories (Section 3.1), but depend on the cooling type and interpretation of the thermal NS radiation.

The existence of the same critical temperatures for several NSs at once is quite unexpected. Initially we expected different joint confidence regions of T_{cn} and T_{cp} for different pairs of NSs. The result is even more surprising taking into account simplicity of our cooling models. It would be interesting to confirm (or reject) these results using more advanced cooling models and a larger number of objects.

We have checked that our results are rather insensitive to variations of the NS mass M as long as M does not pass through the threshold value $M_{cr} = 1.442\, M_\odot$ (of switching on the direct Urca). This fact is a consequence of the main simplification of our models: the constancy of critical temperatures throughout the NS core. In particular, the standard cooling curves for NSs with masses lower than M_{cr} practically coincide (see, e.g., Fig. 2). The same takes place for the enhanced cooling curves of NSs (with masses $M \gtrsim M_{cr}$), if protons or neutrons in their cores possess moderate or strong superfluidity with $T_c \gtrsim 10^8$ K (just as for the joint confidence regions of T_{cn} and T_{cp} obtained above).

We have assumed in our analysis that the NS ages t are known (Section 8.1.3). Then the confidence regions of T_{cn} and T_{cp} for each star were determined from an error bar of the surface temperature T_s obtained from the observations. Introduction of the error bars of Δt instead of the fixed values of t would lead to additional broadening of the confidence ranges of T_{cn} and T_{cp} for each NS and to slight broadening of the joint confidence regions of T_{cn} and T_{cp}. Let us mention that the characteristic ages of PSR 0656 + 14, Geminga and PSR 1055 – 52 are determined to within a factor of ~ 3. The uncertainty in ages of young NSs is higher which, however,

should not cause stronger broadening of the T_{cn} and T_{cp} regions due to the weak slope of the cooling curves at $t = 10^3 - 10^4$ yr (see Fig. 20).

For the black body interpretation of the thermal radiation from NSs, our simulations predict strong neutron superfluidity, $T_{cn} \approx 10^{9.7} - 10^{10.0}$ K, and weak proton superfluidity in the NS cores. This conclusion is in qualitative agreement with the result by Page [124]. Strong proton superfluidity is also possible in the presence of moderate neutron superfluidity. In such cases one superfluidity (n or p) is noticeably stronger than the other. In both the cases of 'black body' and 'atmospheric' interpretations of the observations the largest contrast of T_{cn} and T_{cp} takes place for NS cooling with the direct Urca process allowed. Notice that such a superfluidity is predicted by Takatsuka and Tamagaki [92].

In neither case do we need simultaneously strong superfluidities of n and p to explain the observations. This indicates that the equation of state of the NS cores cannot be too soft (the softness would mean weak nucleon–nucleon repulsion at small separations which would induce especially strong pairing, Section 3.1).

Finally let us mention that we can satisfy the observations by varying the only parameter, T_{cp}, if we assume the presence of neutron superfluidity with $T_{cn} \approx 10^{8.1} - 10^{8.3}$ K. For standard cooling, this parameter should lie in the moderate range $10^{8.0} - 10^{9.0}$ K, while for enhanced cooling it should be larger, $10^{9.45} - 10^{9.65}$ K.

9. Conclusions

We have described one of a few methods to study the fundamental properties of matter of density around the nuclear matter density or several times higher. The method is based on theoretical simulations of cooling of neutron stars and comparison of the results with the observations of the thermal radiation from isolated cooling neutron stars.

We have described all the basic elements of the theory of cooling of neutron stars with standard nuclear composition: stellar heat capacity (Section 3), neutrino cooling (Sections 4–6), the relationship between the internal and surface stellar temperatures (Section 7.2.1). However we did not intend to discuss all the cooling problems in detail but focused on a relatively new direction of the theory which was initiated by the remarkable paper by Page and Applegate [5]. These authors were the first who noticed that neutron star cooling could be very sensitive to the superfluidity of neutrons and protons in their cores. The temperatures of the superfluidity onset, in turn, are sensitive to the equation of state of superdense matter. This opens the principal possibility of exploring nucleon superfluidity and, accordingly, the equation of state in the neutron star cores.

The effects of superfluidity were included in cooling simulations long before Page and Applegate [5]. However they had not been the objects of special attention; systematic analysis of the effects of superfluidity on the neutrino luminosity and the heat capacity were absent, and the effects were described by oversimplified expressions (Section 7.1). We have tried to fill in this gap and presented the results of detailed calculations of the heat capacity and neutrino emissivities in superfluid matter in the framework of the Bardeen–Cooper–Schrieffer theory (Sections 3–6). Our consideration is done in a unified manner. The results are mainly presented in the form of simple fit expressions convenient for practical applications. Thus we have produced a rather elaborated method to include the effects of superfluidity in simulations of neutron-star cooling. This method can be extended easily to neutron star models with superfluid hyperons.

For illustration, we have presented (Section 7.2) the results of cooling simulations of neutron stars whose cores contain superfluid neutrons and protons. For simplicity, the critical temperatures T_{cn} and T_{cp} have been assumed constant over the neutron star core. We have analyzed the effect of superfluidity on the enhanced and standard cooling and showed that this effect is really crucial. If standard cooling of medium-aged ($10^2 - 10^5$ yr) neutron stars with non-superfluid cores goes much slower than cooling enhanced by the direct Urca process, this is not so in the presence of superfluidity. As a whole, the nucleon superfluidity strongly reduces the difference between standard and enhanced cooling. This enables one, in principle, to explain the majority of observational data by the standard cooling of the stars with superfluid cores. On the other hand, this circumstance disproves a widely accepted point of view that the direct Urca process necessarily induces rapid cooling.

We have compared (Section 8.2) the results of cooling simulations with the observational data on the thermal radiation of neutron stars. In almost all the cases (for different methods of inferring the surface temperatures from observational data) the observations can be explained in the models of standard and enhanced cooling of a neutron star with a superfluid core. It is important that the required values of the critical temperatures T_{cn} and T_{cp} do not contradict to the values predicted by various microscopic theories of nucleon superfluidity in superdense matter (Section 3.1). However our results should be regarded as preliminary; they cannot allow us to identify reliably superfluidity and equation of state in neutron star cores. To impose more stringent constraints one needs to carry out more elaborated simulations of neutron star cooling taking into account the density dependence of T_{cn} and T_{cp} in the stellar core. It would be very desirable to make an equation of state of matter, used in cooling simulations, consistent with the critical temperatures. For this purpose, one needs a representative set of equations of state of superdense matter (from soft to stiff ones), supplemented by the values of $T_{cn}(\rho)$ and $T_{cp}(\rho)$, calculated from the same microscopic models. This would enable one to construct a set of more realistic cooling curves and improve thus the 'calibration' of neutron stars as natural thermometers of superfluidity in their cores. Comparing theory with observations one would be able to constrain strongly the set of allowable equations of state. Unfortunately, simultaneous microscopic calculations of the equations of state and superfluid gaps are almost absent. On the other hand, the surface temperatures of the neutron stars cannot be determined uniquely from observations so far.

We hope that after appearance of self-consistent calculations of the equations of state and superfluid gaps and after the launch of orbital observatories of a new generation (*AXAF, XMM, ASTRO-E, SXG*), which will produce more reliable data on the surface temperatures of neutron stars, this method will enable one to reach a deeper understanding of the nature of superdense matter.

Acknowledgments. We are grateful to D A Baiko, V G Bezchastnov, P Haensel, A B Koptsevich, G G Pavlov, M G Urin, D N Voskresensky, and V E Zavlin for discussions of the problems included in this review. Our special thanks are to A D Kaminker and A Y Potekhin for reading the manu-

script of the review and making useful comments. The review is partly based on the course of lectures "White dwarfs and neutron stars" given by one of the authors (D G Yakovlev) to 6th-year students specializing in 'Cosmic studies' at the St.-Petersburg State Technical University. The work was supported in part by RFBR (grant No. 99-02-18099) and INTAS (96-0542).

References

1. Shapiro S L, Teukolsky S A *Black Holes, White Dwarfs, and Neutron Stars* (New-York: Wiley-Interscience, 1983)
2. Imshennik V S, Nadyozhin D K, in *Soviet Scientific Reviews* (Section E: Astrophysics and Space Physics Reviews Vol. 2, Ed R A Sunyaev) (Harwood Academic Publishers, 1982) p. 75
3. Lewin W H G, Van Paradijs J, Van den Huevel E P G (Eds) *X-ray Binaries* (Cambridge: Cambridge Univerisity Press, 1995)
4. Pines D, in *Neutron Stars*: *Theory and Observation* (Eds J Ventura, D Pines) (Dordrecht: Kluwer Acad. Publ., 1991) p. 57
5. Page D, Applegate J H *Astrophys. J. Lett.* **394** L17 (1992)
6. Pavlov G G et al., in *The Lives of the Neutron Stars* (Eds M A Alpar, Ü Kiziloğlu , J van Paradijs) (Dordrecht: Kluwer, 1995) p. 71
7. Pavlov G G, Zavlin V E, in *Neutron Stars and Pulsars* (Eds N Shibazaki et al.) (Tokyo: Universal Academy Press, 1998) p. 327
8. Haensel P, Pichon B *Astron. Astrophys.* **283** 313 (1994)
9. Negele J W, Vautherin D *Nucl. Phys. A* **207** 298 (1973)
10. Pethick C J, Ravenhall D G *Ann. Rev. Nucl. Particle Sci.* **45** 429 (1995)
11. Lorenz C P, Ravenhall D G, Pethick C J *Phys. Rev. Lett.* **70** 379 (1993)
12. Friman B L, Maxwell O V *Astrophys. J.* **232** 541 (1979)
13. Botermans W, Malfliet R *Phys. Rep.* **198** 115 (1990)
14. Baym G, Pethick C J *Landau Fermi-Liquid Theory* (New York: Wiley, 1991)
15. Pandharipande V R *Nucl. Phys. A* **174** 641 (1971)
16. Reid R V *Ann. Phys.* **50** 411 (1968)
17. Pandharipande V R, Smith R A *Phys. Lett. B* **59** 15 (1975)
18. Ruderman M *Astrophys. J.* **366** 261 (1991)
19. Lattimer J M et al. *Phys. Rev. Lett.* **66** 2701 (1991)
20. Prakash M et al. *Astrophys. J. Lett.* **390** L77 (1992)
21. Pethick C J *Rev. Mod. Phys.* **64** 1133 (1992)
22. Bahcall J N, Wolf R A *Phys. Rev.* **140** 1445 (1965)
23. Bahcall J N, Wolf R A *Phys. Rev.* **140** 1452 (1965)
24. Migdal A B *Usp. Fiz. Nauk* **105** 781 (1971)
25. Sawyer R F *Phys. Rev. Lett.* **29** 382 (1972)
26. Scalapino D J *Phys. Rev. Lett.* **29** 386 (1972)
27. Maxwell O V et al. *Astrophys. J.* **216** 77 (1977)
28. Muto T, Tatsumi T *Prog. Theor. Phys.* **79** 461 (1988)
29. Haensel P *Prog. Theor. Phys. Suppl.* **91** 268 (1987)
30. Schaab Ch et al. *Nucl. Phys. A* **605** 531 (1996)
31. Iwamoto N *Phys. Rev. Lett.* **44** 1637 (1980)
32. Burrows A *Phys. Rev. Lett.* **44** 1640 (1980)
33. Schaab Ch et al. *Astrophys. J. Lett.* **480** L111 (1997)
34. Kaplan D B, Nelson A E *Phys. Lett. B* **175** 57 (1986); erratum: **179** 409 (1986)
35. Nelson A E, Kaplan D B *Phys. Lett. B* **192** 193 (1987)
36. Brown G E et al. *Phys. Rev. D* **37** 2042 (1988)
37. Pandharipande V R, Pethick C, Thorsson V *Phys. Rev. Lett.* **75** 4567 (1995)
38. Cherepashchuk A M *Usp. Fiz. Nauk* **166** 809 (1996) [*Phys. Usp.* **39** 759 (1996)]
39. Imshennik V S, Nadyozhin D K *Usp. Fiz. Nauk.* **156** 561 (1988) [*Sov. Phys. Usp.* **31** 461 (1988)]
40. Soyeur M, Brown G E *Nucl. Phys. A* **324** 464 (1979)
41. Itoh N et al. *Astrophys. J.* **285** 304 (1984)
42. Pethick C J, Thorsson V *Phys. Rev. Lett.* **72** 1964 (1994)
43. Itoh N et al. *Astrophys. J. Suppl.* **102** 411 (1996)
44. Kaminker A D, Yakovlev D G, Haensel P *Astron. Astrophys.* **325** 391 (1997)
45. Kaminker A D et al. *Astron. Astrophys.* **343** 1009 (1999)
46. Chiu H-Y, Salpeter E E *Phys. Rev. Lett.* **12** 413 (1964)
47. Boguta J *Phys. Lett. B* **106** 255 (1981)
48. Voskresenskiĭ D N, Senatorov A V *Pis'ma Zh. Eksp. Teor. Fiz.* **40** 395 (1984) [*JETP Lett.* **40** 1212 (1984)]
49. Voskresenskiĭ D N, Senatorov A V *Zh. Eksp. Teor. Fiz.* **90** 1505 (1986) [*JETP* **63** 885 (1986)]
50. Schaab Ch et al. *Astron. Astrophys.* **321** 591 (1997)
51. Flowers E G, Ruderman M, Sutherland P G *Astrophys. J.* **205** 541 (1976)
52. Voskresenskiĭ D N, Senatorov A V *Yad. Fiz.* **45** 657 (1987) [*Sov. J. Nucl. Phys.* **45** 411 (1987)]
53. Page D, in *The Many Faces of Neutron Stars* (Eds R Buccheri, J van Paradijs, M A Alpar) (Dordrecht: Kluwer Acad. Publ., 1998) p. 538
54. Levenfish K P, Shibanov Yu A, Yakovlev D G *Phys. Scripta T* **77** 79 (1998)
55. Yakovlev D G, Kaminker A D, Levenfish K P, in *Neutron Stars and Pulsars* (Eds N Shibazaki et al.) (Tokyo: Universal Academy Press, 1998) p. 195
56. Yakovlev D G, Kaminker A D, Levenfish K P *Astron. Astrophys.* **343** 650 (1999)
57. Levenfish K P, Shibanov Yu A, Yakovlev D G *Astron. Lett.* **25** 417 (1999)
58. Thorne K S *Astrophys. J.* **212** 825 (1977)
59. Haensel P *Acta Phys. Pol. B* **25** 373 (1994)
60. Nomoto K, Tsuruta S *Astrophys. J.* **312** 711 (1987)
61. Lattimer J M et al. *Astrophys. J.* **425** 802 (1994)
62. Gudmundsson E H, Pethick C J, Epstein R I *Astrophys. J.* **272** 286 (1983)
63. Bardeen J, Cooper L N, Schrieffer J R *Phys. Rev.* **108** 1175 (1957)
64. Bohr A, Mottelson B R, Pines D *Phys. Rev.* **110** 936 (1958)
65. Migdal A B *Nucl. Phys.* **13** 655 (1959)
66. Cooper L N, Mills R L, Sessler A M *Phys. Rev.* **114** 1377 (1959)
67. Chen J M et al. *Nucl. Phys. A* **555** 59 (1993)
68. Ishihara T et al. *Prog. Theor. Phys.* **30** 601 (1963)
69. Henley E M, Wilets L *Phys. Rev. B* **133** 1118 (1964)
70. Kennedy R, Wilets L, Henley E M *Phys. Rev. B* **133** 1131 (1964)
71. Kennedy R C *Nucl. Phys. A* **118** 189 (1968)
72. Tamagaki R *Prog. Theor. Phys.* **39** 91 (1968)
73. Anderson P W, Morel P *Phys. Rev.* **123** 1911 (1961)
74. Balian R, Werthamer N R *Phys. Rev.* **131** 1553 (1963)
75. Ginzburg V L, Kirzhnits D A *Zh. Teor. Eksp. Fiz.* **47** 2006 (1964) [*Sov. Phys. JETP* **20** 1346 (1965)]
76. Wolf R A *Astrophys. J.* **145** 834 (1966)
77. Ginzburg V L *Usp. Fiz. Nauk* **97** 601 (1969) [*Sov. Phys. Usp.* **12** 241 (1970)]
78. Baym G, Pethick C J, Pines D *Nature* (London) **224** 673 (1969)
79. Hoffberg M et al. *Phys. Rev. Lett.* **24** 775 (1970)
80. Amundsen L, Østgaard E *Nucl. Phys. A* **437** 487 (1985)
81. Amundsen L, Østgaard E *Nucl. Phys. A* **442** 163 (1985)
82. Wambach J, Ainsworth T L, Pines D, in *Neutron Stars*: *Theory and Observation* (Eds J Ventura, D Pines) (Dordrecht: Kluwer Acad. Publ., 1991) p. 37
83. Baldo M et al. *Nucl. Phys. A* **536** 349 (1992)
84. Takatsuka T, Tamagaki R *Prog. Theor. Phys. Suppl.* **112** 27 (1993)
85. Tamagaki R *Prog. Theor. Phys.* **44** 905 (1970)
86. Takatsuka T, Tamagaki R *Prog. Theor. Phys.* **46** 114 (1971)
87. Takatsuka T *Prog. Theor. Phys.* **47** 1062 (1972)
88. Takatsuka T *Prog. Theor. Phys.* **48** 1517 (1972)
89. Elgarøy Ø et al. *Phys. Rev. Lett.* **77** 1428 (1996)
90. Elgarøy Ø et al. *Nucl. Phys. A* **607** 425 (1996)
91. Takatsuka T, Tamagaki R *Prog. Theor. Phys.* **97** 263 (1997)
92. Takatsuka T, Tamagaki R *Prog. Theor. Phys.* **97** 345 (1997)
93. Takatsuka T, Tamagaki R *Prog. Theor. Phys.* **98** 393 (1997)
94. Muzikar P, Sauls J A, Serene J W *Phys. Rev. D* **21** 1494 (1980)
95. Chao N-C, Clark J W, Yang C-H *Nucl. Phys. A* **179** 320 (1972)
96. Takatsuka T *Prog. Theor. Phys.* **50** 1754 (1973)
97. Baldo M et al. *Nucl. Phys. A* **515** 409 (1990)
98. Elgarøy Ø et al. *Nucl. Phys. A* **604** 466 (1996)
99. Elgarøy Ø, Hjorth-Jensen M *Phys. Rev. C* **57** 1174 (1998)
100. Sedrakian A, Alm T, Lombardo U *Phys. Rev. C* **55** 582 (1997)
101. Civitareze O, Reboiro M, Vogel P *Phys. Rev. C* **56** 1840 (1997)
102. Krotscheck E *Z. Phys.* **251** 135 (1972)
103. Clark J W et al. *Phys. Lett. B* **61** 331 (1976)
104. Takatsuka T *Prog. Theor. Phys.* **71** 1432 (1984)
105. Chen J M et al. *Nucl. Phys. A* **451** 509 (1986)

106. Ainsworth T L, Wambach J, Pines D *Phys. Lett. B* **222** 173 (1989)
107. Wambach J, Ainsworth T L, Pines D *Nucl. Phys. A* **555** 128 (1993)
108. Broglia R A et al. *Phys. Rev. D* **50** 4781 (1994)
109. Elgarøy Ø et al. *Phys. Rev. D* **54** 1848 (1996)
110. Pethick C J, Ravenhall D G, in *The Many Faces of Neutron Stars* (Eds R Buccheri, van J Paradijs, M A Alpar) (Dordrecht: Kluwer Acad. Publ., 1998) p. 49
111. De Blaiso F V, Lazzari G *Phys. Rev. C* **52** 418 (1995)
112. Barranco F et al. *Phys. Rev. C* **58** 1257 (1998)
113. Takatsuka T, Tamagaki R *Prog. Theor. Phys.* **94** 457 (1995)
114. Bailin D, Love A *Phys. Rep.* **107** 325 (1984)
115. Iwasaki M *Prog. Theor. Phys.* **120** 187 (1995)
116. Balberg S, Barnea N *Phys. Rev. C* **57** 409 (1998)
117. Tabakin F *Ann. Phys.* (N. Y.) **30** 51 (1964)
118. Schaab Ch, Weber F, Weigel M K *Astron. Astrophys.* **335** 596 (1998)
119. Lifshitz E M, Pitaevskii L P *Statisticheskaya Fizika* (Statistical Physics) Ch 2 (Moscow: Nauka, 1978) [Translated into English (Oxford: Pergamon Press, 1980)]
120. Levenfish K P, Yakovlev D G *Astron. Rep.* **38** 247 (1994)
121. Levenfish K P, Yakovlev D G, in *Strongly Coupled Plasma Physics* (Eds H M van Horn, S Ichimaru) (Rochester: Univ. of Rochester Press, 1993) p. 167
122. Mühlschlegel B *Z. Phys.* **155** 313 (1959)
123. Maxwell O V *Astrophys. J.* **231** 201 (1979)
124. Page D *Astrophys. J.* **428** 250 (1994)
125. Levenfish K P, Yakovlev D G *Astron. Lett.* **20** 43 (1994)
126. Baiko D A, Yakovlev D G *Astron. Astrophys.* **342** 192 (1999)
127. Van Riper K A, Lattimer J M, in *Isolated Pulsars* (Eds K A van Riper, R Epstein, C Ho) (Cambridge: Cambridge Univ. Press, 1993) p. 122
128. Flowers E G, Sutherland P G, Bond J R *Phys. Rev. D* **12** 315 (1975)
129. Maxwell O V *Astrophys. J.* **316** 691 (1987)
130. Yakovlev D G, Levenfish K P *Astron. Astrophys.* **297** 717 (1995)
131. Itoh N, Tsuneto T *Prog. Theor. Phys.* **48** 1849 (1972)
132. Pizzochero P M *Astrophys. J. Lett.* **502** L153 (1998)
133. Levenfish K P, Yakovlev D G *Astron. Lett.* **22** 47 (1996)
134. Okun' L B *Leptons and Quarks* (Moscow: Nauka, 1990) [Translated into English (Amsterdam: North-Holland, 1984)]
135. Kaminker A D, Haensel P, Yakovlev D G *Astron. Astrophys.* **345** L14 (1999)
136. Kaminker A D, Haensel P *Acta Phys. Pol.* **30** 1125 (1999)
137. Stabler R *Ph.D. Thesis* (New York: Cornell University, 1960)
138. Chiu H-Y *Ann. Phys.* (N. Y.) **26** 364 (1964)
139. Morton D C *Nature* (London) **201** 1308 (1964)
140. Bowyer S et al. *Nature* (London) **201** 1307 (1964)
141. Tsuruta S, Cameron A G W *Can. J. Phys.* **44** 1863 (1966)
142. Tsuruta S *Phys. Rep.* **56** 237 (1979)
143. Tsuruta S, in *X-ray Astronomy* (Eds R Giacconi, G Setti) (Dordrecht: Reidel, 1980) p. 73
144. Tsuruta S, in *Pulsars* (Eds W Sieber, R Wielebinski) (Dordrecht: Reidel, 1981) p. 331
145. Tsuruta S *Comments on Astrophys.* **11** 151 (1986)
146. Tsuruta S *Phys. Rep.* **292** 1 (1998)
147. Glen G, Sutherland P *Astrophys. J.* **239** 671 (1980)
148. Van Riper K A, Lamb F *Astrophys. J. Lett.* **244** L13 (1981)
149. Yakovlev D G, Urpin V A *Pis'ma Astron. Zh.* **7** 157 (1981)
150. Richardson M B et al. *Astrophys. J.* **255** 624 (1982)
151. Umeda H et al. *Astrophys. J.* **408** 186 (1993)
152. Umeda H, Tsuruta S, Nomoto K *Astrophys. J.* **433** 256 (1994)
153. Umeda H et al. *Astrophys. J.* **431** 309 (1994)
154. Page D, Baron E *Astrophys. J. Lett.* **354** L17 (1990) erratum: *Astrophys. J. Lett.* **382** L11 (1991)
155. Page D *Astrophys. J. Lett.* **479** L43 (1997)
156. Gnedin O Y, Yakovlev D G *Astron. Lett.* **19** 104 (1993)
157. Gnedin O Y, Yakovlev D G, Shibanov Yu A *Astron. Lett.* **20** 409 (1994)
158. Page D *Revista Mexicana de Fisica* **41** (Suppl., 1) 178 (1995)
159. Tsuruta S et al. *Astrophys. J.* **176** 739 (1972)
160. Tsuruta S, in *Physics of Dense Matter* (Ed C J Hansen) (Dordrecht: Reidel, 1974) p. 209
161. Tsuruta S *Astrophys. Space Sci.* **34** 199 (1975)
162. Van Riper K A *Astrophys. J.* **329** 339 (1988)
163. Van Riper K A *Astrophys. J. Suppl.* **75** 449 (1991)
164. Page D *Astrophys. J.* **442** 273 (1995)
165. Shibanov Yu A, Yakovlev D G *Astron. Astrophys.* **309** 171 (1996)
166. Heyl J S, Hernquist L *Astrophys. J. Lett.* **491** L95 (1997)
167. Heyl J S, Hernquist L *Astrophys. J. Lett.* **489** L67 (1997)
168. Heyl J S, Hernquist L *Monthly Not. R. Astron. Soc.* **298** 17 (1998)
169. Heyl J S, Hernquist L *Monthly Not. R. Astron. Soc.* **300** 599 (1998)
170. Heyl J S, Hernquist L *Monthly Not. R. Astron. Soc.* (1998) (in press)
171. Heyl J S, Kulkarni S R *Astrophys. J. Lett.* **506** L61 (1998)
172. Chabrier G, Potekhin A Y, Yakovlev D G *Astrophys. J. Lett.* **477** L99 (1997)
173. Potekhin A Y, Chabrier G, Yakovlev D G *Astron. Astrophys.* **323** 415 (1997)
174. Page D, in *Neutron Stars and Pulsars* (Eds N Shibazaki et al.) (Tokyo: Universal Academy Press, 1998) p. 183
175. Malone R C *Ph.D. Thesis* (New York: Cornell University, 1974)
176. Richardson M B *Ph.D. Thesis* (State University of Alabama, 1980)
177. Nomoto K, Tsuruta S *Astrophys. J. Lett.* **250** L19 (1981)
178. Nomoto K, Tsuruta S, in *Accreting Neutron Stars* (Eds J Trümper, W Brinkmann) (Garching: Max Planck Institut, 1982) p. 275
179. Nomoto K, Tsuruta S, in *Supernova Remnants and Their X-ray Emission* (Eds J Danziger, P Gorenstein) (Dordrecht: Reidel, 1983) p. 509
180. Nomoto K, Tsuruta S *Astrophys. J. Lett.* **305** L19 (1986)
181. Schaab Ch, Weigel M K *Astron. Astrophys.* **336** L13 (1998)
182. Alpar M A et al. *Astron. Astrophys.* **177** 101 (1987)
183. Shibazaki N, Lamb F K *Astrophys. J.* **346** 808 (1989)
184. Van Riper K A *Atrophys. J.* **372** 251 (1991)
185. Van Riper K A, Epstein R I, Miller G S *Astrophys. J. Lett.* **381** L47 (1991)
186. Shibazaki N, Mochizuki Y *Astrophys. J.* **438** 288 (1995)
187. Van Riper K A, Link B, Epstein R I *Astrophys. J.* **448** 294 (1995)
188. Reisenegger A *Astrophys. J.* **442** 749 (1995)
189. Haensel P, Urpin V A, Yakovlev D G *Astron. Astrophys.* **229** 133 (1990)
190. Yakovlev D G, in *Strongly Coupled Plasma Physics* (Eds H M van Horn, S Ichimaru) (Rochester: Univ. of Rochester Press, 1993) p. 157
191. Shalybkov D A *Astron. Lett.* **20** 182 (1994)
192. Urpin V A, Shalybkov D A *Astron. Rep.* **39** 332 (1995)
193. Goldreich P, Reisenegger A *Astrophys. J.* **395** 250 (1992)
194. Yakovlev D G, Shalybkov D A *Astrophys. Space Sci.* **176** 171, 191 (1991)
195. Miralles J A, Urpin V A, Konenkov D Yu *Astrophys. J.* **503** 368 (1998)
196. Urpin V A, Konenkov D Yu, in *Neutron Stars and Pulsars* (Eds N Shibazaki et al.) (Tokyo: Universal Academy Press, 1998) p. 171
197. Urpin V A, Muslimov A G *Monthly Not. R. Astron. Soc.* **256** 261 (1992)
198. Urpin V A, Van Riper K A *Astrophys. J. Lett.* **411** L87 (1993)
199. Tsuruta S, in *Physics and Astrophysics of Neutron Stars and Black Holes* (Amsterdam: North Holland, 1978) p. 635
200. Finley J P, Ögelman H, Kiziloğlu Ü *Astrophys. J. Lett.* **394** L21 (1992)
201. Halpern J P, Ruderman M *Astrophys. J.* **415** 286 (1993)
202. Ögelman H, Finley J P, Zimmermann H U *Nature* (London) **361** 136 (1993)
203. Brinkmann W, Ögelman H *Astron. Astrophys.* **182** 71 (1987)
204. Schaab C, Balberg S, Schaffner-Bielich J *Astrophys. J. Lett.* **504** L99 (1998)
205. Haensel P, Gnedin O Y *Astron. Astrophys.* **290** 458 (1994)
206. Prakash M, Ainsworth T L, Lattimer J M *Phys. Rev. Lett.* **61** 2518 (1988)
207. Baade W, Zwicky F *Phys. Rev.* **45** 138 (1934)
208. Hewish A et al. *Nature* (London) **217** 709 (1968)
209. Wolff R S et al. *Astrophys. J.* **202** L15 (1975)
210. Toor A, Seward F D *Astrophys. J.* **216** 560 (1977)
211. Korpela E J, Bowyer S. *Astron. Astrophys. Suppl.* **188** 4301 (1996)
212. Mignani R P, in *Neutron Stars and Pulsars* (Eds N Shibazaki et al.) (Tokyo: Universal Academy Press, 1998) p. 335
213. Martin C, Halpern J P, Schiminovich D *Astrophys. J. Lett.* **494** L211 (1998)
214. Shearer A et al. *Astron. Astrophys.* **335** L21 (1998)

215. Zavlin V E, Pavlov G G, Shibanov Yu A *Astron. Astrophys.* **315** 141 (1996)
216. Rajagopal M, Romani R W *Astrophys. J.* **461** 327 (1996)
217. Zavlin V E, Shibanov Yu A, Pavlov G G *Astron. Lett.* **21** 149 (1995)
218. Potekhin A Y *J. Phys. B* **27** 1073 (1994)
219. Shibanov Yu A et al., in *Isolated Pulsars* (Eds K A van Riper, R I Epstein, C Ho) (Cambridge: Cambridge Univ. Press, 1993) p. 174
220. Rajagopal M, Romani R W, Miller M C *Astrophys. J.* **479** 347 (1997)
221. Page D, Shibanov Yu A, Zavlin V E, in *Röntgenstrahlung from the Universe* (Eds H U Zimmermann, J E Trümper, H Yorke) (Garching: Max-Planck Institut für Extraterrestrische Physik, 1996) p. 173
222. Zavlin V E, Pavlov G G, Trümper J *Astron. Astrophys.* **331** 821 (1998)
223. Becker W, Trümper J *Astron. Astrophys.* **326** 682 (1997)
224. Becker W, Trümper J *Astron. Astrophys.* **341** 803 (1999)
225. Potekhin A Y, Pavlov G G *Astrophys. J.* **483** 414 (1997)
226. Bezchastnov V G, Pavlolv G G, Ventura J *Phys. Rev. A* **58** 180 (1998)
227. Bignami G F et al. *Astrophys. J. Lett.* **456** L111 (1996)
228. Becker W, Aschenbach B, in *The Lives of Neutron Stars* (Eds M A Alpar et al.) (Dordrecht: Kluwer Acad. Publ., 1995) p. 47
229. Alpar M A, Nandkumar R, Pines D *Astrophys. J.* **288** 191 (1985)
230. Gotthelf E V, Vasisht G *Astrophys. J. Lett.* **486** L133 (1997)
231. Gotthelf E V, Petre R, Hwang U *Astrophys. J. Lett.* **487** L175 (1997)
232. Vasisht G, Gotthelf E V. *Astrophys. J. Lett.* **486** L129 (1997)
233. Gotthelf E V, Petre R, Vasisht G *Astrophys. J. Lett.* **514** L105 (1999)
234. Thompson C, Duncan R C *Astrophys. J.* **473** 322 (1996)
235. Kouveliotou C et al. *Nature* (London) **393** 235 (1998)
236. Kouveliotou C et al. *IAU Circular* 7003 (1998)
237. Hurley K et al. *Nature* (London) **397** 41 (1999)
238. Mereghetti S, Israel G L, Stella L *Monthly Not. R. Astron. Soc.* **296** 689 (1998)
239. Walter F M, Wolk S J, Neuhäuser R *Nature* (London) **379** 233 (1996)
240. Walter F M, Matthews L D *Nature* (London) **389** 358 (1997)
241. Pavlov G G et al. *Astrophys. J. Lett.* **472** L33 (1996)
242. Zane S, Turolla R, Treves A *Astrophys. J.* **471** 248 (1996)
243. Haberl F et al. *Astron. Astrophys.* **326** 662 (1997)
244. Kulkarni S R, van Kerkwijk M H *Astrophys. J. Lett.* **507** L49 (1998)
245. Haberl F, Motch C, Pietsch W *Astron. Nachricht.* **319** 97 (1998)
246. Schwope A D et al. *Astron. Astrophys. Lett.* **341** L51 (1999)
247. Neuhäuser R, Trümper J E *Astron. Astrophys.* **343** 151 (1999)
248. Craig W W, Hailey Ch J, Pisarski R L *Astrophys. J.* **488** 307 (1997)
249. Hailey Ch J, Craig W W *Astrophys. J. Lett.* **455** L151 (1995)
250. Lyne A G et al. *Nature* (London) **381** 497 (1996)
251. Zavlin V E, Pavlov G G, Trümper J (1999) (submitted to *Astrophys. J.*)
252. Zavlin V E, Trümper J, Pavlov G G (1999) (to be submitted to *Astrophys. J.)*
253. Ögelman H, in *Lives of Neutron Stars* (Eds M A Alpar, Ü Kiziloğlu, J van Paradjis) (Dordrecht: Kluwer Acad. Publ., 1995) p. 101
254. Anderson S B et al. *Astrophys. J.* **414** 867 (1993)
255. Possenti A, Mereghetti S, Colpi M *Astron. Astrophys.* **313** 565 (1996)
256. Meyer R D, Pavlov G G, Mészàros P *Astrophys. J.* **433** 265 (1994)
257. Halpern J P, Wang F Y-H *Astrophys. J.* **477** 905 (1997)